Mutation analysis of tissue sections and single cells using low-volume polymerase chain reaction

Dissertation

der Fakultät für Geowissenschaften

der Ludwig-Maximilians-Universität München

vorgelegt

von

Veronika Mayer

03. März 2010

Acknowledgement

Contents

1 Abstract

In modern molecular genetic diagnostics a trend towards very small amounts of DNA down to the analysis of single cells can be observed in recent years. Therefore, techniques for precise isolation and transfer of specific sample material are required prior to analysis.

In this work sample isolation was achieved using laser microdissection in combination with a low-pressure single particle adsorbing transfer system. Isolated samples were transferred horizontally to a planar chemically structured polymerase chain reaction (PCR) glass slide instead of into reaction tubes as is the case in most other microdissection techniques. On this glass slide, a low-volume PCR in a total reaction volume of 1 µl is performed. Reduction of the reaction volume has the potential to dramatically increase the efficiency and sensitivity of PCR compared to PCR in larger reaction volumes of up to 50 µl. It is therefore applicable to analyses at the single cell level.

In the first part of this work, three colon polyps of two patients at risk for colorectal cancer (CRC) were characterized simultaneously regarding mutations of the two proto-oncogenes *BRAF* and *KRAS* and microsatellite instability (MSI) status. Major aspects in CRC development are microsatellite instability, CpG island methylator phenotype and mutations in certain genes. The genes *BRAF* and *KRAS* are components of the MAPK ERK signalling pathway and gain-of-function mutations of either of them leads to the activation of the pathway and therefore to cell proliferation.

Low-volume multiplex PCR directly from formalin-fixed paraffin-embedded polyp tissue sections (hyperplastic polyp, sessile serrated and tubular adenoma) was performed. It was demonstrated that hotspot mutations of *BRAF* and *KRAS* occurred simultaneously in the same sample isolated from one polyp of a patient. Furthermore, mutations in both genes, besides the hotspots, were detected very often in the same samples. In contrast, it was shown recently that mutations at the hotspots of *BRAF* (mutation V600E) and *KRAS* (codons 12, 13, 59, 61 and 63) are mutually exclusive in precursor lesions of sporadic microsatellite stable and MSI CRC. Compared to the CRC classification suggested by Jass, the results obtained in this work indicate an association with the serrated pathway model comprising mutations in *BRAF* and *KRAS* and MSI or

microsatellite stability. It was shown that characterization of such colon polyps is important for a better molecular understanding of colorectal cancer development.

In the second part of this work a genetic test system for the specific detection of mutations in the adenomatous polyposis coli (*APC*) gene was established that is applicable to polar body diagnosis. Familial adenomatous polyposis of the colon is an autosomal dominant inherited disorder caused by mutations in the tumor suppressor gene *APC.* A characteristic of this severe disease is the development of hundreds to thousands of polyps in the colon starting in the first decade of age which untreated evolve into malignant colorectal carcinomas. In preimplantation genetic diagnosis (PGD), mutation analysis has to be performed on only few or even single cells e. g. blastomeres, blastocyst cells and polar bodies. Mutation analysis must therefore be carefully validated and optimized as regards amplification efficiency and the evaluation of allelic drop out rates before application to PGD.

A multiplex nested PCR protocol in 1 µl reaction volume, followed by sequencing and fragment length analysis was applied in order to detect mutations in the *APC* gene. High amplification efficiency and low allelic drop out rates for polymorphic microsatellite markers and mutation-specific amplification products of various mutations in the *APC* gene were obtained from fixed single cells. This novel approach enables a reliable validation of genetic testing using diploid single lymphocytes, and will open a wide range of single cell diagnostics. Moreover, this fast and reliable technique for mutation analysis combining laser microdissection, horizontal transfer, low-volume PCR and subsequent analysis can also be optimized for several other questions in molecular research.

Zusammenfassung

In der modernen molekulargenetischen Diagnostik gibt es in den letzten Jahren einen Trend zur Untersuchung äußerst geringer DNA-Mengen bis hin zur Analyse von Einzelzellen. Daher sind Methoden zur präzisen Isolierung und dem Transfer von spezifischem Probenmaterial vor Beginn der Untersuchung erforderlich.

In dieser Arbeit wurde die Probengewinnung durch Laser-Mikrodissektion in Kombination mit einem Unterdruck-Einzelpartikel-Transfersystem erzielt. Die isolierten Proben wurden durch horizontalen Transfer auf einen flachen, chemisch behandelten Polymerase-Kettenreaktions (PCR)-Glasobjektträger überführt anstatt, wie bei der Mehrzahl der Mikrodissektionsmethoden, in Reaktionsgefäße. Auf diesem Objektträger wurde eine sogenannte „low-volume" (LV)-PCR in einem Gesamtreaktionsvolumen von 1 µl durchgeführt. Die Reduzierung des Reaktionsvolumens ermöglicht eine erhebliche Steigerung der PCR-Effizienz und -Empfindlichkeit gegenüber größeren Reaktions-volumina von bis zu 50 µl. Aus diesem Grund ist diese Methode auch auf Einzelzellen anwendbar.

Im ersten Teil dieser Arbeit wurden drei Darmpolypen zweier Krebsrisiko-Patienten gleichzeitig bezüglich des Mikrosatellitenstatus' sowie auftretender Mutationen in den Proto-Onkogenen *BRAF* und *KRAS* untersucht. Hauptaspekte bei der Darmkrebsentstehung sind Mikrosatelliteninstabilität (MSI), Methylierung von CpG Inseln von Genpromotoren und Mutationen in bestimmten Genen. Die Gene *BRAF* und *KRAS* sind Komponenten des MAPK ERK Signalwegs. Funktionsgewinn-Mutationen in einem der beiden Gene führt zur Signalwegsaktivierung und infolgedessen zu vermehrtem Zellwachstum.

Eine LV-multiplex-PCR wurde direkt ohne Zwischenschritte mit fixiertem Polypengewe-be (hyperplastischer Polyp, sessil serratiertes und tubuläres Adenom) durchgeführt. Es wurde gezeigt, dass Mutationen in häufig mutierten Bereichen von *BRAF* und *KRAS* gleichzeitig in derselben Probe eines Polypen eines Patienten vorkommen. Darüber hinaus wurden andere Mutationen in beiden Genen häufig gleichzeitig in denselben Proben nachgewiesen. Im Gegensatz dazu haben mehrere Studien nachgewiesen, dass sich sogenannte „Hotspot"-Mutationen von *BRAF* (V600E) und *KRAS* (Codons 12, 13, 59, 61 und 63) in Vorläuferläsionen von sporadischem Darmkrebs (mikrosatelliten-stabil oder -instabil) gegenseitig ausschließen. Verglichen mit der vorgeschlagenen

Einteilung nach Jass weisen die Ergebnisse dieser Arbeit eine gewisse Übereinstimmung mit dem „Serratierten Karzinogeneseweg" auf. Dieser beinhaltet Mutationen in den Genen *BRAF* und *KRAS* sowie Mikrosatelliteninstabilität oder -stabilität. Es konnte gezeigt werden, dass die Charakterisierung solcher Darmpolypen für ein besseres molekulares Verständnis der Darmkrebsentstehung wichtig ist.

Im zweiten Teil der Arbeit wurde ein genetisches Testsystem zum spezifischen Nachweis von Mutationen im *APC* Gen etabliert, das auch für die Polkörperdiagnose anwendbar ist. Familiäre adenomatöse Polyposis ist eine autosomal dominant vererbte Krankheit, die durch Mutationen im Tumorsuppressorgen *APC* verursacht wird. Ein Merkmal dieser schweren Krankheit ist die Entstehung hunderter bis tausender Darmpolypen beginnend im ersten Lebensjahrzehnt, die unbehandelt ein erhöhtes Krebsrisiko bergen. In der Präimplantationsdiagnostik stehen wenige oder sogar nur eine einzige Zelle für eine Untersuchung zur Verfügung, z. B. Blastomeren, Blastocysten oder Polkörper. Daher muss die Mutationsanalyse bezüglich Amplifikationseffizienz und Allel-Ausfallraten sorgfältig überprüft und optimiert werden, bevor sie in der Präimplantationsdiagnostik angewendet werden kann.

Zum Nachweis der *APC* Mutationen wurden eine LV-multiplex-PCR und anschließende Sequenz- sowie Fragmentlängenanalysen durchgeführt. Sowohl bei den polymorphen Mikrosatellitenmarkern als auch bei den spezifischen PCR-Produkten verschiedener *APC* Mutationen wurden eine hohe Amplifikationseffizienz und geringe Allel-Ausfallraten mit fixierten Einzelzellen erzielt. Dieser neuartige Ansatz ermöglicht die zuverlässige Etablierung eines genetischen Testsystems für diploide Lymphozytenzellen. Darüber hinaus erlaubt diese schnelle und zuverlässige Art der Mutationsanalyse eine Anpassung an viele verschiedene Fragestellungen, sowohl im Bereich der molekularbiologischen als auch der Einzelzell-Forschung.

2 Introduction

2.1 Molecular genetic diagnostics

Exiting advances in developing more sensitive and faster methods for analyzing increasingly less biological sample material have been made in recent years. A trend towards very small amounts of DNA down to the analysis of single cells can be observed (Hagen-Mann et al. 2005). Existing cytogenetic analysis methods like fluorescence *in situ* hybridization (FISH) or comparative genome hybridization (CGH) have been modified and optimized to be applicable for single cells. For example, the combination of such high-throughput and high-resolution methods with whole genome amplification (WGA) techniques display a great advantage in analyzing small amounts of starting material (Speicher and Carter 2005, Fiegler et al. 2007). In this context, chip and array technologies play an increasingly important role in molecular genetic diagnostics (Reyes et al. 2002, Auroux et al. 2002, Matsubara et al. 2005, Dittrich et al. 2006). A sensitive and reliable analysis of the smallest amounts of sample material constitutes the basis not only of forensic case work (Yeung et al. 2006) but also of preimplantation genetic diagnosis (PGD) and tumour tissue analysis. The major aspect of PGD is the analysis of few or single cells. A rising number of genetic and inherited disorders is now applicable to PGD (Findlay 2000, Kuliev et al. 2007, Spits and Sermon 2009). Analysis of small tissue samples and few or even single cells demonstrates a fundamental factor for heterogeneous tumour tissue examination (Hoque et al. 2003, Klein 2005).

In all these cases sample material must be isolated or gained in an appropriate manner prior to analysis.

2.2 Laser microdissection and SPATS

The retrieval and isolation of specific sample material and single cells and their precise positioning for further analysis therefore constitutes a basic aspect of modern molecular and genetic diagnostics. Up to now, different methods for the isolation of single cells or particles have been in routine laboratory use, e.g. extraction via fluorescence-activated

cell sorting (FACS) (Herzenberg et al. 2002, Nunes et al. 2003), hand or glass needle microdissection (Weimer et al. 2001, Croner et al. 2004, Bazan et al. 2005) and a broad variation of laser-based microdissection techniques such as laser capture (Schütze and Lahr 1998, Simone et al. 1998, Curran et al. 2000), laser pressure catapulting (Thalhammer et al. 2003, Bazan et al. 2005, Kirschner and Plaschke-Schluetter 2007) or isolation via gravity effects (Di Martino et al. 2004).

For isolation of fresh single cells floating in a medium, FACS is the method of choice used prior to analysis. However, the cells either need to be identified using fluorescence-labelled antibodies which bind to specific surface markers of the cell membrane or are sorted by size and shape (Bonner et al. 1972). This method is thus disadvantageous when analyzing solid tissue samples as, for example, tumour biopsies. Instead, microdissection techniques enable the precise manipulation and isolation of genetic material within a range of several micrometers, from fragments of histological tissue sections down to single cells or single chromosomes (Lechner et al. 2003, Thalhammer et al. 2004).

Two main types of laser-based microdissection methods can be distinguished: laser capture and laser cutting microdissection. In laser capture microdissection an infrared laser with diameters ranging from 7 to 30 μm is used. The laser melts parts of a thermoplastic membrane, mounted on a plastic cap which is located directly above the cells or sample material of interest. These cells then attach or adhere to the membrane and can be picked up from the tissue section once the membrane has cooled down. Using this method, only relatively large samples can be isolated whereas laser cutting methods allow precise isolation of small numbers or even single cells from tissue sections. This is achieved by using a UV laser with diameters less than 1 μm where the sample of interest is surrounded with the laser beam and cut out of the section (for review, see Murray 2007). Independent of which type of laser microdissection is used, the isolated samples are transferred into reaction tubes. In most cases cells are transferred in the cap of the tube containing a droplet of fluid, e. g. a lysis buffer, in which the sample was collected and further processed. Although the isolation process is performed under optical control, there may be certain difficulties in controlling the presence of the sample in the cap due to the relatively large size and the opaqueness of the cap with the droplet containing a small sample, e. g. a single cell (Schütze and Lahr 1998).

For this reason the isolation of sample material in this work was achieved using laser microdissection in combination with the recently developed low-pressure single particle adsorbing transfer system (SPATS). Samples were isolated using conventional laser cutting microdissection and were then adsorbed to a sample collection grid via low-pressure instead of transferring it into a tube cap via laser pressure catapulting or gravity effects. This approach allows the transfer of the isolated material to a planar chemically structured glass slide with micrometer precision (Woide et al. 2009). The deposition of a single particle specifically to a reaction centre on a planar chemically-structured polymerase chain reaction (PCR) device is facilitated by microscopic control of the entire process including sample transfer and release. After samples are isolated and transferred, further processing and analysis can be performed starting with PCR.

2.3 Polymerase chain reaction

Low-volume PCR

In general, PCR is performed in a total reaction volume of 10 to 50 µl using at least 1 up to 25 ng/µl of template DNA per reaction (Hunt 2008). This is an effective approach in normal routine laboratory analysis where sufficient amounts of genomic DNA are available. However, when only a limited amount of template DNA is available, e. g. from small biopsy samples or in PGD, there is a need for analyzing only a few or even single cells. As it was shown recently, reduction of the reaction volume has the potential to dramatically increase the efficiency and sensitivity of PCR and is therefore applicable to analyses at the single cell level (Schmidt et al. 2005, Proff et al. 2006, Lutz-Bonengel et al. 2007). In this context, miniaturization of PCR devices displays a great advantage and replaces PCR performed in a conventional reaction tube. Low-volume PCRs can be performed on so-called PCR chips which vary in size, architecture, material and PCR procedure. Differentiation can be made concerning single or multi-chamber chips, planar PCR devices with chemically modified surface structures or multi-channel chips. In stationary PCR devices, the PCR mixture does not move during PCR while it flows or is pumped through micro channels in the continuous-flow PCR devices. Altogether, a markedly reduced thermal mass of the entire PCR system effects rapid heating and cooling rates and therefore enables PCR reactions in less time with increased efficiency (for review, see Zhang and Xing 2007).

On the planar PCR glass slide used for this work, a 1-µl droplet of PCR mixture forms its own 'virtual' reaction chamber, held together by surface tension due to the hydrophilic/hydrophobic chemically structured surface (Schmidt et al. 2005, Woide et al. 2007).

Nested PCR

The principle of nested PCR is the amplification of a specific sequence using two different pairs of primers in two sequent PCR reactions. The first or outer primer pair amplifies a specific locus as in conventional PCR reactions. The second or inner (nested) primer pair binds within a position of the first amplification product and generates a secondary PCR product which is shorter than the first one. Nested PCR increases the specificity of the PCR reaction as the probability of amplifying an additional homologous sequence is reduced. A higher yield of specific PCR product serves as template in the secondary amplification and replaces unspecific DNA fragments (Hashimoto et al. 1995). Combination of a low-volume PCR with nested primers additionally raises the yield of specific PCR product compared to a single PCR reaction and allows several subsequent analyses using low amounts of DNA or single cells as template.

2.4   Colorectal cancer

In Germany, colorectal cancer (CRC) is the second most frequent tumour disease and cause of death amongst all cancer syndromes in men and women. Every year, CRC is diagnosed in about 37,000 men and 36,000 women for the first time. Despite this high incidence, a continuous decline of mortality rates in the last decades due to improved diagnosis and therapy can be observed. The mean age of disease diagnosis is 69 years for men and 75 years for women (source: Robert Koch-Institut). For these reasons, understanding and researching this severe disorder constitutes the basis for further improvement in diagnosis and therapy and should also result in better prevention.

Colorectal cancer is a very heterogeneous disorder and the term includes all cases of cancer in the colon, rectum and anus.

The majority of CRC cases are sporadic, 10% constitute inherited forms of CRC and about 20% are familial polygenic (St. John et al. 1993, Salovaara et al. 2000, Peto and

Houlston 2001, Olsson and Lindblom 2003, Aaltonen et al. 2007). Hereditary non-polyposis colorectal cancer (HNPCC) syndromes constitute a major part of inherited cancer with about 5-10% and about 2% of all CRC account for familial adenomatous polyposis (FAP) (Lynch 1999, Turnbull and Hodgson 2005). Inherited cancer is mainly differentiated by the number of polyps or adenomas found in the colon. Other inherited cancer syndromes like Peutz-Jeghers syndrome, familial juvenile polyposis or Cowden syndrome are very rare (Turnbull and Hodgson 2005, Friedl and Propping 2007).

In HNPCC (OMIM 120435, 120436) polyps occur in the colon with a proximal colonic predominance. Usually, a significantly less number of polyps is observed compared to FAP, hence the name non-polyposis syndrome. Despite a relatively small number of polyps, the risk of malignant transformation is very high for an individual polyp. Carcinogenesis is accelerated in HNPCC with development of adenomas to carcinomas occurring in 2-3 years compared to 8-10 years. In the majority of cases autosomal dominant inheritance is observed in HNPCC but in cases with *de novo* germ line mutations in one person family anamnesis cannot be taken into account for diagnosis (Lynch 1999). The genetic basis for HNPCC are germ line mutations in one of the DNA mismatch repair (MMR) genes *MLH1*, *MSH2*, *MSH6* and *PMS2*. Mutations in *MLH1* (chr. 3p21.3) and *MSH2* (chr. 2p16) account for the majority of cases (Wang et al. 2003, v. d. Klift et al. 2005). HNPCC is defined as familial CRC including cases with mismatch repair gene mutation and microsatellite instability as well as cases with microsatellite stable tumours designated as 'familial colorectal cancer type X' (Lindor et al. 2005). The DNA mismatch repair system is responsible for exact replication of DNA in the cell. Patients with a germ line mutation on one allele of an MMR gene have an increased risk of developing cancer, and tumourigenesis is induced when an additional alteration occurs at the second allele. Loss-of-function of the system, e. g. due to mutations in both alleles of a repair gene leads to accumulation of errors and mutations in the genome. Specific repeating motifs, the so-called microsatellite regions are prone to such replication errors. Defect in the MMR system results in shortened or elongated microsatellite sequences and this effect, called microsatellite instability (MSI; Fig. 1) is a hallmark of tumours in HNPCC patients (Gebert and v. Knebel Doeberitz 1999, Lynch 1999). For detecting MSI in colorectal cancer specific criteria were defined and a set of specific microsatellite markers including BAT25, BAT26 and BAT40 which are used

here, was determined in a National Cancer Institute workshop on microsatellite instability in 1998 (Boland et al. 1998).
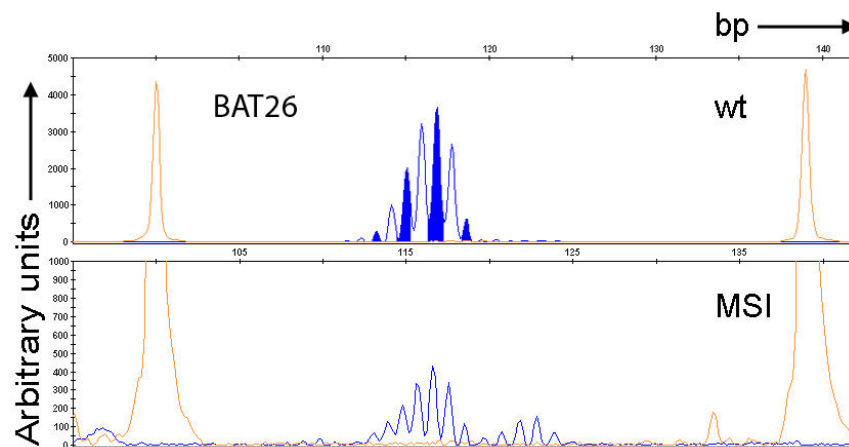
Fig. 1: Microsatellite instability (MSI) is indicated by changes in the resulting regular peak pattern of the wild type (wt) BAT26 marker.

In addition to microsatellite marker analysis on the genomic level for detecting MMR deficiency, the immunohistochemical staining of proteins in cells of tumour tissue enables analysis of mismatch repair gene expression. Presence or absence of the analogous protein can be detected using labelled antibodies binding to the protein in the cells. However, the sensitivity of immunohistochemical staining analysis is reduced compared to MSI analysis due to false positive signals when a non-functional protein is present in the cell (Holinski-Feder and Morak 2010).

Familial adenomatous polyposis of the colon (OMIM 175100) is an autosomal dominant disorder or, in rare cases, recessively inherited by mutations in *MUTYH* (Groden et al. 1991, Sampson et al. 2005). FAP is characterized by hundreds to thousands of adenomas occurring in the colon starting in the second decade of life and is therefore classified as a polyposis syndrome. In the majority of cases, mutations of the adenomatous polyposis coli (*APC*) gene (chr. 5q22.2) are responsible for developing FAP (Nakamura 1995). The protein product of the *APC* gene is an important component of the wnt signaling pathway which is responsible, among other factors, for cell proliferation (Clevers 2004). The main function of *APC* is the regulation of the intracellular ß-catenin level. In non-proliferating cells APC in combination with other proteins in their active conformation phosphorylate ß-catenin; the resulting degradation leads to a low ß-catenin level in the cell. Disruption of this pathway due to mutations in the *APC* gene inhibits phosphorylation of ß-catenin and results in a high intracellular ß-

catenin concentration. Free ß-catenin is translocated into the nucleus and activates transcription factors responsible for cell proliferation. In normal colon mucosa the activation of the wnt signaling pathway leads to increased proliferation of cryptic stem cells. Cells evolved from these stem cells at the bottom of a crypt replace older and apoptotic cells at the top of the crypt. Thus, the colon mucosa is permanently renewed. Most of the mutations in the *APC* gene are nonsense point mutations or frame-shifts due to insertions or deletions which result in truncated non-functional proteins (Nakamura 1995, Ballhausen 2000). In rare cases FAP can be recessively inherited by mutations in *MUTYH* involved in base excision repair of 8-oxo-Guanine.

For several decades the adenoma – carcinoma sequence was thought to be the only carcinogenesis pathway through which cancer could evolve. This so-called Vogelstein pathway described the accumulation of multiple mutations in several genes, mostly beginning with an initial *APC* mutation. Over the years, point mutations in the *KRAS* and *TP53* genes were shown to contribute to carcinogenesis and development of colorectal cancer. A chromosomal instability with an aberrant number of chromosomes as well as chromosomal translocations could then also be detected (Vogelstein et al. 1988, Fearon and Vogelstein 1990, Mitelman et al. 2007). This pathway was supposed to provide the explanation for CRC evolution not only in FAP, which is initiated by *APC* mutations, but also in sporadic cases (Fearon and Vogelstein 1990).

Despite two mutually exclusive types of genetic instability (microsatellite and chromosomal instability), the existence of only one main pathway with certain variations for sporadic and inherited CRC development based on the adenoma – carcinoma sequence was supposed (Kinzler and Vogelstein 1996). The occurrence of Lynch syndrome patients with MSI-high (MSI-H) and mutations in *APC*, *KRAS* and *TP53* seems to confirm this fact. However, MSI-H consistent with mutations in MMR genes (characteristics of Lynch syndrome) could rarely be observed in sporadic adenomas. Additionally, mutations in *APC*, *KRAS* or the ß-catenin (Clevers 2004) gene which are associated with initialization and early progress in the Vogelstein pathway could rarely or not at all be found in sporadic MSI-H CRC. In contrast, mutations in the *BRAF* gene and methylation of the *MLH1* promoter are typical genetic alterations in sporadic CRC but not in Lynch syndrome. For these reasons there was a need for defining another pathway which could explain the discrepancies between sporadic and inherited cancer (for review, see Jass 2007).

Microsatellite instability is caused mainly by a non-functional or inactive *MLH1* gene, e. g. due to germ line mutations occurring in Lynch syndrome and somatic loss of heterozygosity. In sporadic CRC an *MLH1* mutation is absent and another explanation for MSI is necessary: the CpG island methylator phenotype (CIMP; Toyota et al. 1999, Issa 2004). Methylation of cytosine appearing in GC-rich sequences (CpG islands) in the genome is an essential epigenetic mechanism necessary for gene expression regulation (Jones and Baylin 2002). Abnormal methylation of especially *MLH1* as well as *MGMT* (*O^6-methylguanine-DNA methyltransferase*) gene promoter in sporadic CRC leads to inactivation of these genes and thus to microsatellite instability. CIMP causing gene silencing due to increased promoter methylation is an important feature in carcinogenesis (Issa 2004). Methylation is not only limited to *MLH1* and *MGMT* but can also occur in apoptosis-associated genes (for review, see Mäkinen 2007). Methylation of different genes results in different grades of microsatellite instability. The aberrant methylation pattern is often caused by mutations in either one of the proto-oncogenes *BRAF* (v-raf murine sarcoma viral oncogene homolog B1) or *KRAS* (v-Ki-ras2 Kirsten rat sarcoma viral oncogene homolog). The combination of CIMP, microsatellite instability and mutations in *BRAF* or *KRAS* are defining criteria for the serrated neoplasia pathway.

On the basis of MSI and CIMP, multiple carcinogenesis pathways were classified in five subgroups, supported by the integration of histological, morphological and clinical characteristics of CRC (Jass 2007).

1: CIMP-H, methylation of *MLH1* resulting in MSI-H, associated with *BRAF* mutation
2: CIMP-H, partial methylation of *MLH1* resulting in MSI-L or MSS, associated with *BRAF* mutation
3: CIMP-L, methylation of *MGMT* resulting in MSI-L or MSS, associated with *KRAS* mutation; chromosomal instability
4: CIMP-negative, no methylation and therefore MSS; chromosomal instability
5: CIMP-negative, inherited MMR deficiency resulting in MSI-H

Microsatellite instability and CIMP are distinguished into high- (H) and low- (L) levels as well as microsatellite stability (MSS) or CIMP-negative (Boland et al. 1998, Ogino et al. 2006). Serrated polyps are the precursor lesions of groups 1 and 2 consistent with the serrated pathway. Precursor lesions of the fourth (Vogelstein pathway) and the last

subtype (Lynch syndrome or HNPCC) are basically adenomas which evolve through the adenoma-carcinoma sequence. Colorectal cancer of subgroup 3 is assumed to develop from either type of polyp (for review, see Jass 2007).

Generally, colon polyps are histologically classified as adenoma, serrated adenoma, sessile serrated adenoma (SSA), hyperplastic polyp (HP) and various subtypes or mixed forms of them (for reviews, see Young and Jass 2006, Mäkinen 2007). Classification is based on tissue and crypt structure, cell morphology and abnormal proliferating features of the crypt cells. One important characteristic of colon polyps, the serrated morphology can be differentiated into top-down or bottom-up morphology, which depends on the type of affected cells (Holinski-Feder and Morak 2010). Top-down neoplasia develops when apoptosis of cells at the crypt top is decreased or delayed which results in a sawtooth-like infolding of the crypt tissue. Abnormal increased proliferation of the crypt stem cells leads to an elongated mitosis area at the bottom of the crypt which results in a similar crypt structure. Both the top-down and the bottom-up neoplasia cause serration of colon polyps. Therefore, classification of polyps exclusively according to their similar or mixed morphology has proven to be difficult.

As shown above, microsatellite instability as well as mutations in the *BRAF* and *KRAS* genes play a major role in colorectal cancer development and classification.

The two proto-oncogenes *BRAF* and *KRAS* both are components of the same intracellular signalling MAPK-ERK pathway. Extracellular signals are transduced via Kras and Braf to several other proteins which finally activate transcription factors in the nucleus. Regulation of cell proliferation, differentiation and apoptosis is performed via this pathway. *KRAS* (v-Ki-ras2 Kirsten rat sarcoma viral oncogene homolog OMIM190070, chr. 12p12.1) a member of the ras superfamily is a small GDP/GTP binding protein attached to the inner cell membrane. Extracellular binding of a ligand triggers, through a series of adaptor proteins and exchange factors, the activation of Kras. Active Kras binds and actives the serine-threonine protein kinase Braf (V-raf murine sarcoma viral oncogene homolog B1; OMIM164757; chr. 7q34) which in turn activates several downstream protein kinases. Hyperactivation of this pathway leads to increased cell proliferation and displays an early event in carcinogenesis (Weinberg 1982, Garnett and Marais 2004, Kranenburg 2005). Mutations in these two genes are responsible for hyperactivation of the pathway. The mutation c.1799 T>A, p.V600E in exon 15 of the *BRAF* gene, an amino acid substitution from valine to glutamic acid, is a

well-characterized activating mutation (Davies et al. 2002, Kumar et al. 2003). Mutations in codons 12, 13, 59, 61 and 63 of the *KRAS* gene can lead to activation of the protein as well (Grimmond et al. 1992). Amino acid substitutions normally modify the protein structure. Depending on which amino acid is exchanged, the protein may not be able to change between its active and inactive conformation any longer or its ligand binding site becomes inaccessible. In the cases mentioned for Braf and Kras, the proteins stay locked in their active conformation which therefore leads to a hyperactivated pathway (Kranenburg 2005).

Due to this significant role in carcinogenesis, the analysis of mutations in the *BRAF* and *KRAS* genes as well as microsatellite instability constitutes a major goal in cancer research. Combination of laser microdissection with the newly developed horizontal low-pressure transfer system SPATS and low-volume multiplex PCR enables the simultaneous and sensitive analysis of smallest polyp tissue particles. In this way heterogeneous colon polyp tissue can be characterized or even mapped due to mutations in *BRAF* and *KRAS* and the microsatellite status down to small and almost homogeneous parts of a single crypt. This approach enables the exact analysis of the molecular nature and the development of a colon polyp which perhaps could promote advances in classification of CRC and the carcinogenesis pathways.

2.5 Single cell analysis and preimplantation genetic diagnosis

The ability to analyze individual single cells plays an increasingly important role in molecular genetic diagnostics. Recently, mutation analysis of inherited monogenic disorders was successfully established (Sermon 2002, Hehr et al. 2009, Spits and Sermon 2009, Vanneste et al. 2009). In preimplantation genetic diagnosis, mutation analysis must be performed on only a few or even single cells.

For couples who wish to have children but are at high risk of passing a genetic disease on to their offspring, PGD offers the possibility to detect such diseases prior to implantation of the embryo. Generally, three types of cells are used for PGD: blastomeres, blastocyst cells and polar bodies. Blastomeres and blastocyst cells are biopsied from the developing embryo at day 3 or 5 postfertilization when it reaches the eight-cell or blastocyst stage, respectively (Sermon et al. 2004, Spits and Sermon

2009). In these cases, two or up to 10 diploid cells are available for analyzing the genetic status of the embryo (McArthur et al. 2005). In contrast, polar bodies develop during meiosis of the oocyte and allow the analysis of only the maternal genome. In polar body diagnosis, only one haploid single cell is available for analysis (Findlay 2000, Sermon et al. 2004).

The low quantity of DNA on single cells leads to a number of complications in mutation analysis which are rarely found in routine diagnostics. Mutation analysis must therefore be carefully validated and optimized as regards amplification efficiency and the evaluation of allelic drop out (ADO) rates before application to PGD, especially polar body diagnosis. The main reason why polar body diagnosis is chosen as an example is the legal situation in Germany where manipulation of embryos is forbidden by law and polar bodies are the only option for PGD (Tomi et al. 2005, Hehr et al. 2007). In all cases time is a limiting factor in PGD and analysis has to be performed in less than 24 h (Tomi et al. 2005, Spits and Sermon 2009).

The goal of the second part of this work is the establishment of a genetic test system for the specific detection of mutations in the *APC* gene (OMIM 611731) (Mayer et al. 2009). A fast and reliable technique for mutation analysis of single cells combining laser microdissection, SPATS and low-volume PCR is presented in this work.

3 Abbreviations

ADO	allelic drop out
APC	adenomatous polyposis coli
bp	base pairs
BRAF	v-raf murine sarcoma viral oncogene homolog B1
cDNA	complementary DNA
CGH	comparative genomic hybridization
CIMP	CpG island methylator phenotype
CRC	colorectal cancer
DNA	deoxyribonucleic acid
F	forward
FACS	fluorescence-activated cell sorting
FAP	familial adenomatous polyposis
FISH	fluorescence *in situ* hybridization
H	high
HE	hematoxylin and eosin
HNPCC	hereditary non-polyposis colorectal cancer
HP	hyperplastic polyp
KRAS	v-Ki-ras2 Kirsten rat sarcoma viral oncogene homolog
L	low
LV	low-volume
MAPK-ERK	mitogen-activated protein kinase extracellular signal-regulated kinase (signalling pathway)
MDA	multiple displacement amplification
MGMT	O^6-methylguanine-DNA methyltransferase
MLH1	mutL homolog 1
MMR	mismatch repair
mRNA	messenger ribonucleic acid
MSH	mutS homolog
MSI	microsatellite instability
MSS	microsatellite stability
mut	Mutation; mutated
MUTYH	mutY homolog

OGG1	8-oxoguanine DNA glycosylase
PCR	polymerase chain reaction
PEN	polyethylene-naphthalate
PGD	preimplantation genetic diagnosis
R	reverse
rpm	rounds per minute
SPATS	single particle adsorbing transfer system
SSA	sessile serrated adenoma
TD	touch down
TP53	tumour protein p53
UV	ultraviolet
WGA	whole genome amplification
wt	wild type

4 Material and Methods

4.1 Patients

4.1.1 Colon polyps

In total, three colon polyps of two patients were analyzed. Polyp 2320-08-IV of patient A was localized in the sigmoid colon. Extended mucosa with elongated crypts and a well matured crypt epithelium was observed. There was no evidence of a neoplastic polyp. It was classified as hyperplastic polyp with no malignant potential. Histological differentiation of the second polyp (4407-09) of patient A and classification as hyperplastic polyp or sessile serrated adenoma (SSA) was not possible. For the father of patient A, a hereditary non-polyposis colon carcinoma (HNPCC or Lynch syndrome) and additional hyperplastic colon polyps and serrated adenomas were diagnosed. He carries a non-functional allele in the *MLH1* gene with an unknown pathomechanism which was assigned to *MLH1* exon 8, c.655A by cDNA analysis. Patient A has inherited the functional copy of her father's *MLH1* gene.

The analyzed polyp (13342-f1) of patient B was localized in the rectum. One part was classified histologically as sessile serrated adenoma, the other part as tubular adenoma. No evidence of a high-grade intraepithelial neoplasia in the tubular adenoma was observed.

For both patients, genomic wild type DNA was analyzed as a reference. DNA was obtained from a blood sample of patient A and from paraffin-embedded normal mucosa tissue of patient B. This reference DNA was provided by the Medical Genetics Center, Munich. All histological characterizations were performed by the Laboratory for Pathology and Cytology of Dr. Funk, Dr. Dettmar and Prof. Dr. Sarbia, Munich, the Klinikum Garmisch-Partenkirchen or the Klinikum München Neuperlach.

Patient consent for molecular analysis of their tissue samples was obtained.

4.1.2 Familial adenomatous polyposis coli

Three patients with familial adenomatous polyposis coli (FAP) heterozygous for mutations in exon 15 of the adenomatous polyposis coli (*APC*) gene (patient C: c.2612delG; patient D and E: c.3183-3187delACAAA) and cells of an unaffected male were used for the establishment of single cell polymerase chain reaction (PCR). The

deletions of all three patients are germ line mutations and are therefore detectable in lymphocyte cells isolated from blood samples.

All three patients wished to have an unaffected child and underwent polar body analysis prior to pregnancy. Therefore, a genetic test system for single cell analysis applicable for polar body diagnosis was established.

4.2 Preparations for laser microdissection

4.2.1 Tissue preparation

After surgical resection from the patients, the colon polyps were immediately formalin-fixed and embedded in paraffin according to standard protocols (Lehmann and Kreipe 2001, Bova et al. 2005). For laser microdissection, 6 µm thick tissue sections of the paraffined tissue blocks were prepared and applied to a 2 µm polyethylene-naphthalate (PEN) membrane mounted on a glass slide (Carl Zeiss MicroImaging GmbH, Munich, Germany). Tissue sections for laser microdissection were unstained but for histological classification some sections of each polyp, mounted on a normal glass slide, were hematoxylin and eosin (HE) stained (Bova et al. 2005). For microsatellite analysis, immunohistological staining relative to *MLH1* gene expression was applied to some tissue sections of each polyp (Bova et al. 2005). Stained and unstained tissue sections were provided by the Laboratory for Pathology and Cytology of Dr. Funk, Dr. Dettmar and Prof. Dr. Sarbia. Histological classification of the colon polyps as well as the analysis of MLH1 staining was provided by the Klinikum Garmisch-Partenkirchen GmbH and the Laboratory for Pathology and Cytology.

For removing the paraffin, PEN-slides with paraffin-embedded tissue sections were incubated for 30 minutes in xylene. Tissue slides were dehydrated in a decreasing ethanol series with incubation for 5 minutes in 100% ethanol, 2 minutes in 90% ethanol and 2 minutes in 70% ethanol. The slides were carefully removed from the solutions to prevent separation of the tissue sections from the PEN slides. Tissue section slides were completely dried at least 30 minutes at room temperature and about 30 minutes at 37°C. They were stored in appropriate slide boxes a t room temperature.

4.2.2   Single cell preparation

Human lymphocytes were isolated from peripheral blood samples (patients C, D, E; Medical Genetic Center). Fixed lymphocytes were prepared according to the following protocol: About 5 to 10 droplets of anti-coagulated blood were incubated in 9 ml of chromosome medium B (Biochrom AG, Berlin, Germany) at 37°C for 71.5 hours. Thereafter 100 µl of colchicine (Biochrom AG, Berlin, Germany) were added and properly mixed with the cell suspension and incubated at 37°C for 30 minutes. The samples were centrifuged for 10 minutes with 1000 rpm (190 rcf; Rotina 35R, Hettich Zentrifugen, Tuttlingen, Germany) at room temperature and supernatant was discarded. The pellets were resuspended in 1 ml 75 mM KCl first and then filled up to 9 ml. The cell suspensions were then incubated at 37°C for 20 minu tes. For fixation of the cells, 1 ml of fixing solution (3:1 v/v methanol/glacial acetic acid) was added and mixed and the samples were incubated for 5 minutes at 4°C. The ce ll suspensions were centrifuged for 10 minutes at 1000 rpm at room temperature and supernatant was discarded. The pellets were resuspended in fixing solution and incubated for 20 to 30 minutes at -20°C. Subsequently, the samples were washed in fixing solution until the cell suspensions were clear without contamination of red blood cells. Fixed cell suspensions were stored at -20°C.

For laser microdissection fixed single lymphocytes were applied to a PEN membrane glass slide (Carl Zeiss MicroImaging GmbH, Munich, Germany). Fixed cell suspensions were washed once with fixing solution and supernatant was removed except for 1 ml in which the pellet was resuspended. Some droplets of this concentrated cell suspension were pipetted to the PEN slides and dried at room temperature.

For cell nucleus staining, slides were incubated for 5 minutes in 5% (v/v) Giemsa solution (Merck KGaA, Darmstadt, Germany) diluted in phosphate buffered saline buffer (PBS Dulbecco, Biochrom AG, Berlin, Germany). After incubation the slides were washed with distilled water and completely dried at 37°C for about 30 minutes. For isolation of single cells slides were always unstained.

4.3   Laser microdissection

Laser microdissection was performed using an inverted optical microscope (Axio Observer.Z1, Zeiss, Oberkochen, Germany) combined with a laser unit providing a

pulsed nitrogen laser beam (wave length 337 nm) (Thalhammer et al. 2004).

Depending on the sample material, laser energy and focus level were adjusted to create a laser spot size of a few micrometers for accurate particle isolation. This was supported by the use of a long distance objective (40x magnification) for adjusting the numerical aperture and therefore further optimize the microdissection procedure. The movement of the microscopic stage was controlled via joystick and the 'Nanosauger' software (XYZ High Precision, Darmstadt, Germany).

For documentation a CCD camera (Rolera-XR Fast1394, Q Imaging, Surrey, Canada) mounted on the microscope and the Q Capture Pro 6.0 software (Q Imaging, Surrey, Canada) was used.

4.4 Single particle transfer via SPATS

Laser microdissected tissue samples or single cells were transferred horizontally via the low-pressure transfer system SPATS (single particle adsorbing transfer system) to the reaction centres of a planar PCR slide with a chemically-modified hydrophilic/hydrophobic surface structure (AmpliGrid, Advalytix-Beckman Coulter GmbH, Munich, Germany).

The SPATS unit consists of a pressure supply unit PLI-100 (Havard Apparatus, Holliston, USA), a micrometer step motor arrangement, a sample-adsorbing head and the control software 'Nanosauger' version 2.5 (XYZ High Precision, Darmstadt, Germany) and is integrated into the inverted optical microscope (Fig. 2) (For detailed technical description and transfer procedure, see Woide et al. 2009).
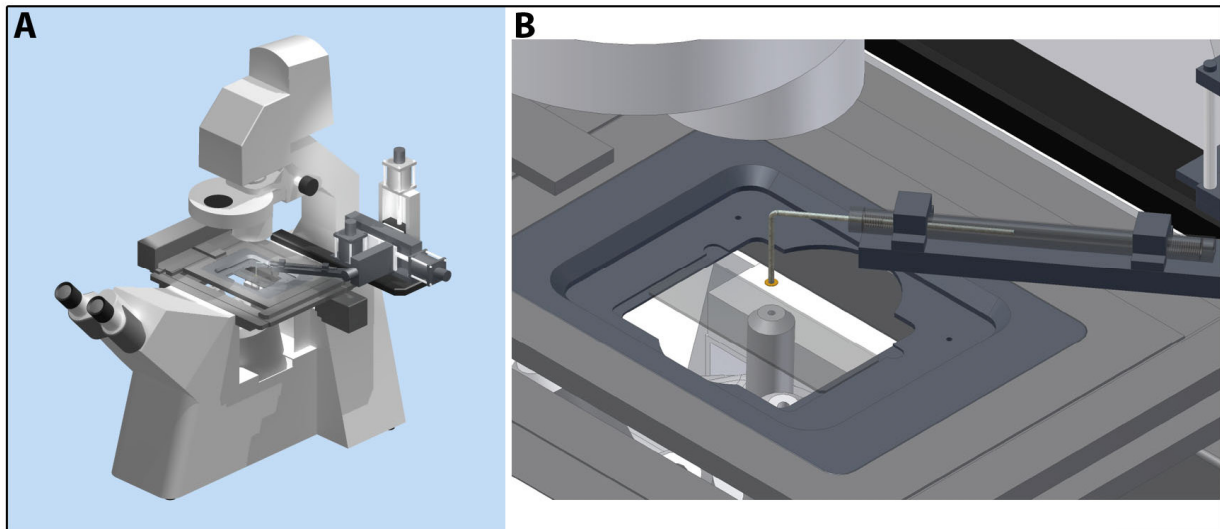
Fig. 2: A) Schematic drawing of the SPATS system integrated to the inverted optical microscope (Axio Observer.Z1, Zeiss, Oberkochen, Germany). B) Detail of the adaptor arm including the sample-adsorbing head.

The sample-adsorbing head was designed to be disposable and consists of a transparent glass tube, a perforated copper disk and a copper grid (Fig. 3). The rectangular bending of the 100 mm long glass tube (Hirschmann Laborgeräte GmbH & Co.KG, Eberstadt, Germany) was done via a Bunsen burner to a ration of 25 to 75 mm. The outer diameter of the glass tube is 1.75 mm and the inner diameter is 1 mm. A perforated copper disk (Plano GmbH, Wetzlar, Germany) with 3.05 mm outer and 1 mm inner diameter was glued to the glass tube with a UV curing adhesive (Norland products, Cranbury, USA) and hardened under UV-light. Afterwards, the copper grid (Plano GmbH, Wetzlar, Germany) with an outer diameter of 3.05 mm and a mesh size of 5 μm was glued to the perforated disc as well and hardened under UV-light. This sample-adsorbing head was sterilized under UV-C irradiation and cleaned with ethanol for repeated use.
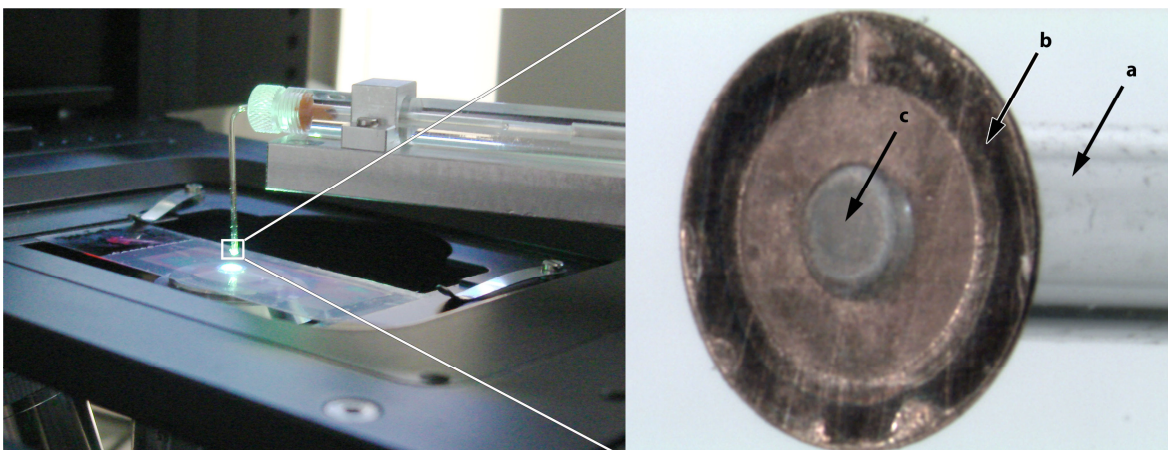
Fig. 3: Picture of the sample-adsorbing head connected to the pressure supply unit via the rotatable adaptor arm. The detail shows the sample-adsorbing head with the glass tube (a), the perforated copper disk (b) and the copper grid (c).

The transfer procedure is summarized as follows. The micrometer stepmotor allows movement of the sample-adsorbing head in xyz-direction necessary for the exact positioning and is controlled via the 'Nanosauger' software. After laser microdissection the sample and the sample-adsorbing head were first centred in the field of view. Then, the sample-adsorbing head was lowered to the glass slide and stopped a few micrometers above the isolated sample (Fig. 4 A). Low-pressure was started and the sample was adsorbed to the grid of the head (Fig. 4 B). In order to prevent loss of the sample, low-pressure was held during the transfer until the sample was released. The sample-adsorbing head was then removed from the slide surface and the sample was transferred to a reaction centre of the chemically-structured PCR slide. Low-pressure was stopped and the sample was released from the grid into a 300 nl sterile water droplet (Fig. 4 C) using a short high-pressure impulse. After the water droplet was dried at room temperature, the sample was located on the hydrophilic reaction centre of the PCR slide (Fig. 4 D). All preparative steps were performed under optical control.
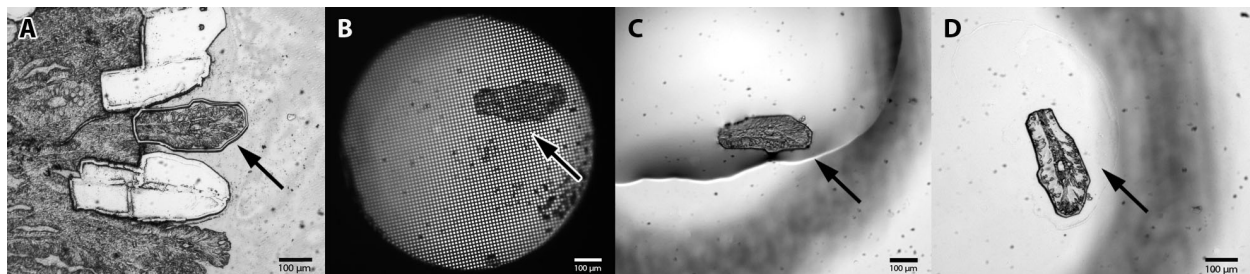
Fig. 4: Transfer procedure of a single particle via the single particle adsorbing transfer system SPATS A) Light microscopic image of a laser microdissected tissue sample (arrows) from a colon polyp. B) The isolated tissue sample is attached to the grid of the sample-adsorbing head. C) The tissue sample was released into a 300 nl droplet of sterile water on the reaction centre of a hydrophilic/hydrophobic structured PCR slide (AmpliGrid, Advalytix-Beckman Coulter GmbH, Munich, Germany). D) Isolated tissue sample at the surface of the PCR slide after the water was evaporated.

4.5   Control DNA

Genomic DNA was isolated from a whole peripheral blood sample of an unaffected male using the All-tissue DNA-Kit (Gen-ial GmbH, Troisdorf, Germany) according to manufacturer's instructions. DNA concentration was determined using the Nanodrop® ND-1000 Spectrophotometer (Peqlab Biotechnologie GmbH, Erlangen, Germany). The

genomic DNA solution was diluted into aliquots of 1 ng/µl, 250 pg/µl, 100 pg/µl, 50 pg/µl and 10 pg/µl. As a positive control, 1 µl of diluted DNA solution was pipetted to a reaction centre of the PCR slide and dried at room temperature.

4.6 Analysis methods

4.6.1 Polymerase chain reactions

4.6.1.1 Low-volume multiplex PCR

Low-volume (LV) PCR reactions were carried out in 1 µl total reaction volume covered with 5 µl mineral oil to prevent evaporation and external contamination (Fig. 5). The reaction mixture was placed in the reaction centres of the hydrophilic/hydrophobic structured PCR slide (AmpliGrid, Advalytix-Beckman Coulter GmbH, Munich, Germany; Fig. 5). After the amplification reaction PCR products from the slides were transferred into 0.2 ml reaction tubes and diluted 1:10 with sterile water.
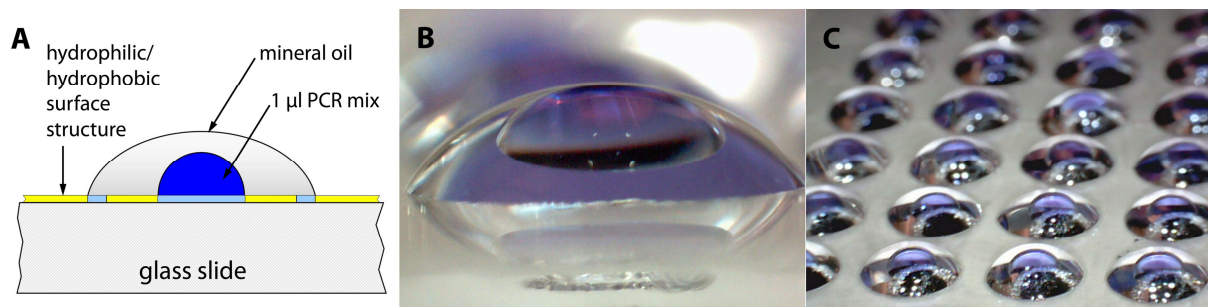
Fig. 5: Image of the planar PCR slide AmpliGrid A) Schematic drawing of the planar PCR slide with the hydrophilic (blue) and hydrophobic (yellow) structured surface. The hydrophilic reaction centre, 1.6 mm in diameter, is covered with 1 µl PCR mixture. A hydrophobic ring around the reaction centre holds the mixture in place. The 5 µl mineral oil, which cover the PCR mix and prevent evaporation, are hold in place by a hydrophilic ring. B) Picture of one single droplet with a blue aqueous solution symbolizing the PCR mixture. C) Detail picture of the planar PCR slide with 48 reaction centres on the size of a normal object slide 76 mm x 25 mm x 1 mm.

Primary PCR was performed using an AmpliSpeed slide cycler (Advalytix-Beckman Coulter GmbH, Munich, Germany) or an Eppendorf Mastercycler with *in situ* adapter (Eppendorf AG, Hamburg, Germany). All low-volume PCR reactions were carried out as multiplex PCR reactions using the QIAGEN® Multiplex PCR Kit (Qiagen GmbH, Hilden, Germany) accordingly to the basic protocol (Tab. 1). Primer concentrations were optimized for each patient-specific PCR reaction and according to the number of primers combined in one multiplex reaction.

Tab. 1: Basic protocol for low-volume multiplex PCR reactions

Reagents	1x	Final concentration
2x Multiplex PCR Master Mix	0.50 µl	1x
5x Q-Solution	0.06 µl	0.3 x
Sterile water	variable	-
Primers	variable	0.15 to 3.0 µM
Advablue or Advagold (partially)	0.05 µl	-
Final volume	**1.00 µl**	

Staining of the PCR mixture with Advablue or Advagold (Advalytix-Beckman Coulter GmbH, Munich, Germany) served as control in the low-volume reaction to exclude mixing of the master mix with the mineral oil during PCR. The staining was used only for the initial testing PCR reactions and not in sample analysis. Primer sequences and locations for the low-volume PCR reactions are listed in table 2 (colon polyps) and 3 (patient-specific single cells).

Tab. 2: Details on primer sequences for colon polyp analysis: Low-volume 6x multiplex PCR reactions were carried out with non-labelled primer pairs for the genes *BRAF* exon 15 and *KRAS* exons 2 and 3 and for microsatellite markers BAT25, BAT26, BAT40.

Primer	Sequence (5'-3')	Location
BAT25-F	TCG CCT CCA AGA ATG TAA GT	4q12
BAT25-R	TCT GCA TTT TAA CTA TGG CTC	
BAT26-F	TGA CTA CTT TTG ACT TCA GCC	2p21
BAT26-R	AAC CAT TCA ACA TTT TTA ACC C	
BAT40-F	ATT AAC TTC CTA CAC CAC AAC	1p12
BAT40-R	GTA GAG CAA GAC CAC CTT G	
Braf15-F-out	TGC TTG CTC TGA TAG GAA AAT G	7q34
Braf15-R-out	TAA CTC AGC AGC ATC TCA GG	
Kras2-F-out	CGT CTG CAG TCA ACT GGA AT	12p12.1
Kras2-R-out	AGA ATG GTC CTG CAC CAG TAA	
Kras3-F-out	TTT TGA AGT AAA AGG TGC ACT G	12p12.1
Kras3-R-out	TGC ATG GCA TTA GCA AAG AC	

Tab. 3: Details on primer sequences for patient-specific single cell analysis: Low-volume 3x multiplex PCR reactions were carried out with primer pairs PC1-F/R for the 1 bp deletion of patient C and PD1-F/R for the 5 bp deletion of patients D and E.

Primer	Sequence (5'-3')	Mutation/location
PC1-F	GAA TAC TAC AGT GTT ACC CAG CTC	c.2612delG
PC1-R	TCA GTG GTA GAC CCA GAA CTT	
PD1-F	CAG TTG AAC TCT GGA AGG CAA	c.3183-3187delACAAA
PD1-R	GGA GAA ACA CAT TCC TGC TGT C	
D5S346-F-FAM	ACT CAC TCT AGT GAT AAA TCG GG	5q22-q23
D5S346-R	AGC AGA TAA GAC AGT ATT ACT AGT T	
D5S82-F-FAM	ATC AGA GTA TCA GAA TTT CT	5q21.3
D5S82-R	CCC AAT TGT ATA GAT TTA GAA GTC	

An overview of the LV-PCR conditions for colon polyp and patient-specific single cell analysis is given in table 4. The conditions were optimized for each multiplex primer combination. The cycle numbers in primary and secondary PCR depend on the total numbers of cycles in both reactions and were adjusted to the yield of secondary PCR product which was checked in gel electrophoresis.

Tab. 4: Overview of PCR conditions for low-volume PCR reactions

Analysis	PCR step	PCR conditions		
Colon polyp analysis	Initial denaturation	97℃	20 min	
	Denaturation	94℃	30 s	|
	Annealing	64℃*	30 s	| 15x
	Extension	72℃	30 s	|
	Denaturation	94℃	30 s	|
	Annealing	50℃	30 s	| 23x
	Extension	72℃	30 s	|
	Final Extension	72℃	7 min	
Single cell analysis	Initial denaturation	97℃	20 min	
	Denaturation	94℃	30 s	|
	Annealing	64℃*	90 s	| 15x
	Extension	72℃	30 s	|
	Denaturation	94℃	30 s	|
	Annealing	50℃	30 s	| 10x or 15x
	Extension	72℃	30 s	|
	Final Extension	72℃	7 min	

*temperature increment of -1℃ per each cycle

For the multiplex PCR with the three microsatellite markers D7S1824, D9S302 and D10S2325 exclusively a LV-PCR was carried out in contrast to the previously mentioned reactions. Primer sequences and locations of the microsatellite markers are shown in table 5. Modified conditions for this multiplex PCR are listed in table 6.

Tab. 5: Details on primer sequences for single cell analysis: Low-volume 3x multiplex PCR reactions were carried out with primer pairs for the microsatellite markers D7S1824, D9S302 and D10S2325.

Primer	Sequence (5'-3')	Location
D7S1824-F-HEX	GCA CCT GTT TGA TTC AGT CA	7q34
D7S1824-R	CCA GCC TGT GTG ACT ATG TG	
D9S302-F-FAM	GGG GAC AGA CTC CAG ATA CC	9q32
D9S302-R	GCG ACA GAG TGA AAC CTT GT	
D10S2325-F-FAM	CTC ACG AAA GAA GCC TTC TG	10p13
D10S2325-R	GAG CTG AGA GAT CAC GCA CT	

Table 6: PCR conditions for low-volume PCR reactions with microsatellite markers

Analysis	PCR step	PCR conditions		
Single cell analysis	Initial denaturation	97℃	20 min	
	Denaturation	94℃	30 s	|
	Annealing	61℃	60 s	| 37x
	Extension	72℃	30 s	|
	Final Extension	72℃	7 min	

After the amplification reaction, PCR products from the slides were transferred into 0.2 ml reaction tubes and diluted 1:6 with sterile water. One microlitre of this dilution was used directly for fragment length analysis.

4.6.1.2   Nested PCR

Aliquots of 1 up to 3 µl of each diluted sample of primary PCR were used as templates in secondary singleplex PCR reactions. PCR was carried out using the QIAGEN® HotStarTaq PCR Kit (Qiagen GmbH, Hilden, Germany) accordingly to the basic protocol (Tab. 7).

Tab. 7: Basic protocol for secondary (nested) PCR reactions

Reagents	1x	Final concentration
2x HotStarTaq Master Mix	6.0 or 12.5 µl	1x
Sterile water	variable	-
Single primer pair	0.5 or 1.0 µl	2.08 µM
Template (primary PCR product)	1.0 to 3.0 µl	-
Final volume	**12.0 or 25.0 µl**	

Secondary PCR was performed using a Primus Advanced96 Peqlab Cycler (Peqlab Biotechnologie GmbH, Erlangen, Germany), a Cyclone25 Peqlab Cycler (Peqlab Biotechnologie GmbH, Erlangen, Germany), a DNA Engine Tetrad 2 Peltier Thermal Cycler, (BIO-RAD, Munich, Germany) or a DYNAD DNA Engine Peltier Thermal Cycler (MJ Research Minneapolis, USA). Primer sequences and analysis methods used are listed in table 8 (colon polyps) and 9 (single cells).

Tab. 8: Details on primer sequences for colon polyp analysis: Nested PCR reactions were carried out with fluorescence-labelled primer pairs for microsatellite markers BAT25, BAT26, BAT40 and with non-labelled primer pairs for the genes *BRAF* exon 15 and *KRAS* exons 2 and 3.

Primer	Sequence (5'-3')	Analysis method
BAT25-F-FAM	TCG CCT CCA AGA ATG TAA GT	Fragment length analysis
BAT25-R-HEX	TCT GCA TTT TAA CTA TGG CTC	
BAT26-F-FAM	TGA CTA CTT TTG ACT TCA GCC	Fragment length analysis
BAT26-R-HEX	AAC CAT TCA ACA TTT TTA ACC C	
BAT40-F-FAM	ATT AAC TTC CTA CAC CAC AAC	Fragment length analysis
BAT40-R-HEX	GTA GAG CAA GAC CAC CTT G	
Braf15-F-in	CTT TAC TTA CTA CAC CTC AG	Gel electrophoresis
Braf15-R-in	AGC ATC TCA GGG CCA AAA AT	Sequencing analysis
Kras2-F-in	TTT TTA TTA TAA GGC CTG CTG	Gel electrophoresis
Kras2-R-in	ATA TTA AAA CAA GAT TTA CCT C	Sequencing analysis
Kras3-F-in	GGT GCA CTG TAA TAA TCC AG	Gel electrophoresis
Kras3-R-in	ACT ATA ATT ACT CCT TAA TGT C	Sequencing analysis

Tab. 9: Details on primer sequences for single cell analysis: Nested PCR reactions were carried out with primer pairs PC2-F/R for the 1 bp deletion of patient C and PD2-F/R for the 5 bp deletion of patients D and E.

Primer	Sequence (5'-3')	Analysis method
PC2-F	AGA ACG CGG AAT TGG TCT AGG CA	Gel electrophoresis
PC2-R	TGA CTT TGG CAA TCT GGG CTG CA	Sequencing analysis
PD2-F	AAG ATG GGC AAG ACC CAA ACA C	Gel electrophoresis
PD2-R	TGC TGT CCA AAA TGT GGT TGG	Sequencing analysis
PD2-F-FAM	AAG ATG GGC AAG ACC CAA ACA C	Fragment length analysis
D5S346-F-FAM	ACT CAC TCT AGT GAT AAA TCG GG	Fragment length analysis
D5S346-R	AGC AGA TAA GAC AGT ATT ACT AGT T	
D5S82-F-FAM	ATC AGA GTA TCA GAA TTT CT	Fragment length analysis
D5S82-R	CCC AAT TGT ATA GAT TTA GAA GTC	

An overview of the secondary PCR conditions for colon polyp and single cell analysis is given in table 10. Variations of PCR conditions in cycle number and annealing temperature depend on different melting temperatures of the primers and were optimized for each primer pair during the establishment of the specific PCR system.

Tab. 10: Overview of PCR conditions for nested PCR reactions

Analysis	Primers	PCR step	PCR conditions		
		Initial denaturation	95℃	15 min	
	BAT25-F/R	Denaturation	94℃	30 s	|
	BAT26-F/R	Annealing	64℃*	30 s	| 15x
	BAT40-F/R	Extension	72℃	30 s	|
Colon polyp analysis	Braf15-F/R-in	Denaturation	94℃	30 s	|
	Kras2-F/R-in	Annealing	50℃	30 s	| 15x or 20x
	Kras3-F/R-in	Extension	72℃	30 s	|
		Final Extension	72℃	7 min	
		Initial denaturation	95℃	15 min	
	PC2-F/R	Denaturation	94℃	30 s	|
	PD2-F/R	Annealing	59/62/64℃	60 s	| 25/x30x
	PD2-F/R-FAM	Extension	72℃	30 s	|
		Final Extension	72℃	7 min	
Single cell analysis		Initial denaturation	95℃	15 min	
		Denaturation	94℃	30 s	|
		Annealing	57℃*	60 s	| 7x
	D5S346-F/R	Extension	72℃	30 s	|
	D5S82-F/R	Denaturation	94℃	30 s	|
		Annealing	50℃	30 s	| 20x or 25x
		Extension	72℃	30 s	|
		Final Extension	72℃	7 min	

*temperature increment of -1℃ per each cycle

4.6.2 Gel electrophoresis

Secondary non-fluorescence-labelled PCR products were separated on 2% agarose or 10% polyacrylamide gels in order to control the presence and quality of amplification products.

For agarose gel electrophoresis 5 µl of PCR solution were mixed with 3 µl of 6x loading dye (Peqlab Biotechnologie GmbH, Erlangen, Germany) and pipetted into the gel slots.

A 100 base pairs (bp) DNA ladder (New England BioLabs, Ipswich, USA) was used as a size standard. Gels were run in 1x Tris-acetate-EDTA buffer at 130 V for 30 to 40 min at room temperature. Agarose gels were ethidium bromide stained and analyzed with a camera detection system (Transilluminator, Peqlab Biotechnologie GmbH, Erlangen, Germany).

For polyacrylamide gel electrophoresis a 10% CleanGel (ETC, Kirchentellinsfurt, Germany) was rehydrated in delect buffer (ETC, Kirchentellinsfurt, Germany) for 2 hours according to the manufacturer's instructions. A mixture of 1 µl PCR solution and 5 µl of loading dye (1:20 dilution of 6x loading dye with delect buffer) was pipetted into each gel slot. The gel was run at 180 V for 40 min and at 390 V for 45 min at 15°C (GenePhor electrophoresis unit, Amersham Biosciences Europe GmbH, Freiburg, Germany). A 100 bp DNA ladder (New England BioLabs, Ipswich, USA) was used as a size standard. Polyacrylamide gels were silver stained with the DNA Silver Staining Kit PlusOne™ (GE Healthcare, Biosciences AB, Uppsala, Sweden) according to the manufacturer's instructions.

4.6.3 Fragment length analysis

A 1 µl aliquot of secondary PCR or a dilution (variable, depending on the PCR reaction) containing fluorescence-labelled primers (FAM, HEX) was mixed with 12.7 µl of Hi-Di™ Formamide (Applied Biosystems, California, USA) and 0.3 µl of GeneScan™-500LIZ™ size standard (Applied Biosystems, California, USA) and prepared for analysis on an AB/Hitachi 3130xL Genetic Analyzer (Applied Biosystems, California, USA). Data were analyzed using GeneScan™ 3.1.2 and GeneMapper® v4.0 software (Applied Biosystems, California, USA).

4.6.4 Sequencing analysis

The PCR products for sequencing were cleaned using 96 filter plates (Multiscreen® PCR µ96, Millipore Corporate, Billerica, USA). The total volume of PCR solution (12-25 µl) and 20 - 100 µl sterile water were added into the filter plate. The liquid passed the filter membrane with the help of a vacuum pump. Once the liquid was completely removed, the DNA was dissolved in 15-20 µl of sterile water and transferred into new PCR tubes or 96 well plates. Double-strand sequencing was performed with the BigDye® Terminator v1.1 Cycle Sequencing Kit (Applied Biosystems, California, USA). Aliquots of the cleaned secondary PCR product were used as template for the

sequencing reaction (Tab. 11) which was performed on a Veriti 96 Well Fast Thermal Cycler (Applied Biosystems, California, USA).

Tab. 11: Protocol for sequencing PCR reactions

Reagents	1x	Final concentration
5x BigDye Buffer	2.0 µl	1x
BigDye cycle terminator	0.5 to 1.0 µl	-
Sterile water	variable	-
Primers	0.2 or 1.0 µl	0.3 or 1.5 µM
Template (secondary PCR product)	1.0 to 4.0 µl	-
Final volume	**10.0 µl**	

PCR conditions for the sequencing reaction are shown in table 12. Primers for sequencing analysis are shown in tables 8 and 9. The amount of template, primers and BigDye cycle terminator used depended on the yield of secondary PCR product which was checked in gel electrophoresis.

Tab. 12: PCR conditions for sequencing reaction

PCR step	PCR conditions		
Initial denaturation	96°C	60 s	
Denaturation	96°C	10 s	|
Annealing	50°C	5 s	| 25x
Extension	60°C	75 s	|
Hold	4°C	forever	

Products of the sequencing reaction were cleaned via sephadex plates (Sephadex[®] G-50, Sigma-Aldrich; 96 plate Multiscreen[®] HTS, HV, Millipore Corporate, Billerica, USA). Sephadex plates were centrifuged for 5 min at 2570 rpm (910 rcf; Universal 320, Hettich Zentrifugen) for removing the water. The complete sequencing PCR solution and 10 µl of sterile water were pipetted onto the sephadex and centrifuged for 5 min at 2570 rpm into a new 96 PCR plate (Thermo-Fast[®] 96 Detection Plate, Thermo Scientific, Waltham, USA). Finally, 20 to 30 µl of sterile water were added and the plate was covered with septa (plate Septa 96-well, Applied Biosystems, California, USA). Sequencing was performed on the AB Hitachi 3730 DNA Analyzer (Applied Biosystems, California, USA) according to the manufacturer's instructions. Data were analyzed using MutationSurveyor v3.10 Software.

5 Results

5.1 Characterization of colon polyp tissue

5.1.1 Analysis of mutations in the genes *BRAF* and *KRAS*

Mutations in exon 15 of the *BRAF* gene and in exons 2 and 3 of the *KRAS* gene were analyzed using three colon polyp tissue sections from two patients. Characterization of colon polyps with regard to the two proto-oncogenes *BRAF* and *KRAS* involved in colorectal cancer development is important for a better molecular understanding of this disease. Information about identification of mutations in the polyp tissue and their localization can be integrated into an increasingly more specific classification of colon polyps. Combination with histological and clinical features enables deeper insights into tumour development.

For One- and Three-letter-code of amino acids used in the text and RNA codon table see appendix.

Patient A, Polyp 2320-08-IV

After histological characterization of the hematoxylin and eosin (HE) stained tissue section, parts of polyp 2320-08-IV were classified as hyperplastic tumour tissue (Fig. 6 A). Comparison of the HE stained section with the unstained tissue section enabled collection of samples from only the hyperplastic tissue area by means of laser microdissection (Fig. 6 B). Samples of different sizes were collected from the tissue section; these samples contained between 10 and 70 cells on average (Fig. 7). Determination of the exact number of cells or cell nuclei in one sample is not possible, as the 6 µm thick tissue section does not contain cells in a regular monolayer. It is therefore possible that only parts of a cell or nucleus are localized within this section.
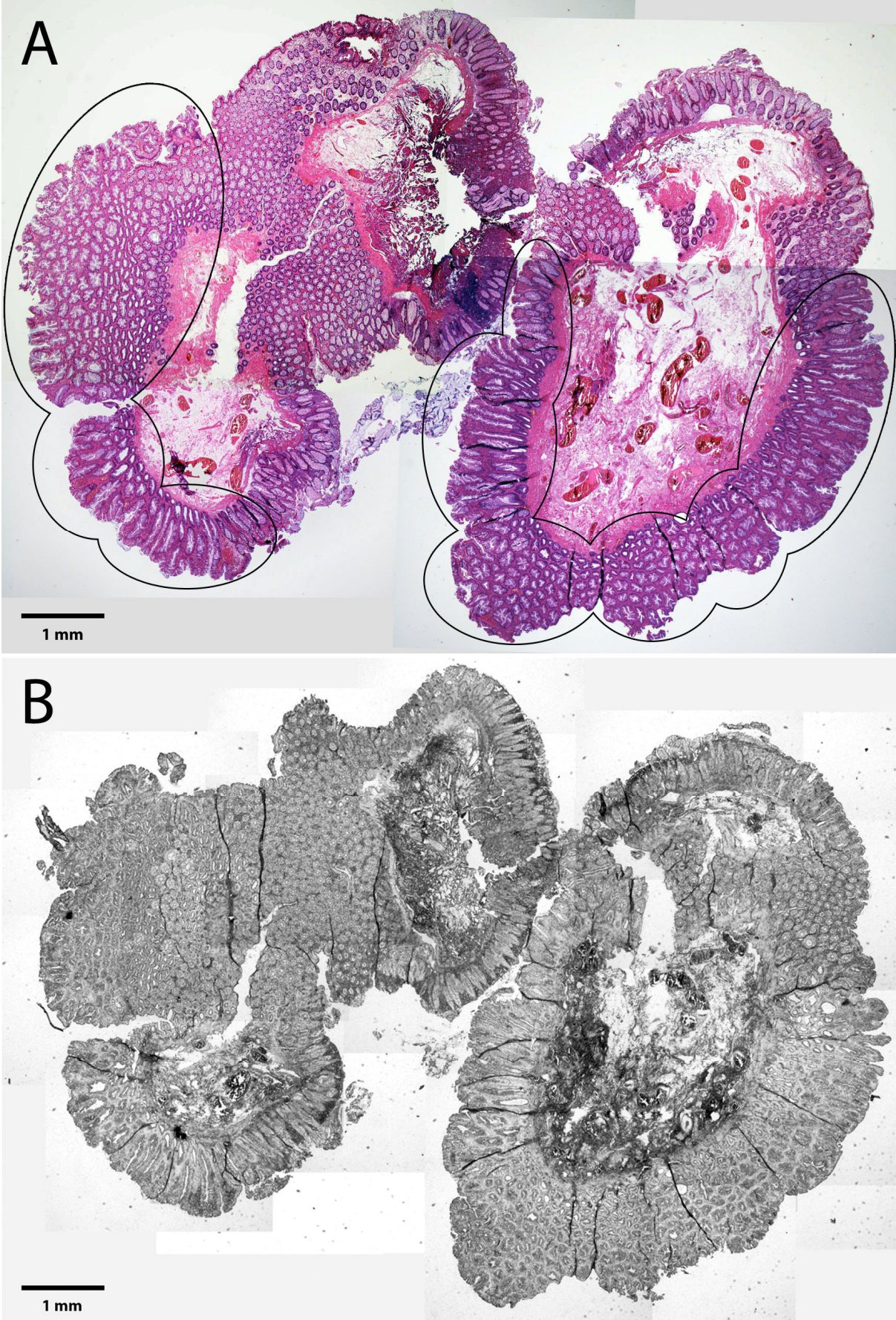
Fig. 6: Colon polyp 2320-08-IV of patient A. A) Image of the HE stained tissue section. The hyperplastic tissue parts of the polyp are highlighted. B) Image of the unstained tissue section used for laser microdissection.
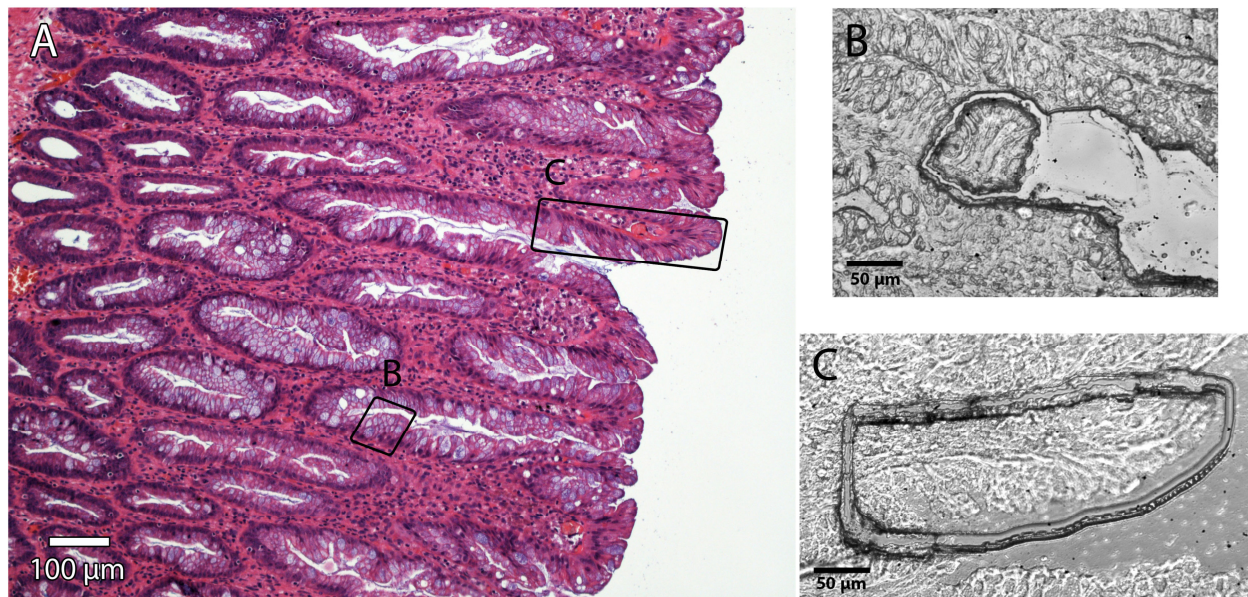
Fig. 7: Detail of polyp 2320-08-IV of patient A. A) Image of the HE stained tissue section with two samples highlighted. B) and C) Detail images of laser microdissected samples using the unstained tissue section. Comparing the sizes of the two samples with the HE stained tissue section enables counting the average number of cells in these isolated samples. Sample B contains 10 and sample C about 70 cells. There is no complete correspondence of the samples in both tissue sections because the tissue sections were gained from different levels of the fixed tissue block.

Sequencing analysis resulted in the detection of 10 different mutations in polyp 2320-08-IV (Tab. 13).

Tab. 13: Mutations of polyp 2320-08-IV of patient A

Gene	Mutation	Codon	Position cDNA	Amino acid	Type	Transversion/ Transition	Known/ unknown
BRAF Exon 15	T>A	GTG>GAG	c.1799	Val600Glu	activating	Transversion	known
	T>C	TCT>CCT	c.1804	Ser602Pro	missense	Transition	unknown
	C>T	TCC>TCT	c.1821	Ser607Ser	silent	Transition	unknown
	C>T	CAT>TAT	c.1822	His608Tyr	missense	Transition	unknown
	G>A	TTG>TTA	c.1839	Leu613Leu	silent	Transition	unknown
KRAS Exon 2	G>A	GAA>AAA	c.7	Glu3Lys	missense	Transition	unknown
KRAS Exon 3	T>C	ATT>ACT	c.137	Ile46Thr	missense	Transition	unknown
	G>A	GGA>GAA	c.143	Gly48Glu	missense	Transition	unknown
	C>T	GCA>GTA	c.176	Ala59Val	missense	Transition	unknown*
	G>T	GGC>TGC	c.229	Gly77Cys	missense	Transversion	unknown

*mutations at the amino acid position with another amino acid substitution are known

The well-known hotspot mutation c.1799 T>A, p.Val600Glu in exon 15 of the *BRAF* gene was detected in 10 samples (Fig. 8). Mosaic forms of this activating mutation dominated in polyp 2320-08-IV and in only one of the 10 samples (10.0%) was the mutation fully manifested. In the overview there is no directed distribution in the appearance of the mutation from the inside to the outside of the polyp tissue or the other way round (Fig. 8 A).
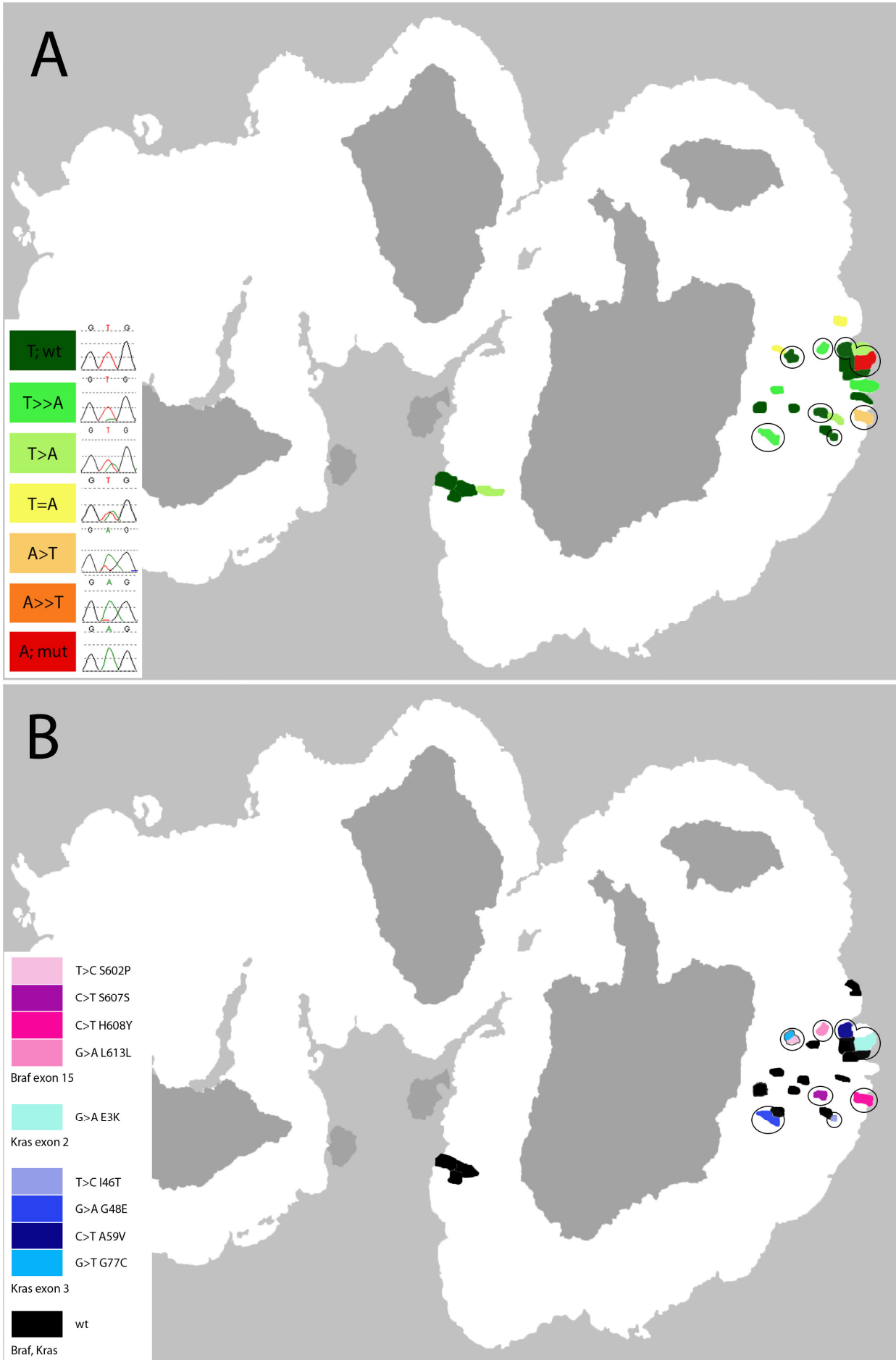
Fig. 8: Schematic drawing of colon polyp 2320-08-IV of patient A. A) The distribution of the hotspot mutation c.1799 T>A, p.Val600Glu in exon 15 of the *BRAF* gene within the polyp tissue section is shown in an overview. The mutation was detected in the range of different forms of mosaicism (T>>A, T>A, T=A, A>T, A>>T) to the fully manifested mutation (A; mut). Samples with the wild type (T; wt) form of the gene are shown in dark green. B) displays the localization of all mutations found in the genes *BRAF* exon 15 and *KRAS* exons 2 and 3. Samples carrying a mutation can be identified using the colour table. If a sample is stained in one colour for one mutation, this means that the sample is wt for the two other exons analyzed. Otherwise, samples are stained in more than one colour. Circled samples in A and B show the comparison of the *BRAF* hotspot mutation status with the other mutations in *BRAF* and *KRAS* found in the same sample. Sequence data are shown in figure 9 and detailed information on all mutations is listed in table 13.

Compared to 10 samples displaying the mutation, sequencing analysis revealed 13 wild type samples in the polyp tissue section. Figure 8 B shows the distribution of all other mutations in *BRAF* and *KRAS* detected in the polyp tissue. Sequence data of polyp 2320-08-IV mutations are shown in figure 9. One of the 13 samples carried the mutation c.1804 T>C, p.Ser602Pro in exon 15 of the *BRAF* gene as well as the mutation c.229 G>T, p.Gly77Cys in exon 3 of the *KRAS* gene. Compared to the samples with the c.1799 T>A, p.Val600Glu mutation in figure 8 A it is shown that there were two samples with mutations in both the *BRAF* gene and in one of the exons of the *KRAS* gene. One sample carried the mutation c.143 G>A, p.Gly48Glu and a mosaic form of the hotspot mutation. In the other sample, the hotspot mutation c.1799 T>A, p.Val600Glu was fully manifested. In addition, the *KRAS* exon 2 mutation c.7 G>A, p.Glu3Lys could be identified. For detailed sequence information on mosaic forms of the c.1799 T>A, p.Val600Glu mutation see figure 8 A.

Two of the 10 mutations found in polyp 2320-08-IV were silent and do not result in an amino acid substitution. The ratio of transversions to transitions is 20.0% (2 of 10) to 80.0% (8 of 10) so that there are four times more transitions than transversions. Except for the activating hotspot mutation c.1799 T>A, p.Val600Glu, most of the detected mutations are not yet described. Detailed information on all mutations for patient A is summarized below starting at page 46.
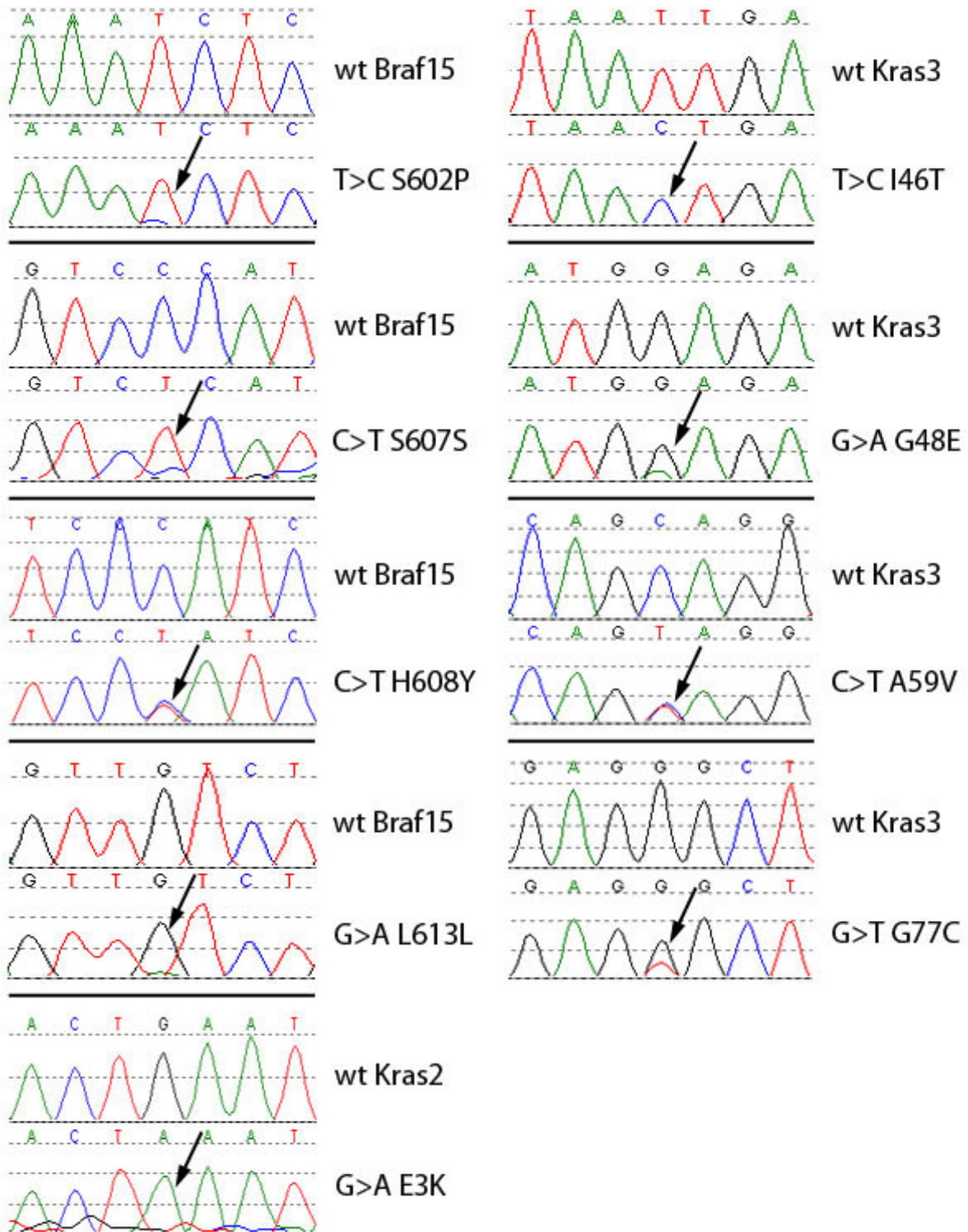
Fig. 9: Sequence data of all mutations found in the 2320-08-IV colon polyp of patient A. Mutations (arrows) in the genes *BRAF* exon 15 and *KRAS* exons 2 and 3 are manifested as mosaic or full mutation. For comparison, the corresponding wild type (wt) sequences are displayed.

Patient A, Polyp 4407/09

A definite histological characterization of the HE stained tissue section of polyp 4407-09 could not be obtained (Fig. 10 A). The polyp could be classified either as hyperplastic polyp or sessile serrated adenoma (SSA) or a mixture or a changeover of both, respectively. Nevertheless, an exact differentiation of tumour and normal tissue was possible (Fig. 10 A). Laser microdissected samples were isolated from all tumour tissue areas using the unstained tissue section (Fig. 10 B).
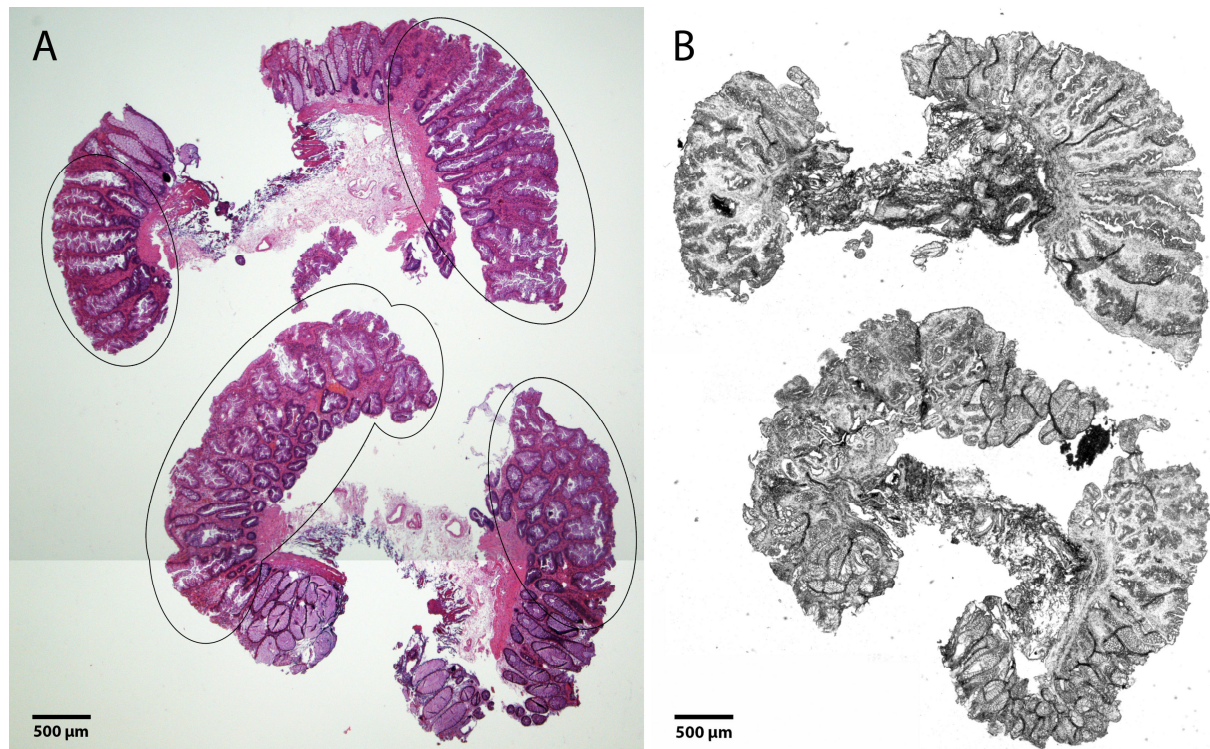
Fig. 10: Colon polyp 4407-09 of patient A. A) Image of the HE stained tissue section. The tumour tissue parts of the polyp are highlighted. B) Image of the unstained tissue section used for laser microdissection.

In polyp 4407-09, 33 mutations including the hotspot mutation c.1799 T>A, p.Val600Glu were detected in sequencing analysis (Tab. 14). In contrast to polyp 2320-08-IV, 8 of 44 samples (18.2%) carrying the hotspot mutation displayed the full manifestation of the mutation. A dominant or regular distribution of the mutation or mosaic forms within the tumour tissue was, as in the first polyp, not observed (Fig. 11 A). In comparison to polyp 2320-08-IV, the ratio of mutated to wild type samples had increased from 0.77 (10 to 13) up to 1.3 (44 to 34). An overview of the 32 other mutations is shown in figure 11 B.

Tab. 14: Mutations of polyp 4407-09 of patient A

Gene	Mutation	Codon	Position cDNA	Amino acid	Type	Transversion/ Transition	Known/ unknown
BRAF Exon 15	G>T	GAT>TAT	c.1780	Asp594Tyr	missense	Transversion	unknown*
	T>A	GTG>GAG	c.1799	Val600Glu	activating	Transversion	known
	T>A+G>T	GTG>GAT	c.1799,1800	Val600Asp	missense	Transversion	known
	C>T	CGA>TGA	c.1807	Arg603X	nonsense	Transition	unknown
	G>A	TGG>TAG	c.1811	Trp604X	nonsense	Transition	unknown
	T>C	AGT>AGC	c.1815	Ser605Ser	silent	Transition	unknown
	G>A	GGG>AGG	c.1816	Gly606Arg	missense	Transition	unknown
	C>T	TCC>TTC	c.1820	Ser607Phe	missense	Transition	unknown
	C>G	CAT>GAT	c.1822	His608Asp	missense	Transversion	unknown
	C>T	CAT>TAT	c.1822	His608Tyr	missense	Transition	unknown
	C>T	CAG>TAG	c.1825	Gln609X	nonsense	Transition	unknown*
	A>G	CAG>CGG	c.1826	Gln609Arg	missense	Transition	unknown*
	T>C	TTG>CTG	c.1837	Leu613Leu	silent	Transition	unknown
	G>A	GGA>AGA	c.1843	Gly615Arg	missense	Transition	unknown
	T>C	ATT>ACT	c.1850	Ile617Thr	missense	Transition	unknown
	G>A	TGG>TGA	c.1857	Trp619X	nonsense	Transition	unknown
KRAS Exon 2	G>A	GGA>AGA	c.28	Glu10Arg	missense	Transition	unknown
	G>C	GTA>CTA	c.40	Val14Leu	missense	Transversion	unknown*
	T>C	TTG>CTG	c.55	Leu19Leu	silent	Transition	unknown
	T>C	CAT>CAC	c.81	His27His	silent	Transition	unknown
KRAS Exon 3	A>G	ACC>GCC	c.148	Thr50Ala	missense	Transition	unknown
	C>A	ACC>ACA	c.150	Thr50Thr	silent	Transversion	unknown
	T>C	CTC>CCC	c.155	Leu52Pro	missense	Transition	unknown
	T>C	GAT>GAC	c.162	Asp54Asp	silent	Transition	unknown
	C>T	CTC>TTC	c.166	Leu56Phe	missense	Transition	unknown
	A>G	GAC>GGC	c.170	Asp57Gly	missense	Transition	unknown
	G>A	GCA>ACA	c.175	Ala59Thr	missense	Transition	known
	A>C	CAA>CCA	c.182	Gln61Pro	missense	Transversion	unknown*
	A>G	GAG>GGG	c.188	Glu63Gly	missense	Transition	unknown
	G>A	GAG>GAA	c.189	Glu63Glu	silent	Transition	unknown
	G>A	AGG>AAG	c.203	Arg68Lys	missense	Transition	unknown
	A>G	AGG>GGG	c.217	Arg73Gly	missense	Transition	unknown
	A>G	AAA>GAA	c.262	Lys88Glu	missense	Transition	unknown

*mutations at the amino acid position but with another amino acid substitution are known

Four of these 32 samples carried more than one mutation referred to all mutations except the hotspot *BRAF* mutation. The first sample, located in the upper left side of the polyp (Fig. 11 B) carried the mutations c.1807 C>T, p.Arg603X and c.1837 T>C, p.Leu613Leu in exon 15 of the *BRAF* gene as well as the mutation c.182 A>C, p.Gln61Pro in exon 3 of the *KRAS* gene. The second one, located in the lower left side of the polyp section (Fig. 11 B) carried the mutations c.1826 A>G, p.Gln609Arg and c.1850 T>C, p.Ile617Thr in exon 15 of the *BRAF* gene additionally to a mosaic form of the c.1799 T>A, p.Val600Glu mutation (Fig. 11 A). The third, very small sample displayed the mutations c.1820 C>T, p.Ser607Phe in exon 15 of *BRAF*, c.148 A>G, p.Thr50Ala and c.166 C>T, p.Leu56Phe in exon 3 of *KRAS* as well as the fully manifested c.1799 T>A, p.Val600Glu mutation. This sample is located in the lower right side of the tissue section (Fig. 11).
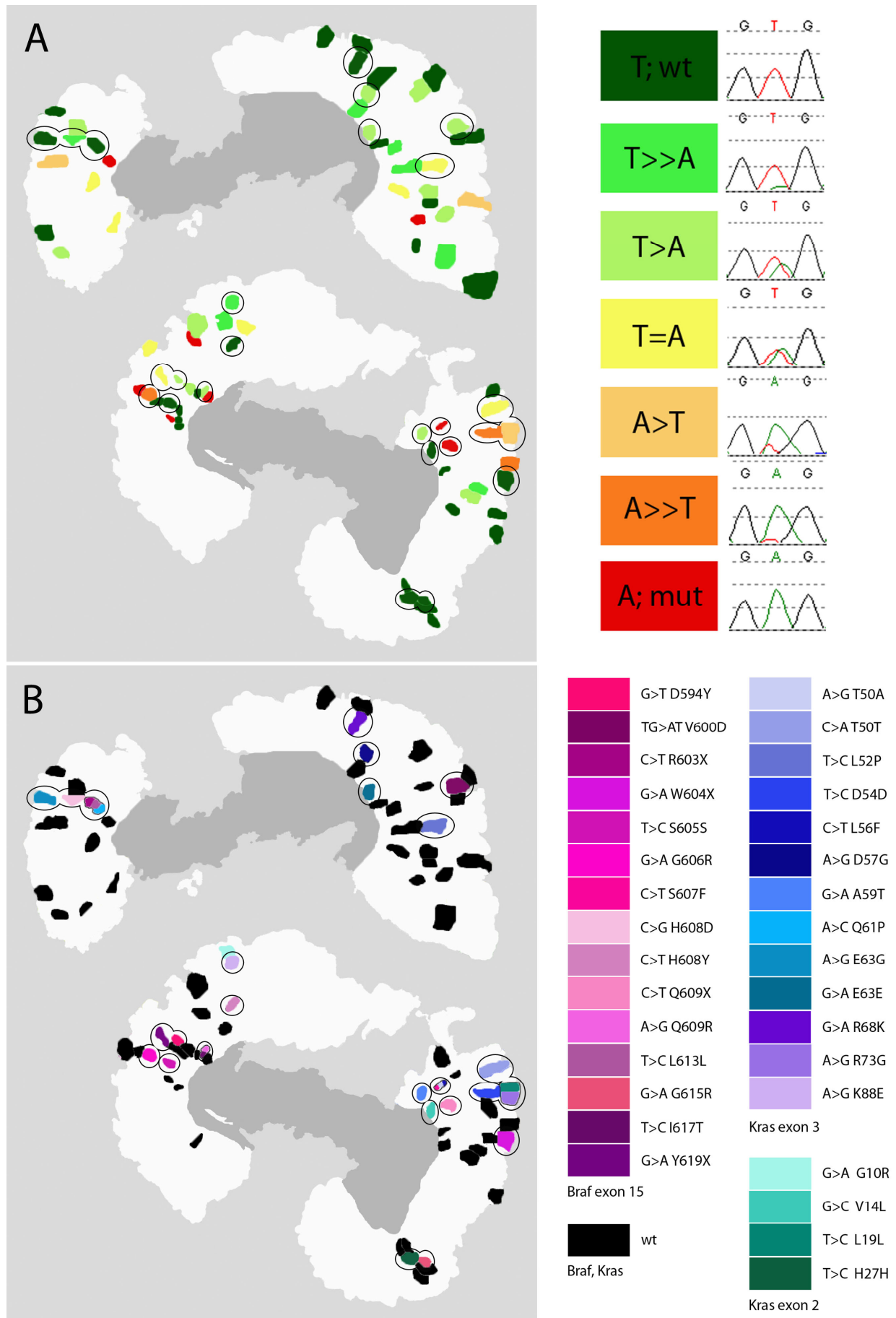
Fig. 11: Schematic drawing of colon polyp 4407-09 of patient A. A) The distribution of the hotspot mutation c.1799 T>A, p.Val600Glu in exon 15 of the *BRAF* gene within the polyp tissue section is shown

in an overview. The mutation was detected in the range of different forms of mosaicism (T>>A, T>A, T=A, A>T, A>>T) to the fully manifested mutation (A; mut). Samples with the wild type (T; wt) form of the gene are shown in dark green. B) displays the localization of all mutations found in the genes *BRAF* exon 15 and *KRAS* exons 2 and 3. Samples carrying a mutation can be identified using the colour table. If a sample is stained in one colour for one mutation, this means that the sample is wt for the two other exons analyzed. Otherwise, samples are stained in more than one colour. Circled samples in A and B show the comparison of the *BRAF* hotspot mutation status with the other mutations in *BRAF* and *KRAS* found in the same sample. Sequence data are shown in figure 12 and detailed information on all mutations is listed in table 14.

The mutations c.55 T>C, p.Leu19Leu in exon 2 and c.217 A>G, p.Arg73Gly in exon 3 of the *KRAS* gene were detected in the last of the four samples which is located in the lower right side of the tissue section. This sample additionally carried a mosaic form of the c.1799 T>A, p.Val600Glu mutation (Fig. 11). Six other samples displayed a mosaic or the fully manifested hotspot mutation beside a second mutation in exon 15 of *BRAF*. In seven cases the samples had mutations in one of the exons of *KRAS* and additionally carried the hotspot mutation. These samples are highlighted in figure 11. Two of 6 samples isolated from the normal tissue area of polyp 4407-09 carried mutations. In one sample the mutation c.1843 G>A, p.Gly615Arg in exon 15 of the *BRAF* gene occurred and in the second sample the mutation c.81 T>C, p.His27His was detected in *KRAS*.

As shown in table 14, seven of the 33 mutations are silent and in four cases nonsense mutations occurred, exclusively in the *BRAF* gene. A nonsense mutation is the exchange of an amino acid codon into a stop codon. The ratio of transversions to transitions for polyp 4407-09 is 21.2% (7 of 33) to 78.8% (26 of 33) which means there are 3.7 times more transitions than transversions. Detailed sequence data of all polyp 4407-09 mutations are shown in figure 12.
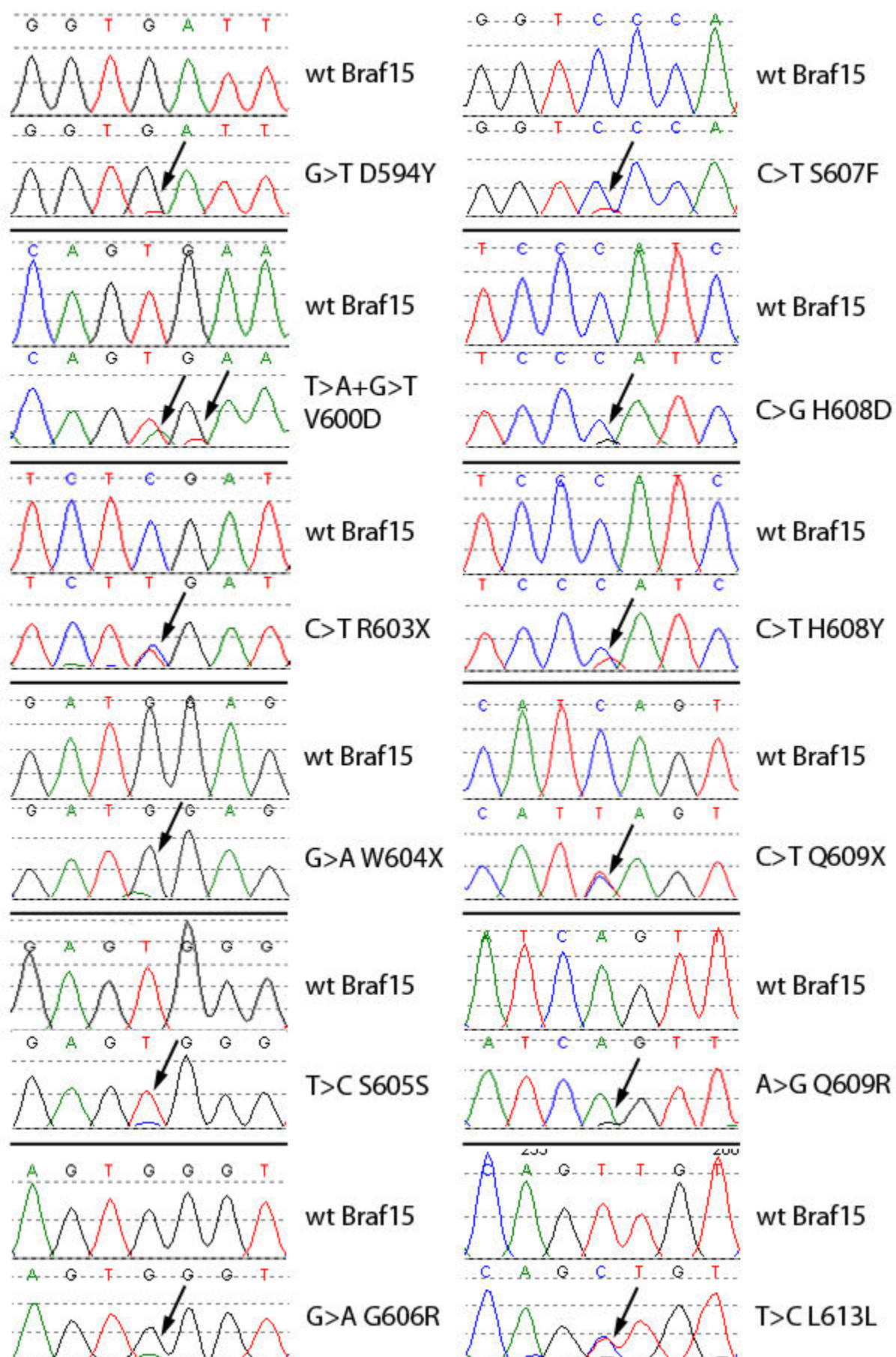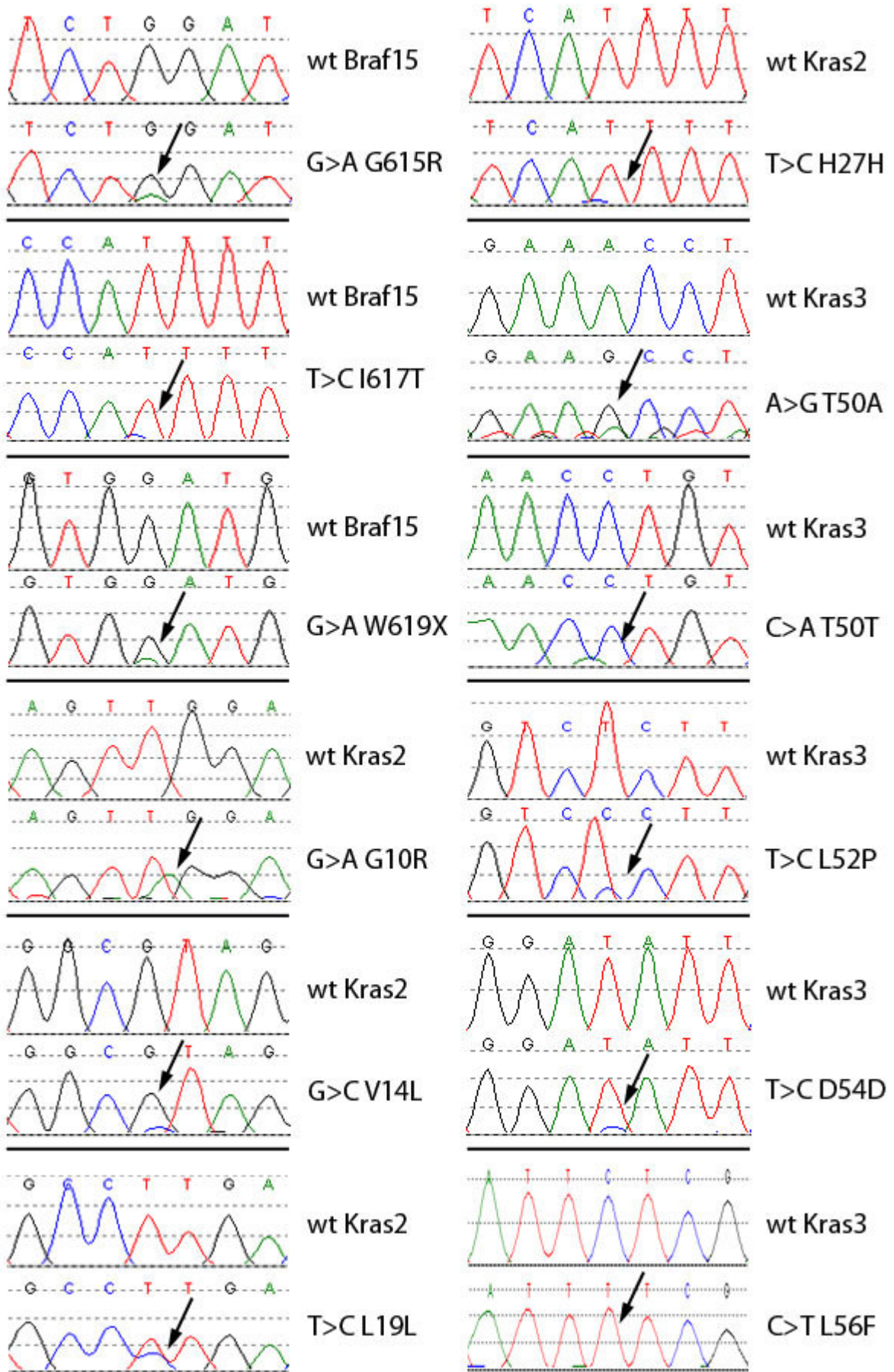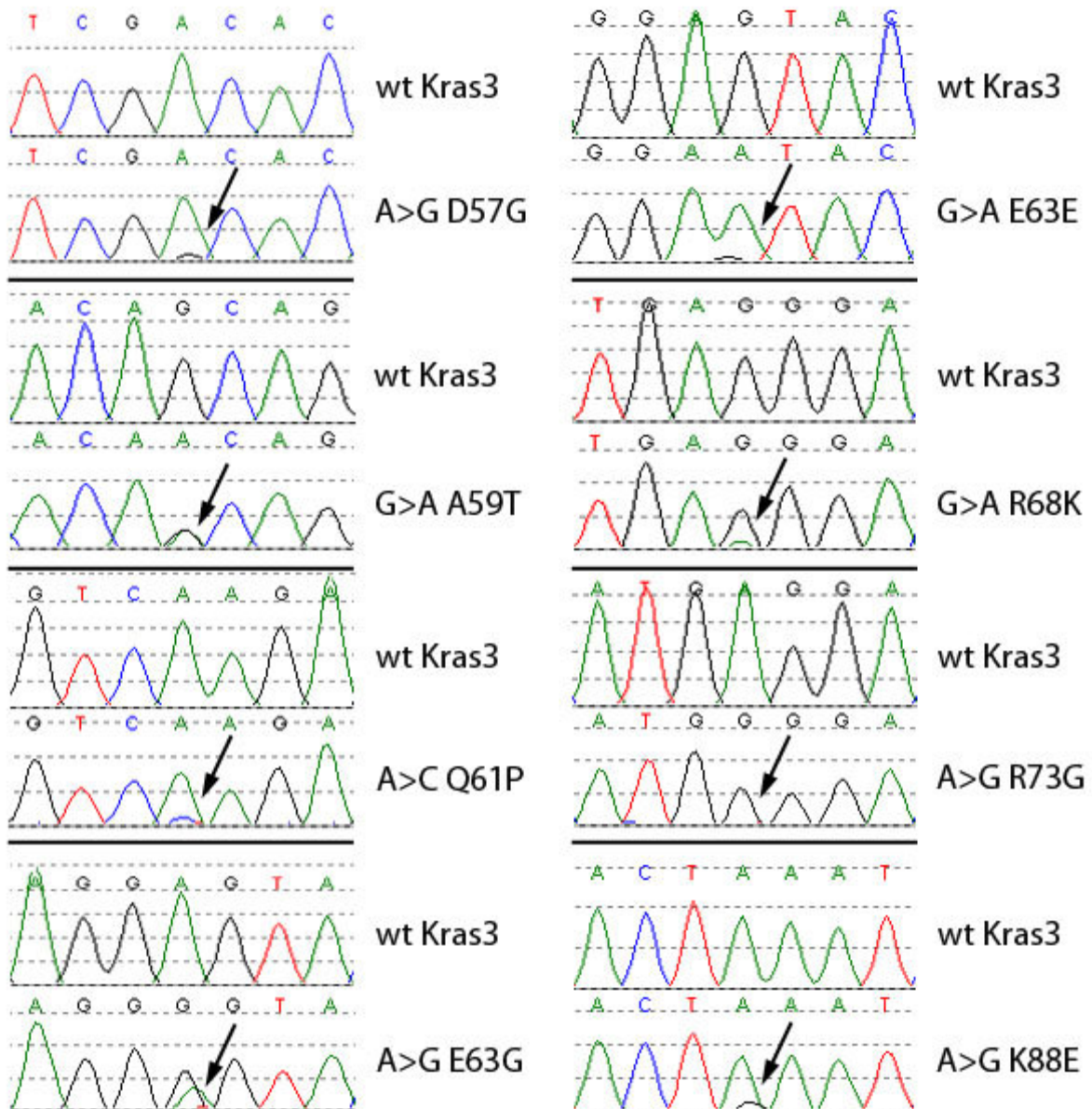
Fig. 12: Sequence data of all mutations found in the 4407-09 colon polyp of patient A. Mutations (arrows) in the genes *BRAF* exon 15 and *KRAS* exons 2 and 3 are manifested as mosaic or full mutation. For comparison, the corresponding wild type (wt) sequences are displayed.

Patient A, Polyps 2320-08-IV and 4407-09

For patient A, a total of 41 different mutations were detected of which 19.5% (8 of 41) were transversions and 80.5% (33 of 41) were transitions. The outcome of this is 4.1 times more transitions than transversions. Furthermore, combining the results of both polyps, some mutations occurred at the same amino acid position but not (except one) at the same nucleotide. In each case two different mutations were detected at amino acid valine 600 (Val600Glu and Val600Asp), serine 607 (Ser607Ser and Ser607Phe), histidine 608 (His608Asp and His608Tyr) and glutamine 609 (Gln609X and Gln609Arg) in the *BRAF* gene. For the substitution of valine into aspartic acid two nucleotide

exchanges were necessary. The mutations at amino acid histidine 608 occurred at the same nucleotide c.1822. In one case the nucleotide was changed from C to G (His608Asp). In the second case the nucleotide changed from C to T (His608Tyr). Only this mutation occurred twice, once in polyp 2320-08-IV and once in polyp 4407-09. The silent mutation Leu613Leu occurred both in polyp 2320-08-IV and 4407-09 but at different nucleotides. In polyp 2320-08-IV, nucleotide c.1839 was changed from G to A and in polyp 4407-09 nucleotide c.1837 was changed from T to C.

Tab. 15: Classification of all mutations of patient A

Gene	Mutation	Amino acid	Classification (PolyPhen)	PSIC
BRAF Exon 15	G>T	Asp594Tyr	probably damaging	2.899
	T>A	Val600Glu	probably damaging	2.120
	T>A+G>T	Val600Asp	probably damaging	2.345
	T>C	Ser602Pro	possibly damaging	1.778
	C>T	Arg603X	probably damaging	2.520
	G>A	Trp604X	probably damaging	4.195
	T>C	Ser605Ser	-	-
	G>A	Gly606Arg	probably damaging	2.492
	C>T	Ser607Phe	probably damaging	2.271
	C>T	Ser607Ser	-	-
	C>G	His608Asp	probably damaging	2.034
	C>T	His608Tyr	benign	0.939
	C>T	Gln609X	probably damaging	2.488
	A>G	Gln609Arg	benign	1.224
	T>C	Leu613Leu	-	-
	G>A	Leu613Leu	-	-
	G>A	Gly615Arg	probably damaging	2.492
	T>C	Ile617Thr	probably damaging	2.181
	G>A	Trp619X	probably damaging	4.195
KRAS Exon 2	G>A	Glu3Lys	benign	1.011
	G>A	Glu10Arg	probably damaging	2.816
	G>C	Val14Leu	probably damaging	2.192
	T>C	Leu19Leu	-	-
	T>C	His27His	-	-
KRAS Exon 3	T>C	Ile46Thr	benign	1.427
	G>A	Gly48Glu	benign	0.450
	A>G	Thr50Ala	benign	0.520
	C>A	Thr50Thr	-	-
	T>C	Leu52Pro	benign	0.696
	T>C	Asp54Asp	-	-
	C>T	Leu56Phe	benign	0.917
	A>G	Asp57Gly	probably damaging	2.237
	C>T	Ala59Val	possibly damaging	1.608
	G>A	Ala59Thr	benign	0.725
	A>C	Gln61Pro	probably damaging	2.788
	A>G	Glu63Gly	probably damaging	2.292
	G>A	Glu63Glu	-	-
	G>A	Arg68Lys	possibly damaging	1.872
	A>G	Arg73Gly	probably damaging	2.542
	G>T	Gly77Cys	benign	0.138
	A>G	Lys88Glu	benign	0.002

In the *KRAS* gene, two mutations occurred each at the amino acid threonine 50 (Thr50Ala and Thr50Thr), alanine 59 (Ala59Val and Ala59Thr) and glutamic acid 63

(Glu63Gly and Glu63Glu). As a comparison with the analysis of genomic DNA of patient A revealed, all mutations are somatic.

A major part of all detected mutations has not yet been described. The c.1799 T>A, p.Val600Glu mutation is known as an activating mutation in the hotspot region of exon 15 of the *BRAF* gene (Davies et al. 2002 and Kumar et al. 2003). Lee and colleagues identified the mutation Asp594Gly (Swiss-Prot variant VAR_018624 in P15056) in non-Hodgkin's lymphoma, a variant of the mutation Asp594Tyr which was detected here at the same amino acid position Asp594 in the *BRAF* gene (Lee et al. 2003). The mutation c.1799,1800 T>A, G>T, p.Val600Asp (Swiss-Prot variant VAR_018628 in P15056) with two nucleotide substitutions was identified in a melanoma cell line (Davies et al. 2002). The mutation c.1827 G>T, p.Gln609His was identified in a malignant melanoma patient which is a variant of the two mutations at amino acid Gln609 detected in polyp 4407-09 (Casula et al. 2004). In the *KRAS* gene the mutation Val14Ile (Swiss-Prot variant VAR_026109 in P01116) was identified in Noonan syndrome type 3 (Schubbert et al. 2006). The mutation variant detected in polyp 4407-09 is a substitution of the amino acid valine to leucine at position 14. As mentioned before, two different mutations at the amino acid position alanine 59 in the *KRAS* gene were detected in the two polyps of patient A. The mutation Ala59Thr (Swiss-Prot variant VAR_016030 in P01116) was identified in a human transitional cell bladder carcinoma cell line and is classified as single nucleotide polymorphism (OMIM_190070_0004; NCBI assay ID: ss38341815) (Grimmond et al. 1992). The mutation Ala59Val identified in polyp 2320-08-IV is not described yet. At the amino acid position glutamine 61 in exon 3 of the *KRAS* gene two different mutations are described. The first mutation, Gln61Arg (Swiss-Prot variant VAR_036306 in P01116) was identified in a colorectal cancer sample and the second one, Gln61His (Swiss-Prot variant VAR_006841 in P01116; NCBI assay ID: rs17851045) was identified in lung carcinoma and is classified as a single nucleotide polymorphism (Fransén et al. 2004, Tam et al. 2006). The amino acid substitution from glutamine to proline (Gln61Pro) detected in polyp 4407-09 has not yet been described.

Nine of the 41 mutations of patient A were silent mutations with no substitution of the amino acid. Eleven mutations were classified as benign, three as possibly damaging and 18 as probably damaging accordingly to the PolyPhen data base (http://genetics. bwh.harvard.edu/pph/)(Tab. 15). This internet tool characterizes amino acid substitutions according to a possible impact on the structure and function of a human protein. The PSIC (Position-Specific Independent Counts) value indicates how often an

amino acid substitution is observed in the protein family. Highly conserved amino acid positions are expressed in big values whereas less conserved positions are expressed in low values. For the two mutations Gln61Pro (ligand CAG) and Glu63Gly (ligand GNP: phosphoaminophosphonic acid-guanylate ester) the disruption of a ligand binding site of the Kras protein is predicted by PolyPhen.

Patient B, Polyp 13342-f1

On the basis of a HE stained tissue section one part of polyp 13342-f1 was classified as sessile serrated adenoma and another part as tubular adenoma (Fig. 13 A). Samples of several crypts were laser microdissected from the sessile serrated as well as from the tubular adenoma using the unstained tissue section (Fig. 13 B).

In total, 6 different mutations were detected in both types of adenomas (Tab. 16). The hotspot mutation c.1799 T>A, p.Val600Glu occurred only in the SSA but not in the tubular adenoma of the polyp (Fig. 14 A). Of 9 mutated samples in the SSA, three displayed the fully manifested mutation, the other 6 samples mosaic forms of it. As in the polyps of patient A, a dominant distribution of the hotspot mutation from the bottom to the top of the crypt or the other way round was not observed. In the SSA, 9 wild type samples were detected so the ratio between mutated and wild type samples is 1:1.

Tab. 16: Mutations of polyp 13342-f1 of patient B

Gene	Mutation	Codon	Position cDNA	Amino acid	Type	Transversion/ Transition	Known/ unknown
BRAF Exon 15	A>G	AAA>AGA	c.1772	Lys591Arg	missense	Transition	unknown
	T>A	GTG>GAG	c.1799	Val600Glu	activating	Transversion	known
	A>G	CGA>CGG	c.1809	Arg603Arg	silent	Transition	unknown
KRAS Exon 2	C>T	GCT>GTT	c.32	Ala11Val	missense	Transition	unknown
	G>A	TTG>TTA	c.57	Leu19Leu	silent	Transition	unknown
KRAS Exon 3	G>A	GAG>GAA	c.228	Glu76Glu	silent	Transition	unknown

An overview of the other 5 mutations in polyp 13342-f1 is given in figure 14 B. Only the silent mutation c.57 G>A, p.Leu19Leu was located in one crypt of the SSA. All other samples in the SSA showed wild type sequences for exons 2 and 3 of the *KRAS* gene. In the tubular adenoma 6 samples with 4 different mutations were detected. In one crypt 3 of 5 samples carried the mutation c.32 C>T, p.Ala11Val, the two other samples had wild type sequences for exons 2 and 3 of *KRAS*. In the second crypt two samples each carried mutations in exon 15 of *BRAF* and one sample carried a mutation in exon 3 of *KRAS*.
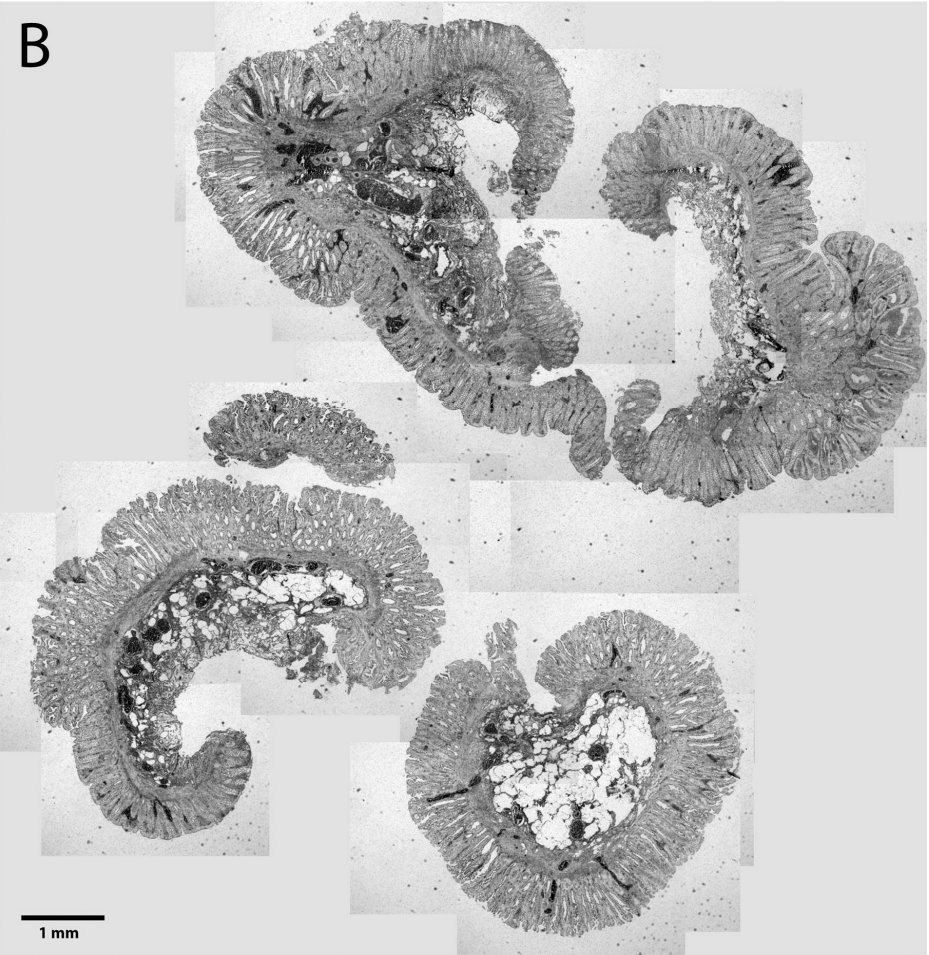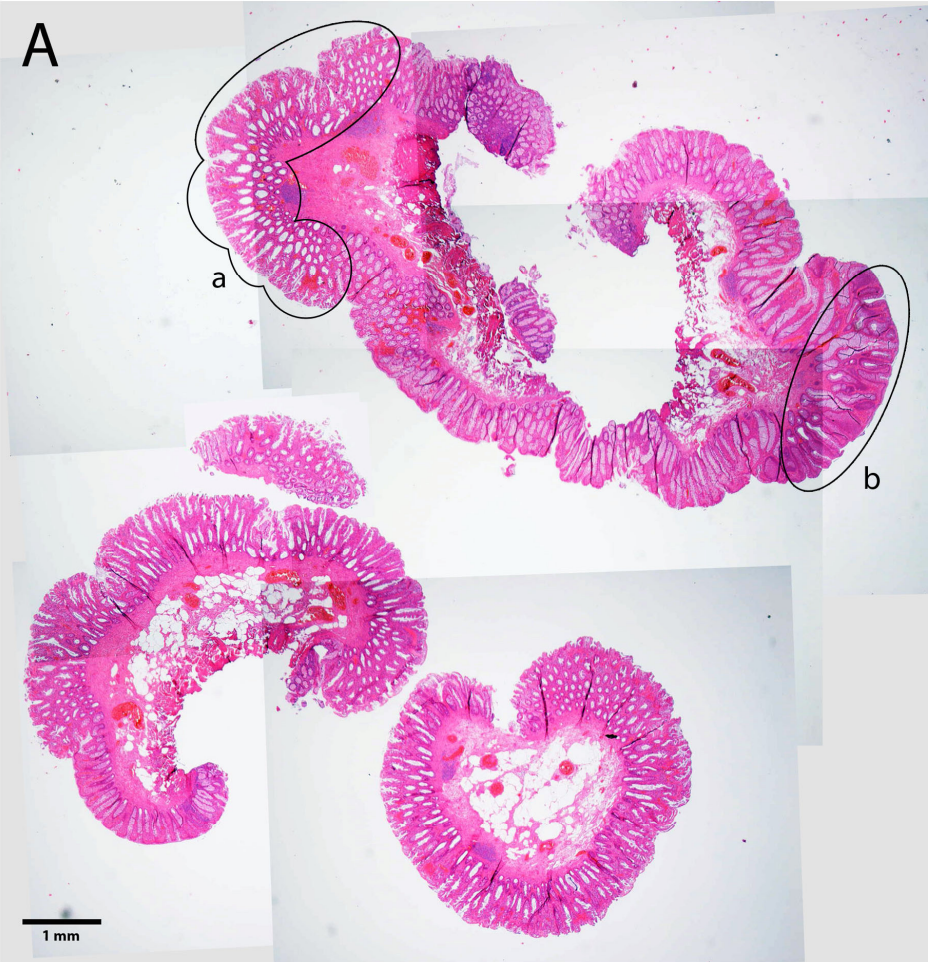
Fig. 13: Colon polyp 13342-f1 of patient B. A) Image of the HE stained tissue section. The tumour tissue parts of the polyp are highlighted. a) sessile serrated adenoma, b) tubular adenoma. B) Image of the unstained tissue section used for laser microdissection.
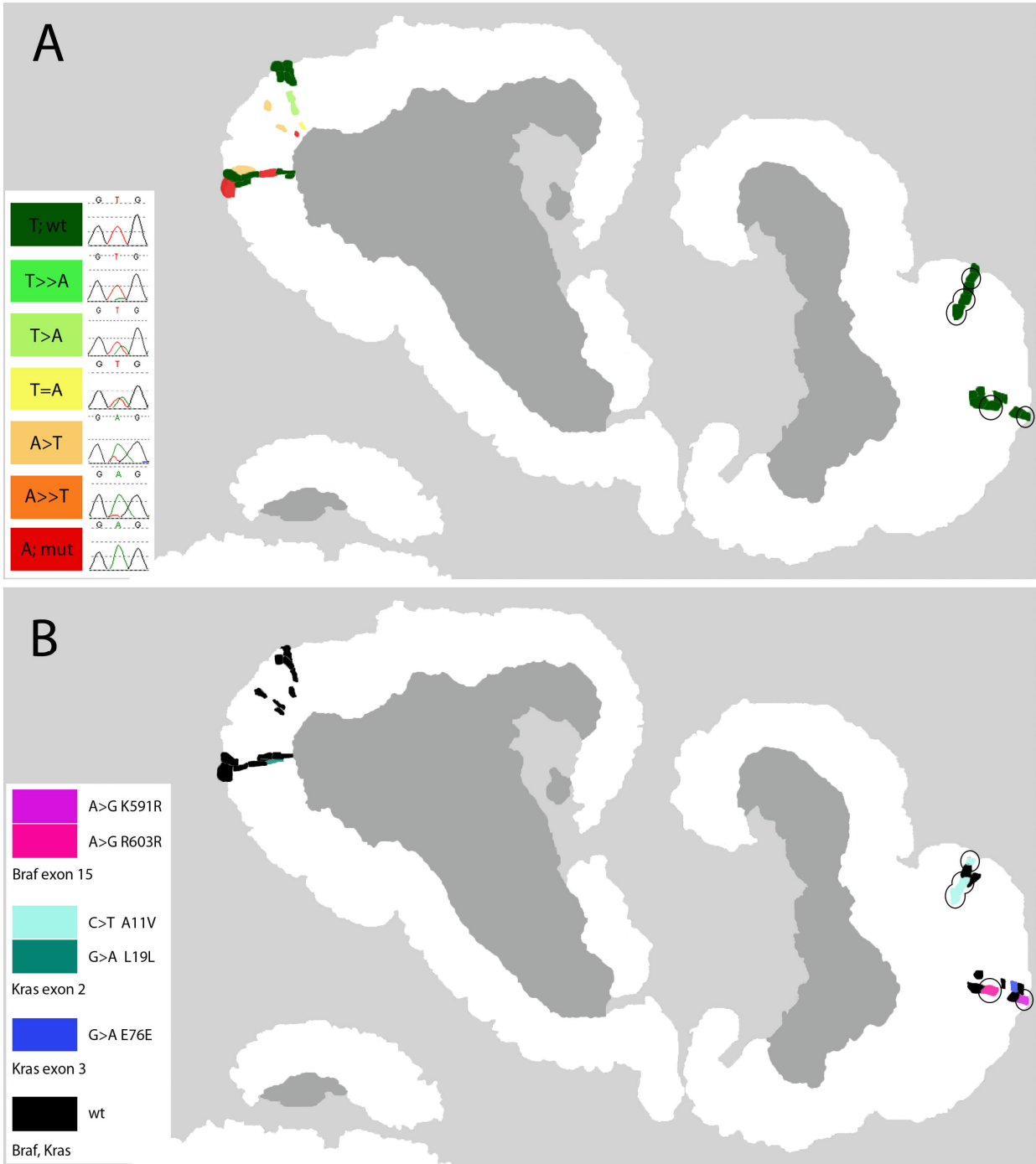

Fig. 14: Schematic drawing of colon polyp 13342-f1 section of patient B. A) The distribution of the hotspot mutation c.1799 T>A, p.Val600Glu in exon 15 of the *BRAF* gene within the polyp tissue section is shown in an overview. The mutation was detected in the range of different forms of mosaicism (T>>A, T>A, T=A, A>T, A>>T) to the fully manifested mutation (A; mut). Samples with the wild type (T; wt) form of the gene are shown in dark green. B) displays the localization of all mutations found in the genes *BRAF* exon 15 and *KRAS* exons 2 and 3. Samples carrying a mutation can be identified using the colour table. If a sample is stained in one colour for one mutation, this means that the sample is wt for the two other exons analyzed. Otherwise, samples are stained in more than one colour. Circled samples in A and B show the comparison of the *BRAF* hotspot mutation status with the other mutations in *BRAF* and *KRAS* found in the same sample. Sequence data are shown in figure 15 and detailed information on all mutations is listed in table 16.

In total, 3 of 6 mutations were silent and the ratio of transversions to transitions is 16.7% (1 of 6) to 83.3% (5 of 6) so there are almost 5 times more transitions than transversions. Nonsense mutations or different nucleotide exchanges at the same amino acid position were not observed. All mutations in polyp 13342-f1 were somatic mutations which resulted from the analysis of normal tissue of patient B. Sequence information on all mutations of patient B are shown in figure 15.
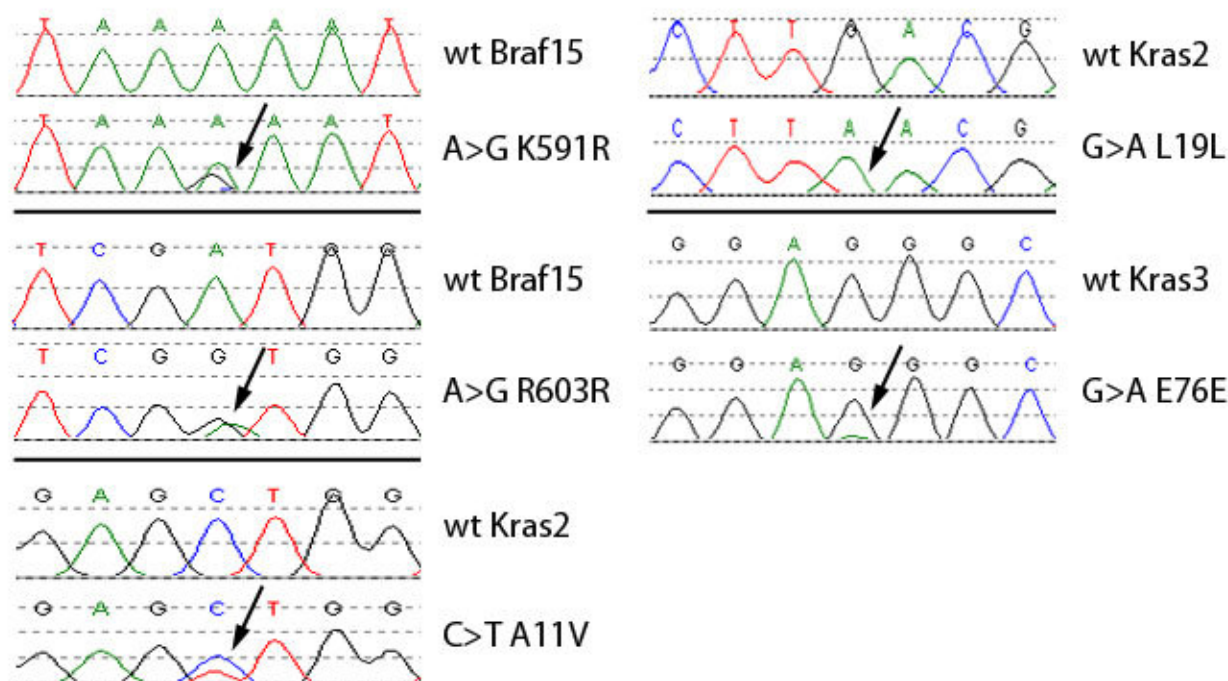

Fig. 15: Sequence data of all mutations found in the 13342-f1 colon polyp of patient B. Mutations (arrows) in the genes *BRAF* exon 15 and *KRAS* exons 2 and 3 are manifested as mosaic or full mutation. For comparison, the corresponding wild type (wt) sequences are displayed.

Except for the activating c.1799 T>A, p.Val600Glu mutation (Davies et al. 2002 and Kumar et al. 2003), the other 5 identified mutations of patient B are not described. Two of the mutations were classified as possibly damaging and one mutation was classified as probably damaging according to PolyPhen (Tab. 17).

Tab. 17: Classification of the mutations of patient B

Gene	Mutation	Amino acid	Classification (PolyPhen)	PSIC
BRAF Exon 15	A>G T>A A>G	Lys591Arg Val600Glu Arg603Arg	possibly damaging probably damaging -	1.678 2.120 -
KRAS Exon 2	C>T G>A	Ala11Val Leu19Leu	possibly damaging -	1.613 -
KRAS Exon 3	G>A	Glu76Glu	-	-

5.1.2 Analysis of microsatellite instability

Microsatellite instability (MSI) status was analyzed using the three microsatellite markers BAT25, BAT26 and BAT40. Additionally, immunohistochemical staining of the MLH1 protein was performed. Defects in the mismatch repair gene *MLH*1 can cause microsatellite instability and additionally may be responsible for mutations in some genes e. g. genes important for cell cycle regulation. Therefore, analysis of microsatellite instability status is an important aspect of colon polyp classification.

Patient A

Fragment length analysis revealed fragment lengths of 122/117 bp (base pairs) for BAT25, 116/118 bp for BAT26 and 126/118 bp for BAT40 as wild type status for patient A (Fig. 16).
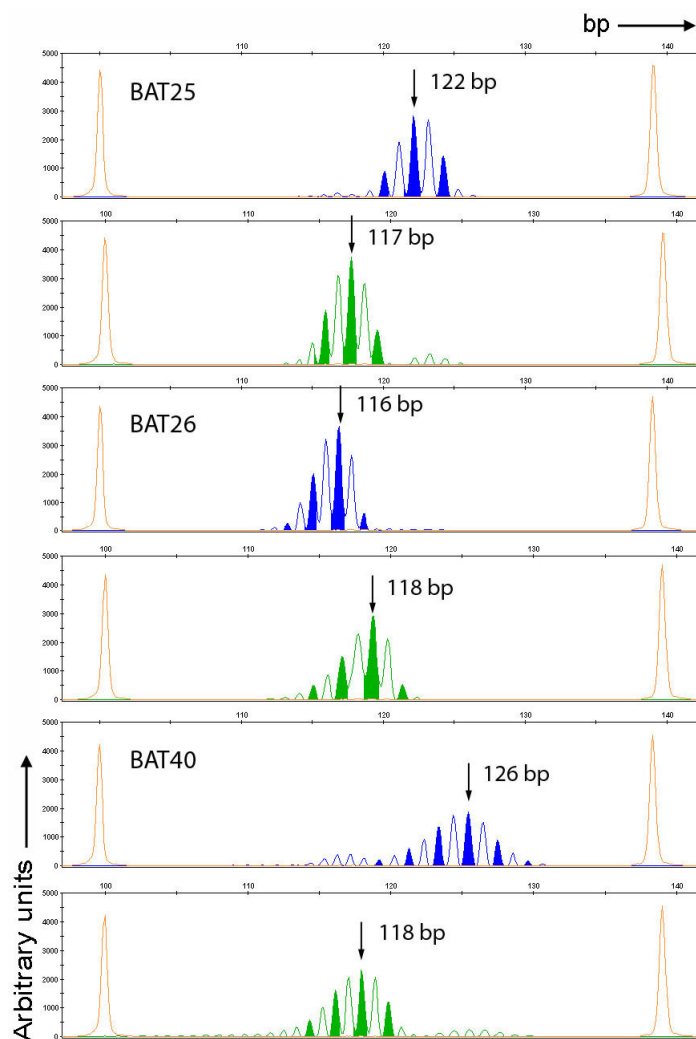

Fig. 16: Fragment length analysis of the microsatellite markers BAT25, BAT26 and BAT40 of patient A. Peak pattern show the wild type distribution of the different marker fragments. Arrows indicate the average fragment length of the markers: BAT25 122/117 bp, BAT26 116/118 bp, BAT40 126/118 bp. Blue: forward primer, green: reverse primer.

An overview of the microsatellite analysis for polyp 2320-08-IV is shown in figure 17 A. In total, 41 samples were analyzed of which two failed amplification (4.9%), 6 show microsatellite instability (14.6%) and 33 were microsatellite stable (80.5%). From the 6 MSI samples, only one sample shows microsatellite instability in two of the three markers (MSI-high). In the other 5 samples only one of the three markers was unstable (MSI-low). Five of six MSI samples were localized at the top of the crypts or at the outer side of the polyp tissue, respectively. Comparison of the marker analysis with the immunohistochemical staining of the MLH1 protein showed a good concordance of the results (Fig. 17). *MLH1* analysis revealed that about 90% of the cells were positive for the presence of the MLH1 protein (Fig. 17 B) and 80.5% of all analyzed samples were microsatellite stable. The assumption that presence of the MLH1 protein causes microsatellite stability (MSS) of the tumour tissue was thus confirmed.

Figure 18 A shows an overview of the microsatellite analysis for polyp 4407-09 of patient A. In total, 113 samples of the polyp were analyzed. Ninety-eight samples were microsatellite stable (86.7%), 13 show microsatellite instability (11.5%) and two failed amplification (1.7%). In 6 of 13 MSI samples, only one of the three markers was unstable (MSI-low). The other 7 samples show microsatellite instability in two of the three markers (MSI-high). All of the 7 MSI-high samples were localized at the top or almost at the top of the crypts. Four of the MSI-low samples were localized at the middle part of the crypts and two of them were even localized at the bottom of one crypt. MLH1 immunostaining shows positive staining of about 80% of the cells which means presence of the MLH1 protein (Fig. 18 B). Compared to the marker analysis (86.7% MSS), a high concordance of the results was obtained (Fig. 18). In the detail image of MLH1 staining of polyp 4407-09 single cells can be differentiated (Fig. 19). Dark brown (positive) stained cell nuclei at the bottom of a crypt are clearly visible (Fig. 19 a). The cells become lighter brown when the distance to the top of the crypt is reduced. Between these brown coloured cells some blue stained (negative) ones are identifiable (Fig. 19 b) which may be a template for microsatellite instability. Non-mitotic epithelial cells encompassing the crypts lack active MLH1 protein and are therefore stained blue.
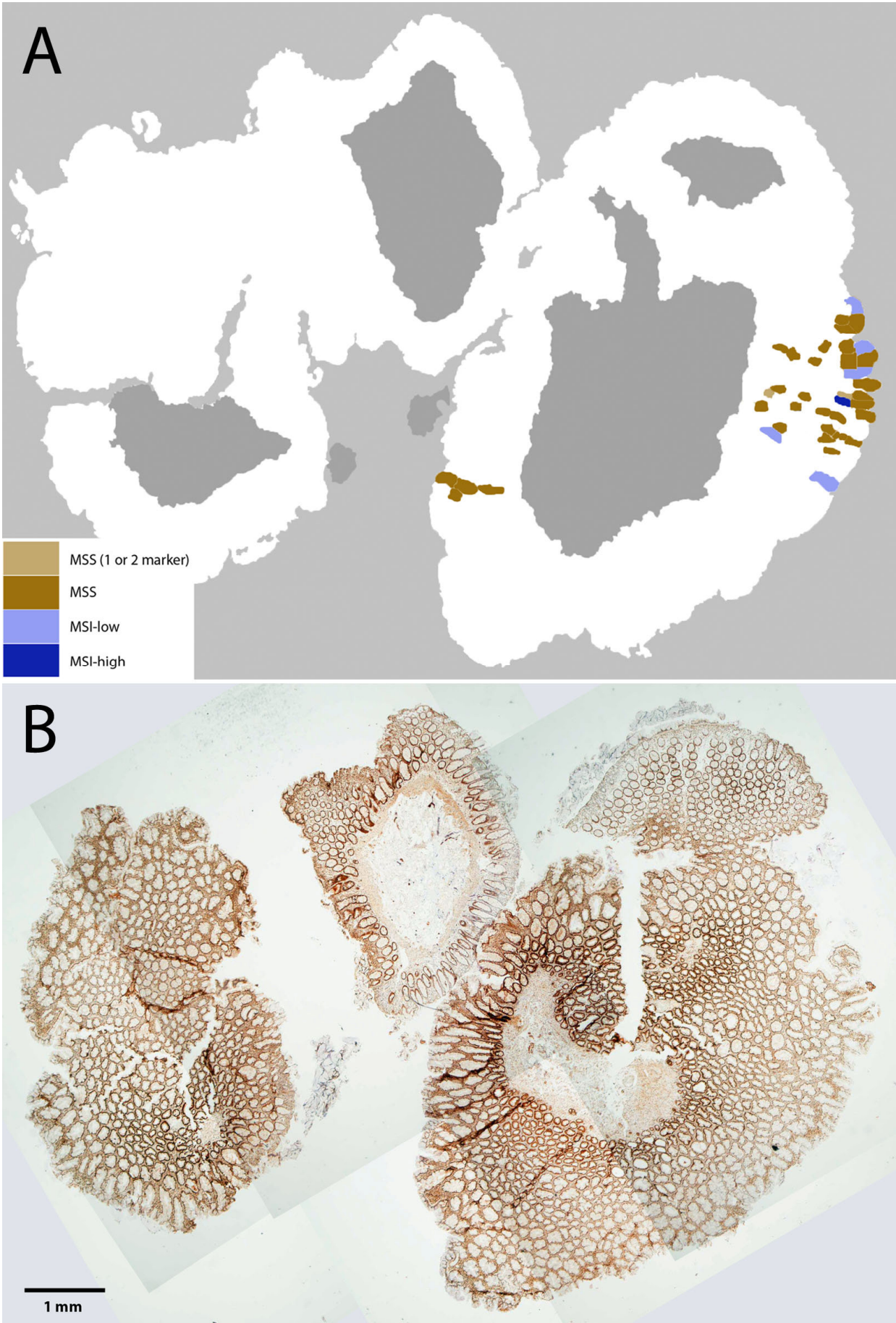
Fig. 17: Analysis of microsatellite instability of polyp 2320-08-IV of patient A. A) Results of fragment length analysis of the microsatellite markers BAT25, BAT26 and BAT40. Light brown: at least one of the

three markers shows microsatellite stability (MSS), results for one or two of the markers failed; brown: MSS; light blue: one of the three markers shows microsatellite instability (MSI-low); dark blue: two or three markers show MSI-high. B) Immunohistochemical staining of the MLH1 protein. Brown staining of nuclei means presence and blue staining means absence of the MLH1 protein in the cell. Positive staining is shown in 90% of the cells in the tumour tissue area.
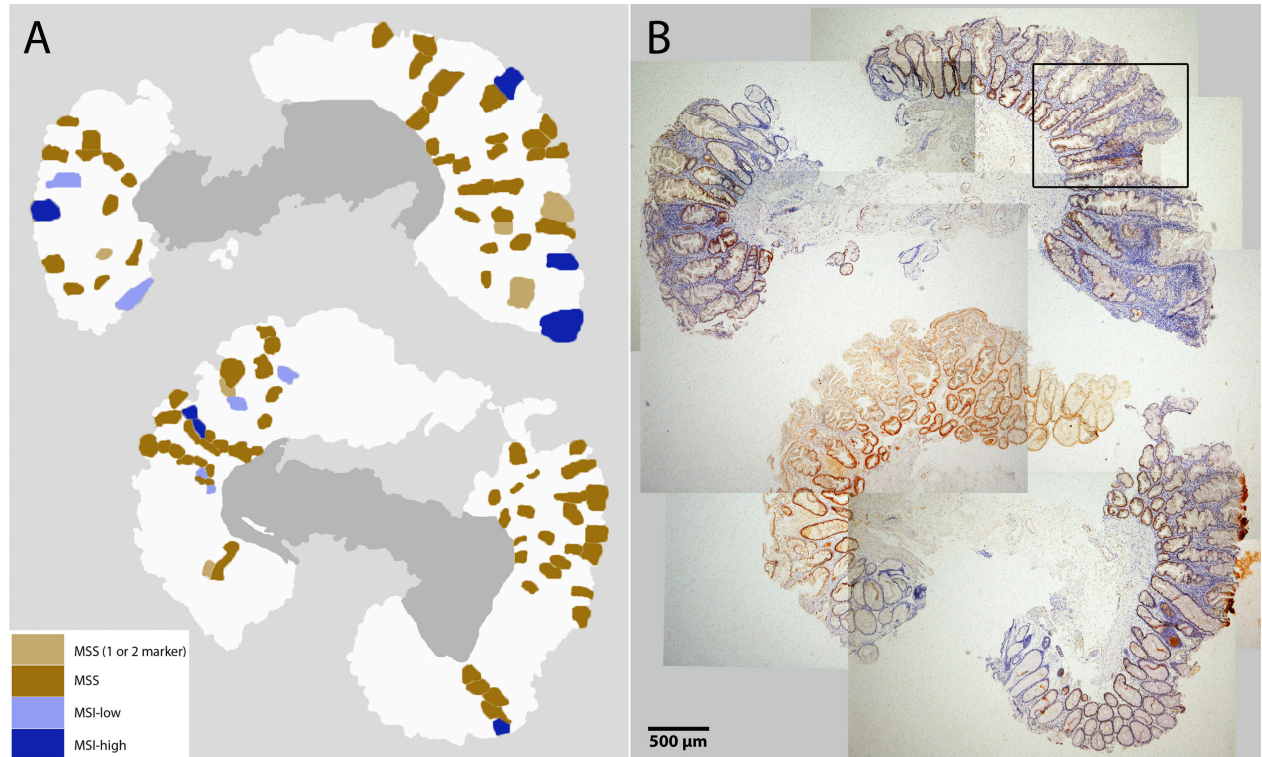
Fig. 18: Analysis of microsatellite instability of polyp 4407-09 of patient A. A) Results of fragment length analysis of the microsatellite markers BAT25, BAT26 and BAT40. Light brown: at least one of the three markers shows microsatellite stability (MSS), results for one or two of the markers failed; brown: MSS; light blue: one of the three markers shows microsatellite instability (MSI-low); dark blue: two or three markers show MSI-high. B) Immunohistochemical staining of the MLH1 protein. Brown staining of nuclei means presence and blue staining means absence of the MLH1 protein in the cell. Positive staining is shown in 80% of the cells in the tumour tissue area.
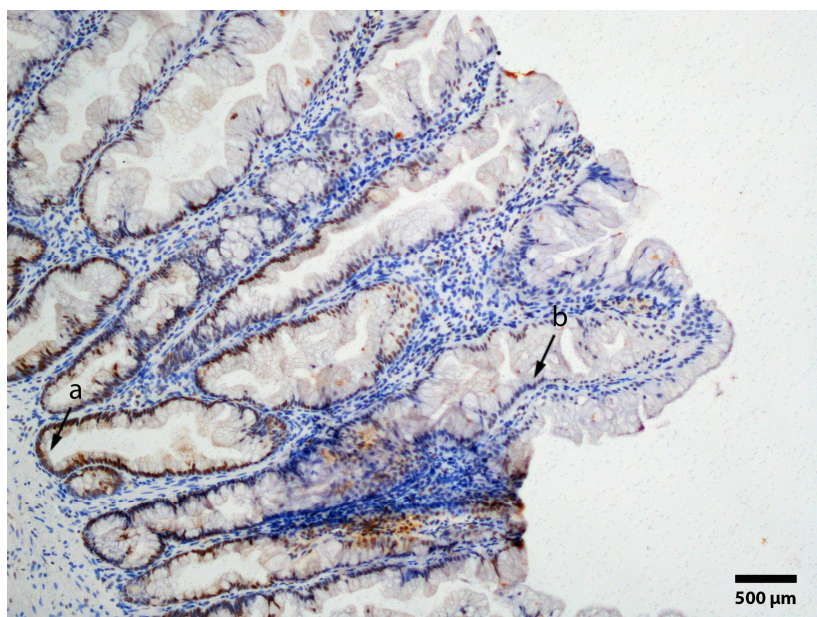

Fig. 19: Detail of figure 18 B. Immunohistochemical staining of the MLH1 protein. a) The arrow indicates the brown staining which represents the presence of the MLH1 protein in the cell nuclei at the bottom of the crypt. b) The arrow indicates the predominantly blue rather than brown staining of the cell nuclei at the top of the crypt which means absence of the MLH1 protein in the cell. Non-mitotic epithelial cells lack the MLH1 protein and are therefore stained blue.

Patient B

For patient B, fragment length analysis revealed fragment lengths of 122/117 bp for BAT25, 116/118 bp for BAT26 and 126/119 bp for BAT40 as wild type status (Fig. 20).

Fig. 20: Fragment length analysis of the microsatellite markers BAT25, BAT26 and BAT40 of patient B. Peak pattern show the wild type distribution of the different marker fragments. Arrows indicate the average fragment length of the markers: BAT25 121/117 bp, BAT26 116/118 bp, BAT40 126/119 bp. Blue: forward primer, green: reverse primer.

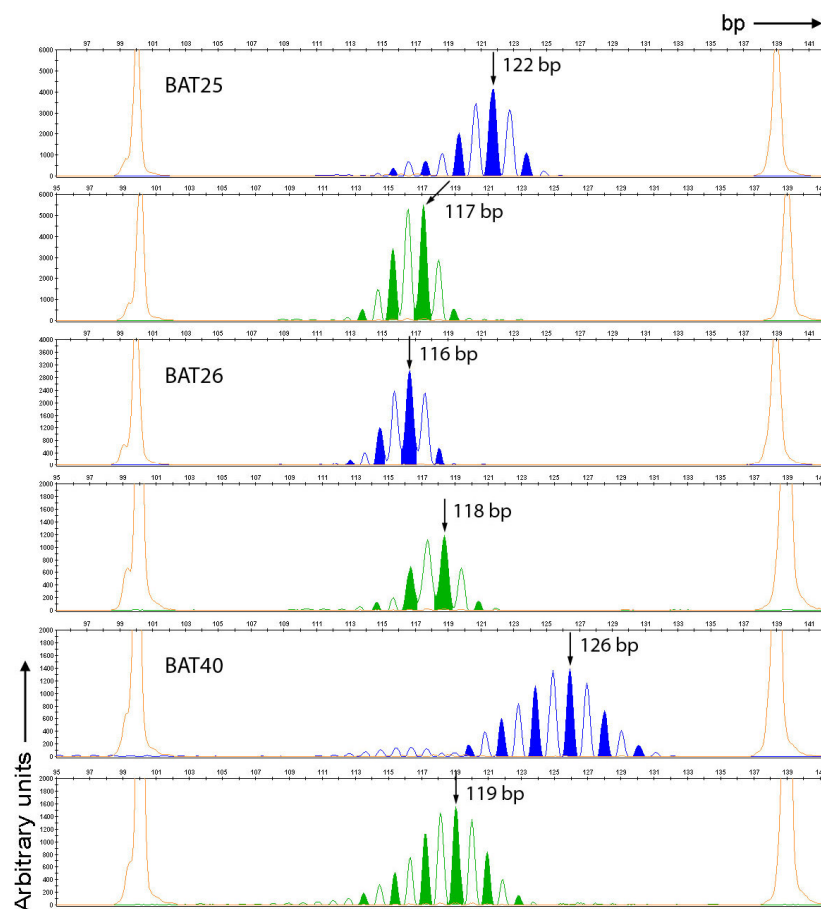The results of microsatellite marker analysis for polyp 13342-f1 is shown in figure 21 A. Fifty-four samples of the polyp tissue were analyzed in total. Amplification failure occurred in 1.9% (1 of 54) of the cases, microsatellite instability was detected in 11.1% (6 of 54) of all samples and 87.0% (47 of 54) of the samples were microsatellite stable. In 5 of the 6 MSI samples only one of the three markers was unstable (MSI-low) and in one sample microsatellite instability in two of the three markers (MSI-high) was detected. Two of the MSI-low samples, at the bottom of the crypt, are localized in the sessile serrated adenoma area of the polyp. The other four MSI samples are localized in the tubular adenoma area of the polyp, in the middle part or at the top of the crypts. Immunohistochemical MLH1 staining yielded about 90% positive stained cells for both the sessile serrated and the tubular adenoma (Fig. 21 B). A high concordance of the results of the marker analysis (87.0% MSS samples) and the MLH1 staining (90% positive stained cells) was obtained (Fig. 21).
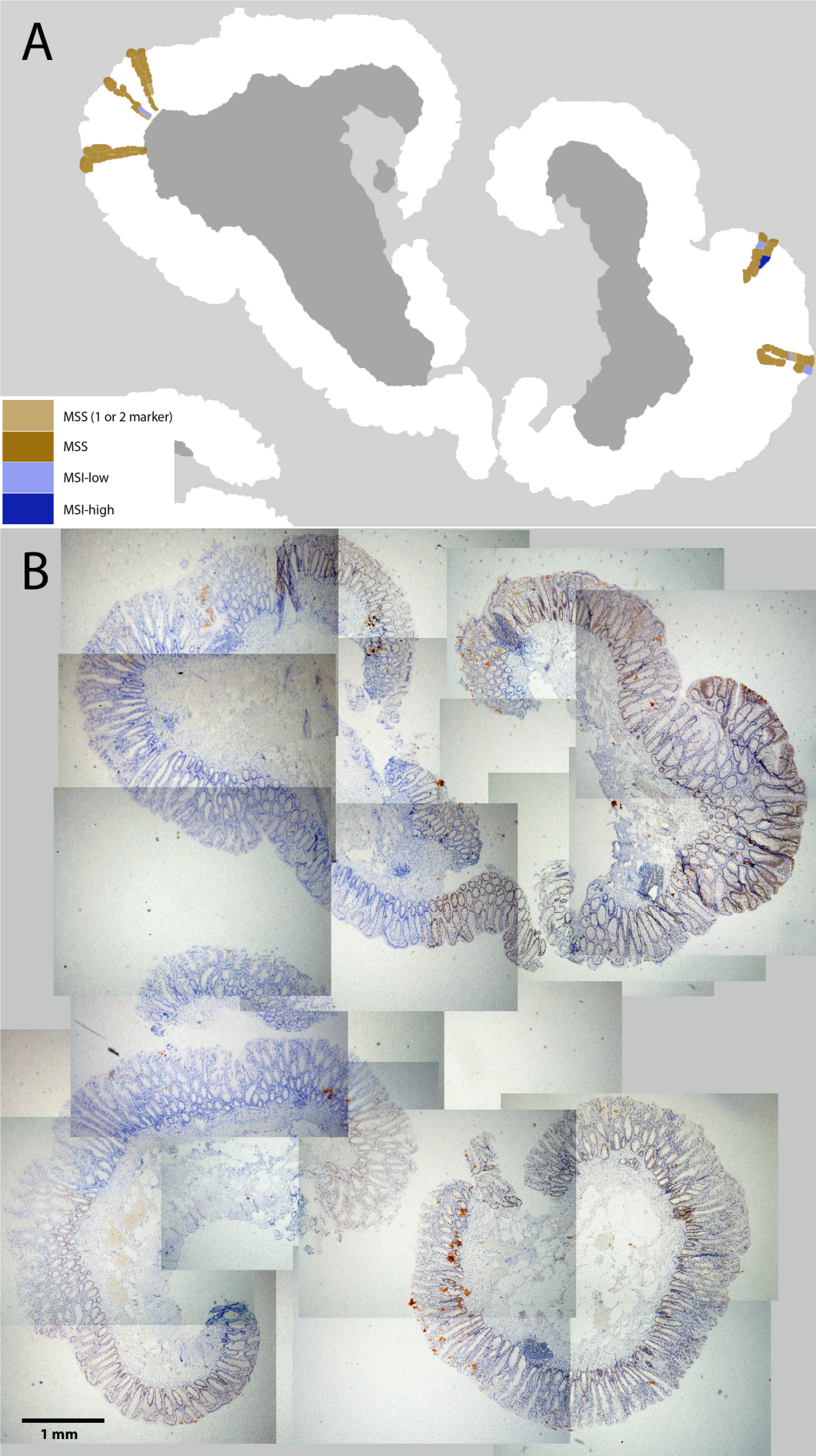
	MSS (1 or 2 marker)
	MSS
	MSI-low
	MSI-high

Fig. 21: Analysis of microsatellite instability of polyp 13342-f1 of patient B. A) Results of fragment length analysis of the microsatellite markers BAT25, BAT26 and BAT40. Light brown: at least one of the three markers shows microsatellite stability (MSS), results for one or two of the markers failed; brown: MSS; light blue: one of the three markers shows microsatellite instability (MSI-low); dark blue: two or three markers show MSI-high B) Immunohistochemical staining of the MLH1 protein. Brown staining of nuclei means presence and blue staining means absence of the MLH1 protein in the cell. Positive staining is shown in 90% of the cells in the tumour tissue area.

5.1.3 Comparison of mutation and microsatellite analysis

When comparing the microsatellite marker analysis of all three polyps with the mutation analysis there is no explicit coherence of samples carrying a mutation and MSI. In polyp 2320-08-IV of patient A, only one of three MSI-low samples carried a mutation in exon 3 of the *KRAS* gene and a mosaic form of the hotspot *BRAF* mutation. The other two samples displayed a wild type sequence in the analyzed *KRAS* gene or the amplification failed in part, respectively (Fig. 22). In the second polyp of patient A, 4407-09, there were only two MSI-low samples which displayed a mosaic form of the *BRAF* hotspot mutation. Four other samples, either MSI-low or -high, were analyzed as wild type for mutations in *BRAF* and *KRAS* (Fig. 23). In polyp 13342-f1 of patient B one of four MSI samples carried a mutation in exon 15 of the *BRAF* gene. Three wild type samples according to *KRAS* or the *BRAF* hotspot mutation showed MSI-low or -high (Fig. 24). Only samples which gave results in at least two of all three parts of analysis were taken into consideration.

An efficiency of 97.6% (203 of 208) for microsatellite marker analysis after low-volume (LV) multiplex polymerase chain reaction (PCR) was achieved for all three colon polyps. In only 2.4% (5 of 208) of all cases, none of the three microsatellite markers was amplified. In contrast, the efficiency for sequencing analysis was slightly lower with 79.8% (166 of 208). The amplification failed in 42 of 208 (20.2%) cases when none of the three gene fragments was amplified in the multiplex PCR.

Fig. 22: Comparison of mutation and microsatellite marker analysis of polyp 2320-08-IV of patient A. A) Distribution of the hotspot mutation c.1799 T>A, p.Val600Glu in exon 15 of the *BRAF* gene within the polyp tissue section. B) Localization of all mutations found in the genes *BRAF* exon 15 and *KRAS* exons 2 and 3. C) Fragment length analysis of the microsatellite markers BAT25, BAT26 and BAT40. Samples which carry a mutation and are microsatellite unstable are circled in all three images.

Fig. 23: Comparison of mutation and microsatellite marker analysis of polyp 4407-09 of patient A. A) Distribution of the hotspot mutation c.1799 T>A, p.Val600Glu in exon 15 of the *BRAF* gene within the polyp tissue section. B) Localization of all mutations found in the genes *BRAF* exon 15 and *KRAS* exons 2 and 3. C) Fragment length analysis of the microsatellite markers BAT25, BAT26 and BAT40. Samples which carry a mutation and are microsatellite unstable are circled in all three images.
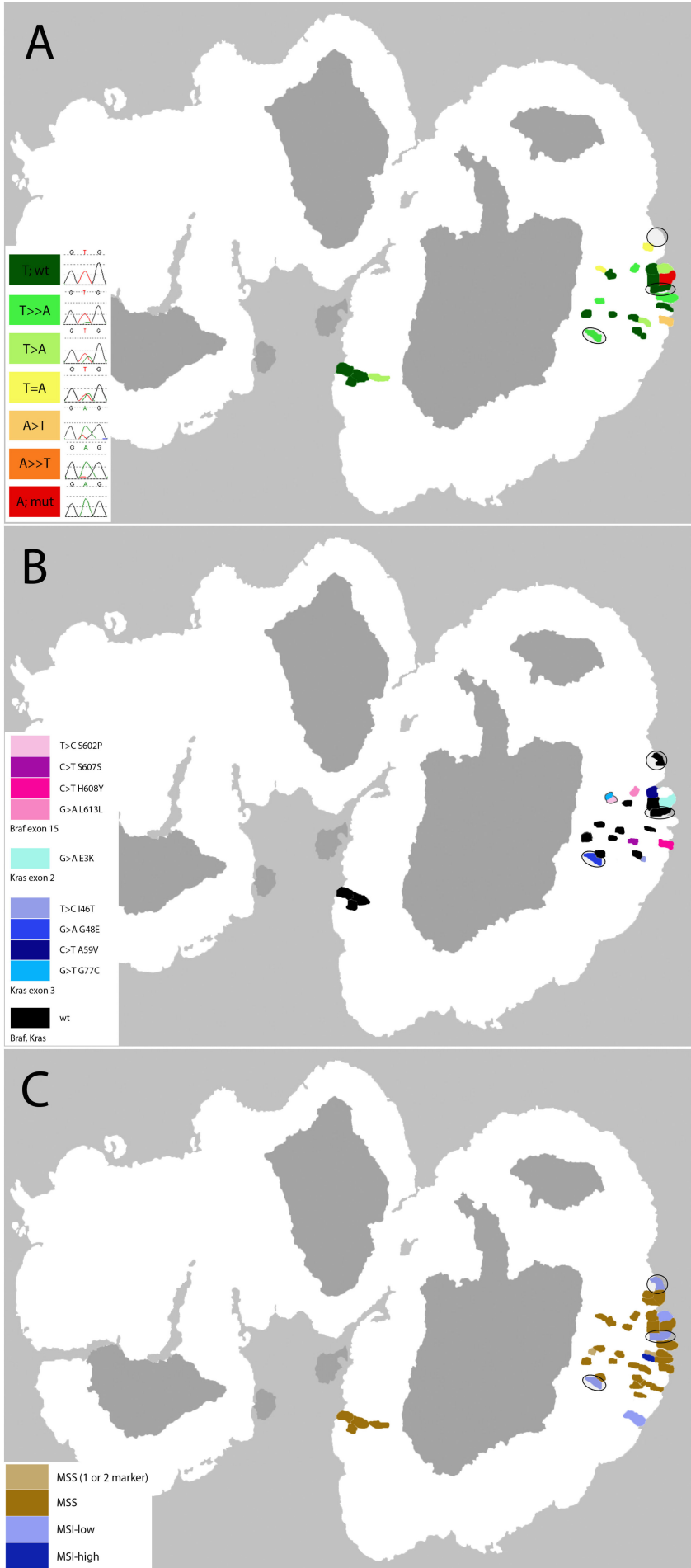
Fig. 24: Comparison of mutation and microsatellite marker analysis of polyp 13342-f1 of patient B. A) Distribution of the hotspot mutation c.1799 T>A, p.Val600Glu in exon 15 of the *BRAF* gene within the polyp tissue section. B) Localization of all mutations found in the genes *BRAF* exon 15 and *KRAS* exons 2 and 3. C) Fragment length analysis of the microsatellite markers BAT25, BAT26 and BAT40. Samples which carry a mutation and are microsatellite unstable are circled in all three images.
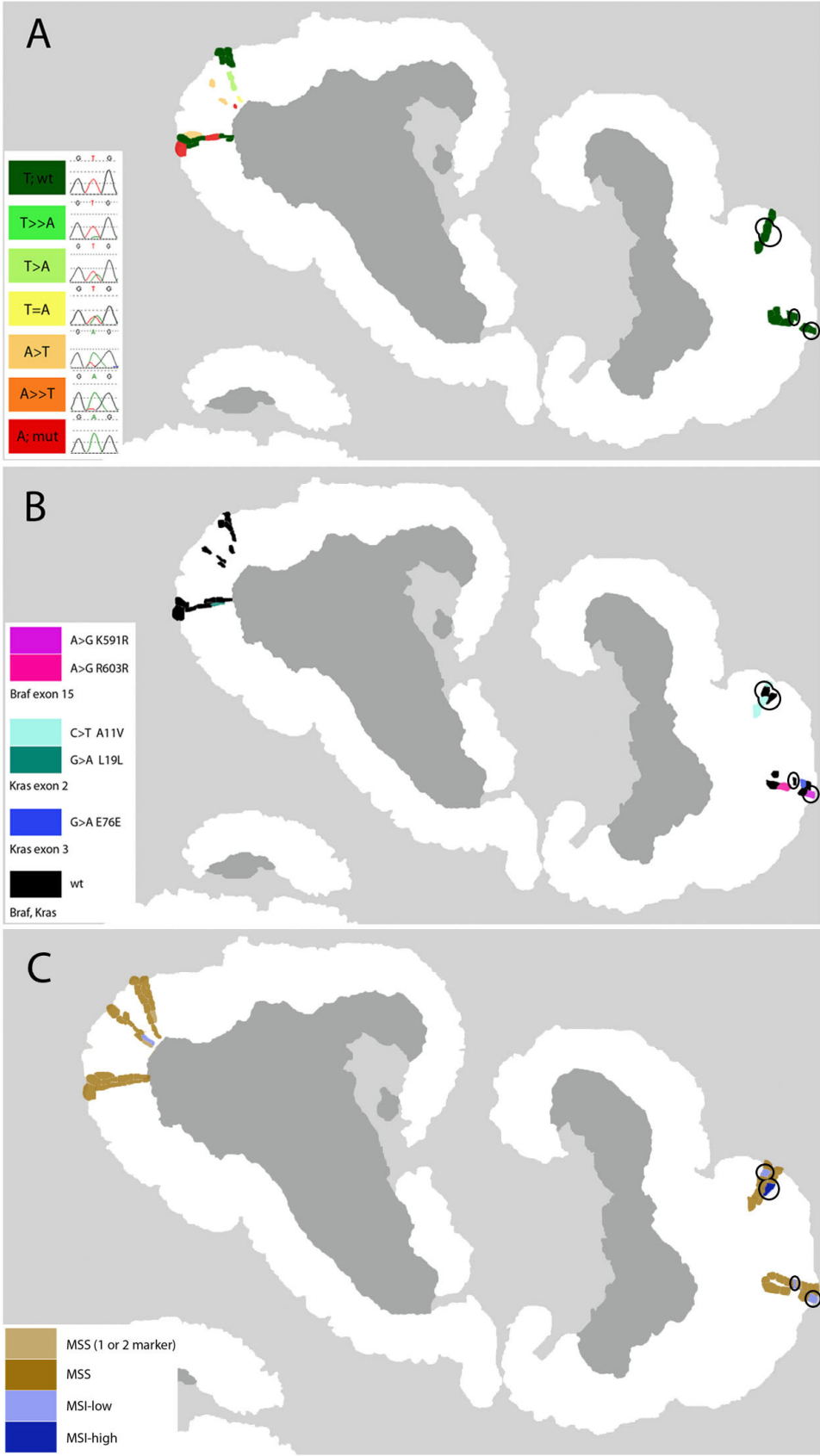
5.2 Mutation analysis of single cells

5.2.1 Efficiency of low-volume multiplex PCR with fixed single cells

The efficiency of a low-volume multiplex PCR combining the three microsatellite markers D7S1824, D9S302 and D10S2325 using fixed single cells was analyzed. In preliminary experiments the combination of the three markers for multiplex PCR was tested and optimized using genomic DNA of an unaffected male. In total, 153 laser microdissected diploid single cells of the same person were amplified. For each marker two alleles were expected; all together a total number of 918 (6x153) alleles could be obtained. A full profile of the three markers consisting of 6 alleles is shown in figure 25.
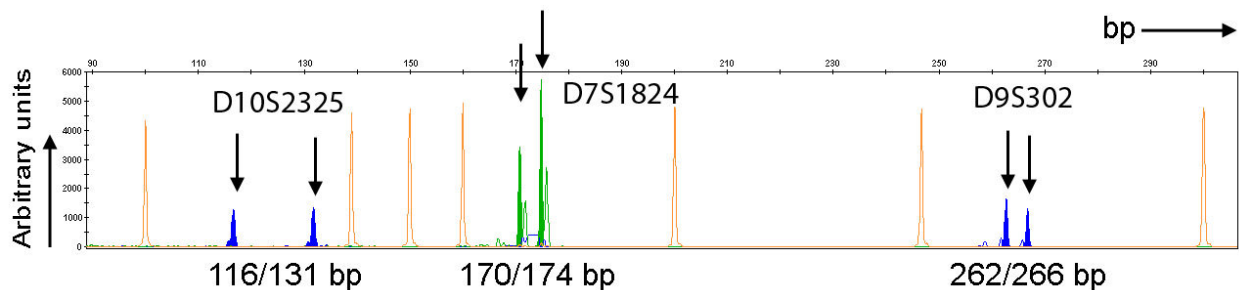

Fig. 25: Results of fragment length analysis of the microsatellite marker PCR using fixed single cells. The full profile consists of 6 alleles, generated with the three primer pairs D10S2325: 116 bp/131 bp; D7S1824: 170 bp /174 bp and D9S302: bp/179 bp. Size standard: orange peaks.

The amplification efficiency ranged from 75.2 to 88.9% for each allele. On average, an amplification efficiency of 80.0% was achieved in the low-volume multiplex PCR (Tab. 18). All 29 negative controls analyzed in fragment length analysis were negative for the expected alleles. In one negative control an additional allele at 264 bp was detected. A full profile with 6 alleles was obtained from all 9 positive controls with 100pg genomic DNA.

Tab. 18: Results of the microsatellite marker PCR with single cells

Marker/ alleles	D7S1824 170 bp/174 bp		D9S302 262 bp/266 bp		D10S2325 116 bp/131 bp		Total
Total number of analyzed cells	153 cells		153 cells		153 cells		918 alleles
Negative amplifications %	18.3 (28/153)	11.1 (17/153)	23.6 (36/153)	24.8 (38/153)	19.0 (29/153)	23.6 (36/153)	20.0 (184/918)
Amplified alleles %	81.7 (125/153)	88.9 (136/153)	76.4 (117/153)	75.2 (115/153)	81.0 (124/153)	76.4 (117/153)	80.0 (734/918)

5.2.2 Establishment of a single cell analysis system for patient-specific *APC* mutations

For the establishment of single cell analysis, fixed cells of three patients carrying heterozygous germ line mutations in the adenomatous polyposis coli (*APC*) gene were used (patient C: c.2612delG, patient D and E: c.3183-3187delACAAA) (Fig. 26).

In an initial experiment the amplification efficiency of stained (Giemsa) and unstained fixed single lymphocytes was compared. Twenty-two stained and 22 unstained cells of each of the patients C and D were amplified in a nested PCR reaction using the primer pairs PC1/PC2 and PD1/PD2 (see tables 3 and 9). The amplification efficiency of the nested PCR product was analyzed using agarose gel electrophoresis. For patients C and D, an amplification product of stained cells was obtained in 27.3% (6 of 22) of cases. In contrast, amplification efficiency of the unstained cells yielded 81.8% (18 of 22) for patient C and 40.9% (9 of 22) for patient D. Only samples with an amplification product were used for sequencing analysis. In total, 24 samples of patient C and 15 samples of patient D (stained and unstained) were sequenced.
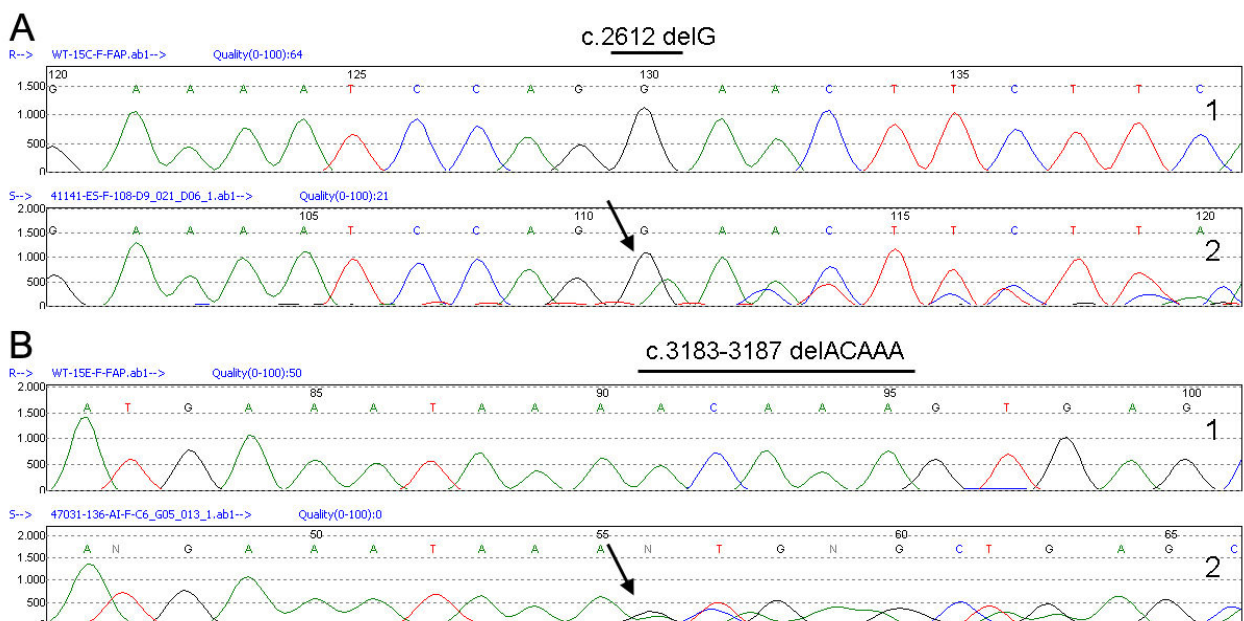
Fig. 26: Specific mutations in the *APC* gene of familial adenomatous polyposis (FAP) patients C, D and E. A) Sequencing shows the heterozygous 1 bp deletion (c.2612delG) (arrow) of patient C. Lane 1: wild type sequence of exon 15; lane 2: forward patient-specific sequence B) shows the wild type sequence in lane 1 and the heterozygous sequence with the 5 bp deletion (c.3183-3187delACAAA) (arrow) of patients D and E in lane 2 (forward).

Sequencing analysis resulted in 17 homozygous samples for patient C including 10 wild type samples and 7 samples carrying the deletion c.2612delG. Two samples were

analyzed as heterozygous which means both the wild type and the mutated allele of patient C were detected in a single cell. Analysis failed in 5 of 24 samples.

For patient D, sequencing analysis resulted in 11 homozygous samples of which 8 were wild type and three showed the deletion c.3183-3187delACAAA. Analysis failed in 4 of 15 samples. Sequencing yielded very low heterozygosity rates of 10.5% (2 of 19) for patient C and 0.0% (0 of 11) for patient D which means that staining of the cells lead to high allelic drop out rates. In keeping with these results, only unstained cells were used in the following experiments.

PCR conditions were optimized comparing different combinations of temperatures and types of PCR in first (LV-PCR) and secondary (nested) PCR. For each of the patients C and D, 16 cells per reaction condition were amplified. The primary PCR was carried out as 'touch down' (TD) PCR or as specific PCR with a 59°C annealing step. 'Touch down' PCR means a temperature increment of -1°C per each cycle starting at 64°C to 50°C and 25 cycles at 50°C (see Tab. 4). The specific PC R was carried out as described in table 6 but with an annealing step at 59°C for 90 s ec and 20 cycles. Secondary PCR was carried out either as TD or as specific PCR. An overview of the combinations for first and secondary PCR is given in figure 27.
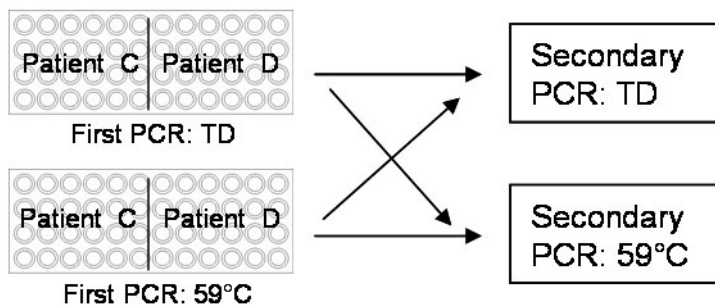
Fig. 27: PCR conditions and combinations in first and secondary PCR. TD: touch down PCR; 59°C: specific PCR with an annealing step at 59°C.

The results of the amplification efficiency for every PCR condition are listed in table 19. When comparing all results, it is obvious that the highest efficiency was achieved with a combination of TD PCR followed by a specific secondary PCR. Although a specific PCR followed by either another specific or a TD PCR yielded the same efficiency for patient C, the combination TD – specific PCR gave the best results for both patients and was chosen for further experiments.

Tab. 19: Amplification efficiency of single cell PCRs carried out with different combinations of PCR conditions.

PCR conditions	TD – TD	TD - 59℃	59℃ – TD	59℃ – 59℃
Patient C	87.5 % (14/16)	100% (16/16)	100% (16/16)	100% (16/16)
Patient D	62.5% (10/16)	81.3 % (13/16)	50.0% (8/16)	37.5% (6/16)

The results of sequencing analysis are summarized in table 20. For each condition and patient 16 cells were analyzed. In most cases, the heterozygosity rates were increased compared to the previous experiment with stained and unstained cells. Nevertheless, further optimization of PCR conditions including temperature, cycle number, primer design and combination were carried out in several experiments.

Tab. 20: Results of the sequencing analysis of single cell PCRs carried out with different combinations of PCR conditions. wt: wild type; mut: mutation.

Patient		PCR conditions			
		TD – TD	TD - 59℃	59℃ – TD	59℃ – 59℃
Patient C	wt	6	6	3	2
	mut	6	8	8	10
	heterozygous	2	2	2	4
	Heterozygosity rate %	14.0 (2/14)	12.5 (2/16)	15.3 (2/13)	25.0 (4/16)
	failed	2	-	3	-
Patient D	wt	4	4	4	4
	mut	6	9	3	1
	heterozygous	-	-	1	1
	Heterozygosity rate %	0.0 (0/10)	0.0 (0/13)	12.5 (1/8)	16.7 (1/6)
	failed	6	3	8	10

In a final experiment, a multiplex PCR was performed for 22 and 21 fixed single lymphocytes and two negative controls for patients C and D respectively and for 65 single cells and 19 negative controls for patient E. The mutation-specific amplification products were part of the initial nested PCR reactions. The amplification products of microsatellite marker PCR served as control for the detection of allelic drop out or contamination events. To detect patient-specific deletions, the PCR products were sequenced (Fig. 26). In addition to sequencing, fragment length analysis (patient D and E) was performed. Amplification efficiency of single cell PCR ranged from 77.3% to

93.8%, shown with gel electrophoresis and fragment length analysis. Heterozygosity rates between 72.2% and 100.0% were achieved. For the 5 bp deletion c.3183-3187delACAAA (patients D and E) heterozygosity efficiency was determined for full profiles of the multiplex PCRs in fragment length analysis. The full profile for patient D (82.3%) consists of the alleles 118/120 bp (D5S346) and 137/142 bp (PD2-FAM), for patient E (57.4%) the alleles 111 bp/119 bp (D5S346), 137 bp/142 bp (PB2-FAM) and 173 bp/179 bp (D5S82) (Fig. 28). All results of this single cell analysis are summarized in table 21.
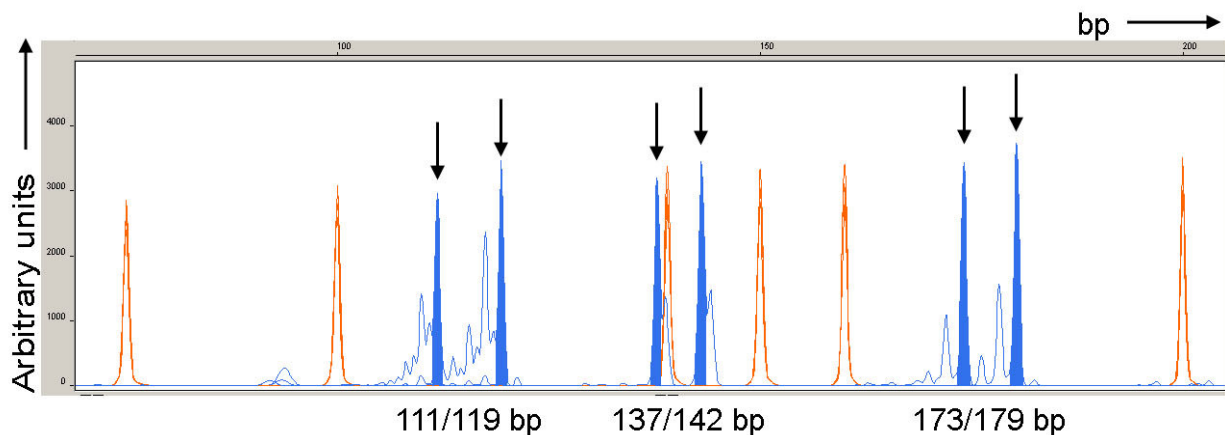
Fig. 28: Results of fragment length analysis of the multiplex PCR for patient E (c.3183-3187delACAAA). The full profile consists of 6 alleles, generated with the three primer pairs D5S346: 111 bp/119 bp; PD2-FAM: 137 bp (mutated)/142 bp (wild type) and D5S82: 173 bp/179 bp. Size standard: orange peaks.

Tab. 21: Results of the final single cell analysis

Patient/Loci	Amplification %	Heterozygosity %	Contamination %	Analysis method
Patient C c.2612delG	77.3 (17/22)	81.3 (13/16)	0.0 (0/16)	Gel electrophoresis Sequencing analysis
Patient D c.3183-3187delACAAA	90.5 (19/21)	72.2 (13/18)	0.0 (0/18)	Gel electrophoresis Sequencing analysis
	85.7 (18/21)	83.3 (15/18)	0.0 (0/18)	Fragment length analysis
Patient D D5S346	85.7 (18/21)	100.0 (18/18)	0.0 (0/18)	Fragment length analysis
Patient E c.3183-3187delACAAA	93.8 (61/65)	83.6 (51/61)	0.05 (3/61)	Fragment length analysis
Patient E D5S346	89.2 (58/65)	93.1 (54/58)	0.02 (1/58)	Fragment length analysis
Patient E D5S82	92.3 (60/65)	76.7 (46/60)	0.0 (0 /60)	Fragment length analysis

6 Discussion

6.1 Characterization of colon polyp tissue

Colorectal cancer (CRC) is the second leading cause of death amongst cancer syndromes in the general population (Robert Koch-Institut, Mäkinen 2007). This complex disease is classified according to clinical, histological, morphological and molecular features but still much work has yet to be done for further understanding of tumour development (Jass 2007). Colorectal cancer is mainly characterized by the occurrence of a variable number and different types of polyps throughout the colon. The histological and morphological characterization of colon polyps enables the determination of carcinogenesis risk in affected patients in many cases (Kirchner and Reu 2008). Despite improved diagnosis and therapy in recent years, several questions remain unsolved. In some cases unequivocal histological differentiation of the type of colon polyp is not possible (Holinski-Feder and Morak 2010). Molecular analysis of colon polyp tissue allows deeper insights into tumourigenesis of a single polyp. Important molecular features for classification include the analysis of the microsatellite instability (MSI) status and occurrence of mutations in the proto-oncogenes *BRAF* and *KRAS* (Boland et al. 1998, Garnett and Marais 2004, Kranenburg 2005, O'Brien et al. 2006).

In the first part of this work small tissue particles isolated from three colon polyp sections of two patients were analyzed simultaneously with regard to mutations in the *BRAF* and *KRAS* genes and the microsatellite instability status.

Isolation of sample material was performed via laser microdissection from 6 µm thick unstained tissue sections of the colon polyps. The size of the isolated particles varied, containing cells between 10 and 70 cells per particle on average (Fig. 7). Estimations of the cell number were reached by comparison of stained and unstained tissue sections but determining the exact number was not possible. Furthermore, cell number variation may occur due to slightly deviant thickness of the tissue sections from one end to the other. Additionally, there is the possibility of isolating only parts of a cell as cells were not arranged in a monolayer within the section. Despite these reasons, successful analysis of samples containing approximately 10 or even less cells could be performed. Varying amplification efficiencies independent of particle size or cell number could be

observed. It is assumed that this is due to different quality of tissue sections influenced by the preparation procedure including fixation and subsequent removal of the paraffin. There is evidence of degradation and fragmentation of DNA caused by fixation with formalin or formaldehyde, respectively. The cross-linking of proteins and DNA within a cell caused by formaldehyde leads to DNA strand breaks; the average DNA fragment length which can be found in fixed tissue is approximately 300 bp (Lehmann and Kreipe 2001, Hunt 2008). Therefore only short sequences were amplified in this work, although amplification failure cannot be completely avoided in doing so. The risk of additional degradation of DNA possibly caused by hematoxylin and eosin (HE) staining was excluded by the use of unstained tissue sections (Burton et al. 1998, Murray 2007). Hematoxylin stains negatively charged molecules like nucleic acids and eosin stains positively charged molecules including positively charged amino acids (Bova et al. 2005). DNA isolation from such stained tissue sections is possible if the tissue is well preserved. Although there is no evidence of HE staining inhibiting polymerase chain reaction (PCR) directly, as a precaution, the problem was circumvented. Furthermore, visibility of tissue structures is dramatically reduced when using HE stained tissue sections without the cover slip which is necessary for laser microdissection (Bova et al. 2005). For this reason, Bazan and colleagues added a droplet of oil directly onto the stained tissue section and visibility was increased when the oil spread over the slide (Bazan et al. 2005). However, this step is a source of increased contamination risk as the sample is in contact with the oil prior to analysis. Moreover, though applicable when performing laser pressure catapulting isolating the sample into a plastic cap, it is not applicable with the recently developed single particle adsorbing transfer system (SPATS; Woide et al. 2009) due to increased capillary forces between sample and slide. Therefore, unstained tissue sections, which also allow a high visibility and a good distinction of crypts and epithelium cells, were used in this work.

An outstanding advantage of the horizontal particle transfer via SPATS is the reliable and precise transfer and release of sample material to the planar chemically structured PCR slide (Schmidt et al. 2005, Woide et al. 2007). The whole procedure is performed under optical control which facilitates easy identification of a sample on the PCR glass slide (Fig. 4). This is in contrast to isolation of single particles into plastic caps because retrieving of the sample is not guaranteed in every case (Schütze and Lahr 1998). Furthermore, horizontal transfer of laser microdissected sample material enables PCR analysis in 1 μl directly from fixed tissue particles. Due to selective isolation and transfer

of specific regions of interest, cross-contamination with cells of the heterogeneous neighbouring tissue can be circumvented. The following aspects and arrangements further reduced the risk of contamination. Ultra-violet light irradiation of the sample adsorbing head and the PCR glass slide ensured sterilization prior to isolation. Moreover, the sample adsorbing head of the transfer system was designed as disposable and was changed prior to isolation of different polyps (Woide et al. 2009). Fewer preparative steps, for example the use of unstained tissue sections and PCR directly from tissue samples, further reduce the risk of contamination. Naturally, appropriate laboratory equipment and cleaning procedures were used.

A fundamental factor of this approach is performing PCR directly from formalin-fixed paraffin-embedded tissue material. In general, relatively large tissue areas are necessary for DNA extraction due to loss of genomic information, e. g. caused by incomplete lysis of the sample material (Bova et al. 2005). Integration of sample denaturation into the first PCR cycle, carried out at 97℃ for 20 minutes, can circumvent this problem. Even the whole genetic information contained in very small samples is conserved and thus accessible for analysis. Mutations in only a few cells from one sample can be detected this way. This displays a great advantage as 'dilution' of mutation information below the detection limit can occur when an excess of wild type DNA is present in the sample (Bazan et al. 2005).

Although DNA extraction of tissue sections is standard in almost all laboratories performing microdissection (Spirio et al. 1998, Umetani et al. 2000, Lehmann and Kreipe 2001, Calabrese et al. 2004), some groups have different approaches. Cawkwell and Quirke also used formalin-fixed tissue particles for direct analysis in PCR reactions. But in contrast to 10 or 70 cells used here, they isolated particles in the range of 1-2 mm^2 consisting of several hundreds of cells. Some droplets of water were applied to the region of interest of the tissue section. Until the tissue was dislodged from the glass slide the samples were transferred into a PCR tube via a pipette (Cawkwell and Quirke 2000). Another approach is the direct use of proteinase K digested, laser capture microdissected sample material as template for PCR without any further washing step. Here as well, a high number of cells ranging from 500-1000 cells per sample were used as template (Dillon et al. 2001). For sensitive detection of mutations rarely occurring in only a few cells within the heterogeneous polyp tissue, it is important to isolate only a small homogeneous region of interest. Thus, the probability of containing cells carrying a mutation is strongly elevated compared to samples consisting of a high proportion of

wild type cells (Bazan et al. 2005). Giuffrè and colleagues could show that laser microdissected samples with approximately 150-500 cells achieved a significantly more specific result in microsatellite analysis when compared to hand microdissection. However, cell lysis prior to DNA extraction using proteinase K lasted 18 hours in that study (Guiffré et al. 2005). In contrast, PCR analysis was performed immediately after sample isolation using the combination of SPATS and low-volume (LV) PCR presented here.

Combined low-volume and nested PCR raises the sensitivity and efficiency of analysis applicable for templates consisting of only few cells. PCR in smaller reaction volumes are significantly more sensitive and efficient when applicable to low amounts of template material compared to PCR in larger reaction volumes (Piyamongkol et al. 2003, Proff et al. 2005, Schmidt et al. 2005, Lutz-Bonengel et al. 2007). In the study of Roehrl and colleagues the efficiency of single cell PCR from stained and fixed tissue sections was investigated. DNA was extracted from the fixed sample material and PCR was performed in 50 µl. Efficiencies of 11 to 25% were achieved for single cell PCR and efficiencies of 26 to 33% were achieved when using clusters of 10-30 cells (Roehrl et al. 1997). In another study, PCR efficiency was optimized for microsatellite marker analysis of fixed colorectal tissue samples using the markers BAT25, BAT26 and BAT40. DNA was extracted and 20 ng/µl of DNA were used as template for PCR. Reduction of fragment length revealed an amplification efficiency of 97% for the markers mentioned (Umetani et al. 2000). The efficiency of microsatellite marker analysis achieved with LV-PCR was in the same range with 96.7 and 98.1% for patients A and B, respectively. In contrast, this high efficiency was obtained using fixed sample material directly for PCR without prior DNA extraction. Another basic difference of this work is the application of a multiplex PCR combining not only the three microsatellite markers but additionally primers for the genes *BRAF* and *KRAS*.

The approach presented in this work combining laser microdissection, horizontal sample transfer and subsequent low-volume multiplex PCR is unique. Although multiplex PCR itself is a standard tool in analysis, it yet has not been applied to fixed tissue samples in a 1 µl PCR.

Analysis of the colon polyps was performed in a simultaneous approach implicating direct sequencing of *BRAF* exon 15 and *KRAS* exons 2 and 3 and microsatellite fragment length analysis. Three tissue sections of patients A and B were characterized

in respect to genetic alterations by isolating small homogeneous regions from single crypts.

Polyps 2320-08-IV and 4407-09 of patient A were classified as hyperplastic polyp and either hyperplastic polyp or sessile serrated adenoma (SSA) respectively (Fig. 6 and 10). In this case a differentiation between the two types of polyps relying only on morphological features was extremely difficult. Distinction is not possible in all cases as overlapping of morphological structures sometimes occur. This example highlights the fact that integration of molecular analysis is a basic aspect of classification and diagnosis on colorectal polyps.

In total, 41 different mutations were detected in the two polyps of patient A, of which only three have been described in the literature. For another 6 mutations, different nucleotide substitutions were described at the same amino acid positions detected here (Tab. 13 and 14). Other studies screening for mutations in *BRAF* and *KRAS* rarely detected some additional mutations besides the hotspot mutations in the sequenced exons (Davies et al. 2002, Lee et al. 2003, Sarkozy et al. 2009). This might occur, on the one hand, depending on the sample material and, on the other hand, due to limited sensitivity in detection when analyzing more than 1 ng of genomic DNA extracted from heterogeneous tissue samples (Grimmond et al. 1992, Fransèn et al. 2004). However, even when using a highly sensitive method like high resolution melting curve analysis such a high number of mutations besides the hotspot mutations in *KRAS* and *BRAF* had not been detected (Seth et al. 2009).

The mutation c.1799 T>A, p.Val600Glu (in the following named V600E) in exon 15 of the *BRAF* gene leads to an amino acid substitution from valine to glutamic acid. This causes the constitutive activation of the protein which is part of the MAP-kinase signalling pathway responsible for cell proliferation, among other functions (Davies et al. 2002, Garnett and Marais 2004). This mutation plays an important role in early tumourigenesis, especially in colorectal cancer (Yang et al. 2004, Young and Jass 2006). The activating V600E mutation was detected in 10 samples of polyp 2320-08-IV and in 44 samples of polyp 4407-09 (Fig. 8 and 11). Considering the crypt structure, it was supposed that a specific distribution of the mutation within one crypt might have been observed. For example, if the mutation occurs in a mitotic stem cell at the bottom of a crypt the clones of this cell were assumed to carry the same mutation too. So the mutation should have been detected along the crypt in almost every cell from the bottom to the top. Due to relatively slight deviations in the crypt structure of hyperplastic

polyps compared to normal polyps (Young and Jass 2006, Mäkinen 2007), a similar mutation detection was expected, at least in polyp 2320-08-IV. However, a predominant distribution of the mutation within the tissue section could not be observed in either polyp. The V600E mutation was detected in different regions of the polyp tissue not limited to either the top or bottom of crypts. In several samples a mosaic form of the mutation was manifested (Fig. 3 and 6, for mosaic forms see colour legend). Mosaic means that not all cells of a sample carry the mutation and/or that cells are either heterozygous or homozygous related to the mutation. Interestingly, in one case the fully manifested mutation was detected in one sample (polyp 2320-08-IV) right next to 3 wild type samples (Fig. 8). A fluent changeover from wild type to mutated samples was not observed. Considering these results it can be concluded that the mutation V600E occurs spontaneously in several cells throughout the polyp tissue independently from one another. Notably, besides the V600E hotspot mutation, a large number of mutations in exon 15 of the *BRAF* gene as well as in exons 2 and 3 of *KRAS* were detected. Most of these mutations were not described yet. This could be due to the fact that only samples with less than 100 cells were analyzed in this work. Usually, when large samples with heterogeneous cell populations were analyzed, genetic information of few cells cannot be detected as this is below the detection limit (Bazan et al. 2005). Remarkably, some of these mutations occur at the same amino acid position but not at the same nucleotide (Tab. 13 and 14). Comparing both polyps of patient A, each had a different mutation pattern independent from one another. Only one mutation, a C to T transition at histidine 608 occurred at the same nucleotide c.1822 in both polyps.

Interestingly, in two samples from a crypt of polyp 4407-09 which was classified as normal, the mutations Gly615Arg in exon 15 of *BRAF* and His27His in exon 2 of *KRAS* were detected (Fig. 10 and 11). This might display a beginning process of tumourigenesis before histologically normal tissue develops aberrant crypt structures. The genetic cause for these results, if the mutations are important for tumourigenesis or are only by-products of cells with a deficient repair system, has to be investigated further.

Recently, several studies verified that mutations in *BRAF* and *KRAS* are mutually exclusive in sporadic MSI CRC (Rajagopalan et al. 2002, Deng et al. 2004, Koinuma et al. 2004, Seruca et al. 2009). Although it is not discussed explicitly in every case, this is mostly related to the V600E mutation in *BRAF* and one of the hotspot mutations at

codons 12 or 13 (and perhaps codons 59, 61 and 63) of the *KRAS* gene (Seth et al. 2009). Mutations in these codons of *KRAS* are associated with activation of the protein function as they are located in important ligand binding sites of the protein (Grimmond et al. 1992, Kranenburg 2005). Both genes are components of the MAPK-ERK signalling pathway and the activation of either *BRAF* of *KRAS* might be sufficient for activation of the pathway. However, it was demonstrated here that V600E occurred together with mutations in the *KRAS* gene in the same samples (Fig. 8 and 11). In one case, the V600E mutation was detected simultaneously with the mutation c.175 G>A, p.Ala59Thr, a well-known hotspot mutation of *KRAS* (Fig. 11; Swiss-Prot variant VAR_016030 in P01116; Grimmond et al. 1992). It might be possible that both mutations occurred in one cell as the analyzed sample consisted of relatively few cells. In the study of Seth and colleagues the G12D hotspot mutation of *KRAS* and the *BRAF* T529A mutation were detected in a cell line and therefore confirmed that both mutations occurred in the same cell (Seth et al. 2009). Regarding this result the authors suggested that it is likely that both mutations can occur in the same cell of primary tumour tissue. Despite these results, it cannot be excluded that the mutations Ala59Thr and V600E of patient A occurred in different cells of the sample as the mutations were detected as mosaic forms rather than fully mutated.

In other samples of polyps 4407-09 and 2320-08-IV, mutations in codons 59, 61 and 63 of the *KRAS* gene were found (Tab. 13 and 14). This demonstrated that hotspot mutations of *BRAF* (V600E, as shown previously for the polyps of patient A) and *KRAS* occurred in the same polyp of one patient. This is an extremely remarkable fact, as even patients having different polyps with either *BRAF* or *KRAS* mutations have shown to be a significantly rare event (Carvajal-Carmona et al. 2007). Furthermore, in three samples of polyp 4407-09 three mutations and, in one sample, four mutations were detected simultaneously. The first sample displayed the mutations Arg603X (X = stop codon) and Leu613Leu (silent) in exon 15 of the *BRAF* gene and Gln61Pro (hotspot codon) in exon 3 of the *KRAS* gene (Fig. 11). It can be assumed that a stop codon leads to more or less inactivation of *BRAF* whereas the mutation in codon 61 leads to activation of *KRAS*. This seems to be consistent with the hypothesis that mutations in *BRAF* and *KRAS* are mutually exclusive. In the second sample the mutations Gln609Arg, Ile617Thr and a mosaic form of V600E were found in exon 15 of the *BRAF* gene (Fig. 11). In this case it remains ambiguous if the entire protein would still be activated due to V600E when all of the three mutations might occur in the same cell.

The third sample carried a mosaic form of V600E additionally to the mutations Leu19Leu (silent) in exon 2 and Arg73Gly in exon 3 of the *KRAS* gene. Normally, silent mutations without amino acid substitution do not have any impact on the protein function. The four mutations Ser607Phe in exon 15 of *BRAF*, Thr50Ala and Leu56Phe in exon 3 of *KRAS* as well as the fully manifested V600E *BRAF* mutation were found in the fourth sample of polyp 4407-09. As visible in figure 11, this is a very small sample compared to others consisting of no more than 10 cells. Since sequencing analysis revealed a very good quality without background signals it is supposed that the mutation V600E could be present homozygously in (almost) every cell of the sample.

In contrast to MSI CRC, simultaneous hotspot mutations of *BRAF* and *KRAS* were detected in sporadic primary carcinomas and lymph node metastasis of MSS CRC (Oliveira et al. 2007). Oliveira and colleagues found that increasingly more *BRAF* and *KRAS* mutations occurred exclusively in advanced tumours (T2-T4 according to the tumour-node-metastasis system) invading the muscularis propria and/or having spread into metastases. Synchronous mutations of *BRAF* and *KRAS*, in contrast, were never detected in the precursor lesions analyzed in that study. The colon polyps analyzed in this work had been classified as hyperplastic polyps and sessile serrated adenoma which are defined as precursor lesions prior to malignant transformation into carcinomas. Therefore, it is astonishing that *BRAF* and *KRAS* mutations occur simultaneously in these early stage polyps.

One part of the polyp of patient B was classified as sessile serrated adenoma and the other part as tubular adenoma (Fig. 13). In total, 6 different mutations were detected in both parts, including the V600E mutation in *BRAF* (Tab. 16). In figure 14 it is clearly visible that the V600E mutation is limited to the SSA and is not present in the tubular adenoma. Another difference of both types is the distribution of the other mutations. In the SSA all samples were wild type for the *KRAS* gene except one silent mutation in *KRAS* (Leu19Leu in exon 2) in one sample. In contrast, in the tubular adenoma two mutations in both genes, *KRAS* and *BRAF*, were detected. In one crypt, almost all cells carried only the mutation Ala11Val in exon 2 of the *KRAS* gene (Fig. 14). This seems to be the result of clonal expansion of one mutated crypt stem cell as was expected previously for polyps of patient A. In another crypt of the tubular adenoma the mutations Lys591Arg and Arg603Arg in exon 15 of *BRAF* and Glu76Glu in exon 3 of *KRAS* were detected in different samples (Fig. 14). None of these mutations detected in the tubular

adenoma is a hotspot mutation either of *BRAF* or of *KRAS*. A striking aspect is the fact that half of the six mutations of patient B were silent mutations with no effect on protein structure and activity. In contrast, most of the mutations of patient A were missense mutations with possible effect on the protein structure or nonsense mutations. Additionally, a lower number of mutations was detected in patient B (6 mutations in 54 samples, 11.1%) than in patient A (41 mutations in 154 samples, 26.6%). Nine of the eighteen samples of the SSA carried a mosaic form of V600E and in three of these the mutation was fully manifested (Fig. 14). A predominant distribution of the mutation related to the crypt structure could not be observed which is consistent with the results of patient A. This seems to confirm the thesis that the V600E mutation occurs spontaneously in different regions of the tissue of SSA or hyperplastic polyps. For statistically significant results, further studies need to be performed.

The large number of mutations detected in the polyps raises the question as to what impact the mutations might have on protein structure and functionality. All mutations detected were somatic, which resulted from mutation analysis of DNA from the corresponding normal tissue or blood. Mutations at the hotspots of the *BRAF* and *KRAS* gene discussed above already cause the constitutional activation of the proteins and lead in the end to cell proliferation. Determining the effects of missense mutations which cause changes in the amino acid sequence is not simple. Chemical and structural features as well as protein functionality analysis are necessary for exact characterization of mutation effects. Generally, mutations which are related to 'less important' sites of the protein might have less impact on activity than mutations at the active centre. Compared to the results obtained from PolyPhen, mutations in *KRAS* exon 3 are more often classified as 'benign' when they are located away from the hotspot codons (Tab. 15). In contrast, mutations near the V600E mutation in exon 15 of *BRAF* are mostly classified as 'probably damaging' (Tab. 15). But reliable statements can be obtained only after protein analysis. In comparison, silent mutations do not change the amino acid sequence of a protein due to the degenerated genetic code (see One- and Three-letter-code of amino acids at the appendix). For almost all of the amino acids more than one combination of bases is available, which ensures a relatively high resistance against mutations.

Compared to missense mutations, nonsense mutations always have negative effects related to the normal protein structure. If a stop codon is introduced into the coding

sequence of a gene, the translation of mRNA terminates before the end of the gene. The resulting mRNA is unstable in most cases when the stop codon occurs at least 50 nucleotides upstream of the last splicing junction. In such cases, a nonsense-mediated mRNA decay is initiated and translation into proteins do not occur (Lykke-Andersen et al. 2001, Maquat 2005). In other cases a premature termination of mRNA translation leads to truncated proteins. The impact of such proteins is difficult to predict and depends on the final length and stability of the truncated protein and which domains are lost or affected. A truncated protein still can exhibit remaining functionality or binding capacity. In the worst case, this may result in a dominant negative effect, when the aberrant protein inhibits the function of normal wild type proteins and results in an actually recessive disorder being caused by a heterozygous mutation (Fearon and Vogelstein 1990). Another possibility is the nonsense-associated alternative splicing, where the exon containing the stop codon is skipped and a stable mRNA is generated (Wang et al. 2002). But in this case as well, the resulting protein structure is changed with an often unknown effect on protein function.

Mutations generating stop codons occurred only in the *BRAF* gene of patient A whereas in the *KRAS* gene or in the polyp of patient B only missense or silent mutations were detected (Tab. 13, 14 and 16).

Another important aspect is the question of possible causes of the mutations found in the polyps of patient A and B. A striking fact is that patient A exhibits a broad spectrum of mutations with no dominance for a specific base substitution or type of mutation. Presumably, deficiency in DNA repair might cause these mutations. Defects or silencing of the mismatch repair (MMR) gene *MLH1* mainly lead to distinctive microsatellite instability which is not the case in either patient A nor B. Mutations or alterations in the MMR genes *MLH1*, *MSH2*, *MSH6* and *PMS2* causative for MMR deficiency furthermore induces an increase in point mutation frequency. However, investigations of premalignant precursor lesions (hyperplastic and adenomatous colorectal polyps) revealed that mutations in *BRAF* and *KRAS* precede silencing of the MMR gene *MLH1* due to hypermethylation in sporadic colorectal cancer (Seruca et al. 2009).

Beside MMR genes, there are many other genes associated with DNA repair. Genes that are involved in base excision repair (BER) include *OGG1* and *MUTYH* as well as further DNA glycosylases like *UNG*, *SMUG1*, *MBD4* and *TDG* (Wood et al. 2001). Of these, *OGG1* and *MUTYH* are responsible for removal and repair of 8-oxoguanine

which mispairs with adenine (Boiteux and Radicella 2000). Deficiency in one of these two genes leads to an excess of G:C to T:A (G>T) transversions in several genes, e. g. in the adenomatous polyposis coli (*APC*) gene triggered by deficiency in *MUTYH* repair causing *MUTYH*-associated polyposis (Al-Tassan et al. 2002, Sampson et al. 2005). The DNA repair gene O^6-methylguanine-DNA methyltransferase (*MGMT*) removes methyl and alkyl groups from the O^6 position of guanine (Wood et al. 2001). Silencing of this gene, e. g. by promoter hypermethylation results in an excess of G:C to A:T (G>A) transitions, for example in the proto-oncogene *KRAS* or the tumour suppressor gene *TP53* (Esteller et al. 2001).

Concerning the mutations of patients A and B, approximately four to five times more transitions than transversions can be observed. Although transversions are expected to occur more often due to the genetic code, a bias with an excess of transitions is observed in mammals. Transition rates depend on the amino acids affected and the nucleotide position in the codon (Brown et al. 1982, Collins and Jukes 1994). However, no prevalence of a specific base substitution like G to A transitions was detected in the polyps analyzed. Mutations occurred relatively equally at all three codon positions (Tab. 13, 14, 16). If an alteration in any of the DNA repair genes is responsible for the point mutations in *BRAF* and *KRAS*, only further study of these genes will unravel the cause.

In general, all three polyps of the two patients were primarily analyzed as microsatellite stable or low-grade MSI. Microsatellite instability is categorized as high-grade MSI (MSI-H), low-grade MSI (MSI-L) and microsatellite stability (MSS) according to the criteria defined at the Bethesda workshop (Boland et al. 1998). Usually, a marker panel of five microsatellite markers is used for analysis. MSS means that none of the markers shows instability. MSI-L is defined as only one of the markers displays instability, and when two or more markers show instability the tissue is classified as MSI-H. Although only three markers (BAT25, BAT26 and BAT40) were analyzed in this work, classification was done according to the defined criteria.

The results of microsatellite marker analysis showed good correlation with the immunohistochemical staining of the MLH1 protein. In polyp 2320-08-IV of patient A 80.5% of the samples were MSS and immunohistochemistry revealed 90% positive staining. Samples of polyp 4407-09 were stable in 86.7% and MLH1 staining revealed 80% positive staining of the tissue. For patient B, samples of polyp 13342-f1 showed MSS in 87.0% and immunohistochemical staining resulted in 90% positive stained cells.

Positive staining of the MLH1 protein means that the protein is present in the cells, which in turn leads to the expectation of microsatellite stability of the cells. Therefore, results of the immunohistochemical staining of MLH1 were confirmed by microsatellite marker analysis.

Differentiation between MSS and MSI-L for the analyzed polyps is not simple, as a definition of the proportions of samples which show MSI and MSS is necessary. Usually, MSI is analyzed using genomic DNA extracted from tissue or tissue sections. In this way, the entire polyp tissue is characterized according to the size of the original sample. Giuffrè and colleagues demonstrated in their study that samples had to be reclassified when comparing the results of hand versus laser microdissected samples. The sensitivity of analysis increased as the size of the samples decreased. They also suggested that in some cases MSI occurs stepwise in relation to a proceeding MMR dysfunction but prior to the complete loss of MMR gene expression (Giuffrè et al. 2005). According to the results, all three polyps were classified as MSS or MSI-L.

Microsatellite instability is a hallmark of mismatch repair deficiency in cells which can be achieved on two different ways: First, an inherited germ line mutation on one allele of a MMR gene and a somatic alteration on the second allele induce inactivation of the gene in patients with hereditary nonpolyposis colorectal cancer (HNPCC/Lynch syndrome). Second, hypermethylation of the promoter region of *MLH1* leads to silencing of the gene in sporadic colorectal cancer (Lynch 1999, Toyota et al.1999). Patient A has inherited the functional allele of the *MLH1* gene of her father. Therefore, the first possibility of *MLH1* inactivation due to inherited germ line mutations can be excluded in this case. Mutation analysis of other MMR genes and analysis of the methylation status was performed neither for patient A nor patient B as this was out of scope of this work. However, according to the results of microsatellite marker analysis and immunohistochemical staining of MLH1 it is supposed that a high-grade CIMP (CIMP-H) associated with *MLH1* promoter methylation can be excluded. But still the possibility of methylation of other genes or *de novo* mutations remains.

Summarized, the *BRAF* hotspot mutation V600E was detected only in sessile serrated adenomas and hyperplastic polyps of both patients but not in the tubular adenoma. Mutations of *BRAF* and *KRAS* previously reported as mutually exclusive were detected in the same samples, even the V600E *BRAF* mutation and a hotspot mutation in *KRAS*. This might be due to a lower cell amount analyzed. A much higher number of mutations

was detected in the polyps of patient A than in the polyp of patient B. Most of the mutations from patient A were unclassified missense or nonsense mutations whereas the mutation pattern of patient B seems to be more innocuous except for the V600E mutation. The cause of point mutations may lie in DNA repair deficiency but must be investigated further. Microsatellite marker analysis and immunohistochemical staining of MLH1 revealed MSS or MSI-L of all three colon polyps.

Both hyperplastic polyps and sessile serrated adenomas are generally referred to as 'serrated polyps', although their biological relationship has not yet been clarified (Mäkinen 2007). Differentiation can be made between simple hyperplastic polyps, which were thought to have no malignant potential, and sessile serrated adenomas with evidence for malignant potential. These serrated polyps were thought to be the precursor lesions of the serrated pathway (Young and Jass 2006, Mäkinen 2007). This pathway is integrated into the five molecular subtypes suggested for colorectal cancer classification (Jass 2007):

1: CIMP-H, methylation of *MLH1* resulting in MSI-H, associated with *BRAF* mutation

2: CIMP-H, partial methylation of *MLH1* resulting in MSI-L or MSS, associated with *BRAF* mutation

3: CIMP-L, methylation of *MGMT* resulting in MSI-L or MSS, associated with *KRAS* mutation; chromosomal instability

4: CIMP-negative, no methylation and therefore MSS; chromosomal instability

5: CIMP-negative, inherited MMR deficiency resulting in MSI-H

The first three subtypes can be summarized in the serrated pathway, responsible mostly for sporadic colorectal cancer. Main steps in this pathway include activation of the MAPK-ERK signalling pathway (via *BRAF* of *KRAS*), inhibition of apoptosis and silencing of specific genes by promoter hypermethylation facilitating MSI. A possible separation of the serrated pathway into sessile serrated and traditional serrated pathways was suggested depending on the affected gene (O'Brien et al. 2006, Mäkinen 2007).

In the sessile serrated pathway, an activating mutation in *BRAF* precedes methylation especially of *MLH1* and/or *MGMT*. Silencing of *MLH1* generates MSI-H and methylation of *MGMT* or partial methylation of *MLH1* produces MSI-L (associated with groups 1 and 2). Tissue alterations develop from the precursor lesions aberrant crypt foci to hyperplastic polyps to sessile serrated adenomas and finally, to serrated adenocarcinomas.

In the traditional serrated pathway, *KRAS* mutations precede methylation of *MGMT* and other tumour suppressor genes, followed by MSI-L or MSS (associated with group 3). Normal mucosa develops from aberrant crypt foci into hyperplastic polyps which may persist in an innocuous state or evolve into serrated adenomas and, in the end, to serrated adenocarcinomas. In both pathways, inhibition of apoptosis is initiated by methylation of genes responsible for cell cycle regulation.

Comparison of the results obtained in this work with the suggested classification reveals similarities and differences. However, one must keep in mind that mainly molecular features were investigated and that for overall classification and diagnosis clinical and morphological features play an equally important role.

The sessile serrated adenomas or hyperplastic polyp, of patients A and B respectively, harbour *BRAF* V600E mutations but the polyps were classified as either MSS or MSI-L. Mutations in *BRAF* and *KRAS* were demonstrated to be a very early event in tumourigenesis, preceding development of hypermethylation and MSI in sporadic CRC (Seruca et al. 2009). So if a sample carries the V600E *BRAF* mutation, methylation of *MLH1* and the resulting MSI would be expected in the same sample rather than in a *BRAF* wild type sample. However, two *BRAF* wild type samples were classified as MSI-H in polyp 4407-09 of patient A (Fig. 23). Although some samples displaying mutations (including V600E) in *BRAF* and/or *KRAS* were classified as MSI-L, other MSI-L or MSI-H samples were wild type for *BRAF* and *KRAS* (Fig. 22-24). Correlations of MSI samples and samples carrying mutations were therefore not detected in this work. Possibly, overall MSI would have been developed in these polyps at a later stage if they had not been removed from the colon. Compared to the second subgroup (and the sessile serrated pathway), a partial methylation of *MLH1* would also lead to low-grad MSI or microsatellite stability. Furthermore, the gradient occurrence of MSI was suggested by the incomplete loss of *MLH1* function, which could be consistent with the MSS or MSI-L status of the analyzed polyps (Giuffrè et al. 2005). The CIMP status, which was not analyzed in these polyps, might provide further information about classification or chronological order of *BRAF* mutations and microsatellite instability.

In the tubular adenoma of patient B, some mutations in *BRAF* and *KRAS* other than the hotspot mutations were detected. This result is consistent with the fourth subgroup according to Jass which also can be defined as the Vogelstein pathway or adenoma-carcinoma sequence. Typical features of this pathway are mutations in the *APC*, *KRAS* or *TP53* genes accompanied by chromosomal rather than microsatellite instability.

As mentioned previously and shown in several studies, mutations in *BRAF* and *KRAS* are mutually exclusive (Rajagopalan et al. 2002, Deng et al. 2004, Koinuma et al. 2004, Weisenberger et al. 2006, Seruca et al. 2009). It was demonstrated that *BRAF* V600E can be used as a molecular marker for sporadic CRC and is an exclusion criteria for HNPCC whereas *KRAS* mutations occur in sporadic as well as in inherited cancers (Domingo et al. 2005, Seruca et al. 2009).

The results obtained in this work give rise to two different interpretations. First, they support the hypothesis that mutations in *BRAF* and *KRAS* are mutually exclusive in precursor lesions, as the mutation V600E and simultaneous mutations in codons 12 and 13 of the *KRAS* gene were not found. Although a mutation in codon 14 of *KRAS* was detected, analysis of its effect on protein activity was outside the scope of this work (Tab. 14; Schubbert et al. 2006). Second, analysis of the three polyps revealed that mutations of *BRAF* and *KRAS* actually occur simultaneously, not only in one sample but in the same polyp of a patient. Furthermore, it has to be considered that mutations in *BRAF* and *KRAS* other than their hotspots occur simultaneously relatively often in the polyps analyzed. Usually, this mutation status was rarely detected, related not only to the hotspot mutations in *BRAF* (V600E) and *KRAS* (codons 12 and 13) but perhaps due to less sensitive analysis methods as mentioned previously (Samowitz et al. 2005). Therefore, this investigation demonstrated that sensitive and precise characterization of colon polyps should be a basic prerequisite for further research and understanding of CRC development.

Based on the results examined so far, it can be assumed that the polyps of patient A were sporadic rather than inherited. However, considering the fact that the father of patient A harbours several polyps like SSAs or hyperplastic polyps in addition to the HNPCC syndrome, a genetic predisposition is suggested. A possible explanation for the development of polyps could be hyperplastic polyposis syndrome. Varying numbers and types of polyps are described by this syndrome, making a clear differentiation from other types of colorectal cancer difficult. Precursor lesions include hyperplastic polyps and sessile serrated adenomas which also can occur spontaneously and appear to be identical to those of hyperplastic polyposis (Minoo et al. 2006, Young and Jass 2006). Minoo and colleagues demonstrated that hypermethylation of multiple gene promoters in normal colorectal mucosa might be due to a genetic predisposition in hyperplastic polyposis (Minoo et al. 2006). It can thus be speculated if hypermethylation of certain

DNA repair genes could cause point mutations in several genes like *BRAF* and *KRAS*. In this case, mutations would be likely to appear throughout the polyp tissue, which might be supported by *BRAF* and *KRAS* mutations in normal mucosa of polyp 4407-09. This hypothesis may be confirmed by the findings of Carvajal-Carmona and colleagues who detected two polyps with V600E *BRAF* mutation and the G12C *KRAS* mutation in the surrounding normal mucosa (Carvajal-Carmona et al. 2007).

These discrepancies reveal that much must be undertaken to further investigate the development and tumourigenesis of colorectal cancer. For patient A, future studies should focus on the familial aspect of cancer development, as it was shown that synchronous *BRAF* and *KRAS* mutations do not occur in sporadic MSS and MSI CRC precursor lesions. Although in this work analysis was limited to the *BRAF* and *KRAS* genes and microsatellite instability status, analysis of a large number of different types of polyps from many patients would give us a better insight into cancer development. For example, the characterization of the hyperplastic polyp (2320-08-IV) of patient A resulted in the detection of *BRAF* V600E which is associated with a certain cancer risk. However, hyperplastic polyps were thought to be innocuous for a long time. Characterization or even mapping of such polyps might reveal further understanding of tumourigenesis of these types of polyps and provide new insights especially into the serrated carcinogenesis pathway. In addition to molecular analyses, clinical information like family anamnesis, number and localization of polyps, age at diagnosis as well as morphological features are essential to cancer research and risk assessment for the patient.

In this work it was shown that characterization or generation of a molecular map of polyp tissue is a valuable tool in future cancer research.

6.2 Mutation analysis of single cells

Single cell analysis plays an important role in numerous fields of genetic testing, especially in preimplantation genetic diagnosis (PGD) (Ao et al. 1998, Klein et al. 1999, Lu et al. 2004, Peng et al. 2007). Recent years have seen a considerable increase in mutation analysis of monogenic diseases in the context of PGD due to advances in single cell analysis techniques. Up to now, mutation analysis of inherited monogenic disorders has been a well-established procedure (Kuliev et al. 2007, Renwick and Ogilvie 2007). As there is a need for validation prior to PGD, a test system is required to optimize the work flow, thus increasing the detection efficiency of mutations and to reduce allelic drop out (ADO). The precise and reproducible accessibility to single cells is a basic prerequisite to establishing such a test system.

In an initial step, the efficiency of low-volume multiplex PCR using fixed lymphocytes was analyzed. LV-PCR was performed in a total reaction volume of 1 µl. Compared to PCR analysis in larger reaction volumes, this leads to an increased amplification sensitivity and efficiency of PCR which is necessary for minute amounts of DNA (Proff et al. 2005, Schmidt et al. 2005). Different combinations of microsatellite markers were tested using genomic DNA as template, and finally the markers D7S1824, D9S302 and D10S2325 fitted best in a multiplex reaction. As PCR was performed with these three fluorescence-labelled microsatellite markers, a single LV-PCR using fixed single cells yielded enough amplification products appropriate for analysis in fragment length analysis. In a statistical study the amplification efficiency of the six specific alleles for all three markers was analyzed in 153 heterozygous single cells of an unaffected male (Fig. 25). The average amplification efficiency of 80% with no value below 75% for each of the six alleles (Tab. 18) was near the range of fresh single cells, which demonstrated the sensitivity of LV-PCR appropriate for single cell analysis (Ray et al. 2001, Lee et al. 2007, Spits et al. 2007). Additionally, a high specificity of the low-volume reaction was shown as in all 191 reactions (153 single cells, 9 positive and 29 negative controls) only one unspecific allele was detected.

Although fluorescent LV-PCR yielded enough PCR products for successful fragment length analysis, the application of single cell amplification with subsequent sequencing analysis was tested. In sequencing analysis, the quality and type of mutations like deletions, insertions or single nucleotide substitutions can be detected. However, a higher yield of starting template is required for successful sequencing reactions which

turned out in serial experiments. Therefore, a nested PCR subsequent to the LV-PCR was introduced. The use of a nested PCR assay enables reducing the number of cycles during the first PCR and thus minimizes the risk of amplifying unspecific products. During the second PCR reaction, amplification products of the first PCR serve as template for the inner primers, and so the yield of specific amplification products increases. In further experimental steps specificity and sensitivity of LV- and nested PCR were increased gradually until PCR products were appropriate for direct sequencing.

For a testing system for patients with specific mutations, microsatellite markers significant for the patients (C, D and E) and primers designed especially for their mutations (heterozygous germ line mutations c.2612delG and c.3183-3187delACAAA) were chosen (Tab. 3 and 9, Fig. 26).

Visibility and recognition of stained single cells which were spread on a microscopic slide is markedly easier than identifying unstained cells. Due to a possible influence of staining on the PCR reaction, amplification efficiency was compared using stained and unstained fixed single lymphocytes of the patients. Gel electrophoresis of secondary PCR products revealed an obviously higher amplification efficiency of unstained (81.8 and 40.9%) rather than stained (27.3%) cells. Discrepancy of amplification efficiencies between the two patients C and D of factor two can presumably be explained by the quality of the blood cells which may vary between several persons dependent upon their constitution. Samples from which PCR products were detected in gel electrophoresis usually produced a result in sequencing analysis independent of staining. However, heterozygosity rates for these samples were extremely low or even absent. In most cases, either the mutated or the wild type allele could be detected in one heterozygous cell.

For this reason, PCR conditions had to be further optimized using exclusively unstained single cells. In the next approach differently combined conditions, 'touch down' or specific PCR in first or secondary reaction, respectively, were compared (Fig. 27). The advantage of specific PCR is the exact adjustment of the annealing temperature according to the melting temperatures of the primers used. For a singleplex PCR this is true but for a multiplex PCR with more than one primer pair slightly different melting temperatures sometimes cannot be avoided for several reasons. When designing primers an optimal length of about 20-25 nucleotides each, amplification of the chosen

DNA region with regard to the final product length and the nucleotide constitution of the specific sequence have been taken into account.

The advantage of a touch down PCR is its higher specificity as stringency of primer binding is increased and unspecific binding can therefore be avoided. The annealing temperature of the first PCR cycle is chosen in relation to the highest melting temperature of all primers used. During the next 15 cycles the annealing temperature decreases by -1°C per cycle. Slightly different melting temperatures of the primers hence have only a lesser impact on efficiency. Therefore, it could be expected that performing a multiplex touch down PCR followed by a second specific singleplex PCR would yield in an optimal result which was confirmed by the analysis results of patients C and D. The highest amplification efficiency (100% and 81.3%) for both patients was achieved by combining the touch down with a subsequent specific PCR. Sequencing analysis revealed a trend for slightly higher heterozygosity rates of up to 16.7% compared to the previous approach yielded in 0 and 10.5%, but still were unacceptable for reliable single cell analysis. Application of fluorescent PCR, which is standard in PGD nowadays, as well as further optimization of PCR conditions and nested PCR protocols (concerning annealing temperature, cycle number and duration time, primer concentrations) were strategies for additionally increasing amplification efficiency and detection sensitivity in this work (Moutou and Viville 1999, Spits and Sermon 2009).

Finally, the successful combination of single cell laser microdissection, single particle transfer and low-volume multiplex PCR is presented. It was shown that fragment length analysis and sequencing analysis could be performed on single cell PCR products. This approach displays not only the establishment of a genetic test system for single lymphocytes; analysis is also applicable to conventional isolated polar bodies, blastomeres or blastocyst cells which are transferred to a planar glass slide (Mayer et al. 2009).

In comparison to other preliminary testing for PGD, some significant differences can be observed. The horizontal transfer of a series of isolated single lymphocytes via the SPATS system to a planar PCR slide constitutes a basic aspect in our approach. Optical control of the entire single cell handling including horizontal transfer ensures the reliability of the system in contrast to other isolation methods (Woide et al. 2009). A striking advantage is the use of easily accessible fixed single lymphocytes. Storage of fixed lymphocytes for several months in sufficient quality for PCR analysis allows

repeated optimization experiments without the need for fresh blood samples. Considering the template DNA quality, primer pairs were chosen which amplify only short sequences no more than 200 bp in length. Furthermore, short fragments increase amplification efficiency and decrease allelic drop out in single cell PCR reactions (Piyamongkol et al. 2003).

In contrast to the majority of investigations for PGD, in this approach heat denaturation of fixed lymphocytes was used prior to the first PCR cycle instead of chemical or enzymatic lysis of the cells (Spits and Sermon 2009). Higher denaturing temperatures of at least 96℃ reduce ADO rates dramatically without affecting amplification efficiency (Ray et al. 1996). Therefore, an initial denaturing step for single cell PCR of 97℃ was chosen. This process enables time savings of up to 1 hour, depending on the lysis method, since the time needed for enzyme incubation or washing can be omitted. The overall time for the single cell analysis procedure, excluding laser microdissection, is about 8-12 hours, depending on which method is used, e. g. fragment length or sequencing analysis. Time is an important factor in PGD, and in polar body diagnosis analysis time is limited to about 20 hours in Germany (Tomi et al. 2005).

Another advantage of heat denaturation is the reduced risk of contamination. Several lysis preparation steps and therefore unessential contact with potentially contaminated reagents or laboratory equipment can be avoided as the isolated cell on the reaction centre of the planar PCR slide is covered only with reaction mix and mineral oil before starting PCR. Precise isolation and transfer of only one single cell under optical control and dry conditions additionally ensures that the risk of co-isolation of contaminating particles such as cell debris or DNA which may be present in aqueous cell solutions is minimized. On the basis of PCR on a glass slide the possibility of releasing contaminant substances from plastic PCR tubes into the reaction mix, especially when the tube is heated, can thus be circumvented (McDonald et al. 2008). Contamination from other sources is reduced to a minimum due to extreme care and appropriate facilities in the laboratory.

The combination of at least two polymorphic markers and a mutation-specific fragment ensure an accurate analysis of the heterozygosity status of a single lymphocyte cell. Such multiplex reactions not only allow the reliable detection of ADO but are an important element for indirect diagnosis with linked polymorphic markers. Although multiplex PCR exclusively carried out with polymorphic markers has the advantage of being applied to many patients with different mutations, we could show that a multiplex

assay combining different markers and mutation-specific primers can also be applied to several patients with the same mutation.

Furthermore, this approach enables the possibility of direct analysis of specific mutations, as nested PCR of single cells yields enough DNA for sequencing analysis (if necessary). This could be the case if linkage analysis for polymorphic markers is not feasible for couples who wish to perform PGD (for review, see Spits and Sermon 2009). Whole genome single cell amplification which enables the combination of several different analysis methods such as mutation, polymorphic marker or STR analysis, comparative genomic hybridization (CGH) or fluorescence *in situ* hybridization (FISH) would display a great facilitation in PGD. Some efforts have been taken to establish whole genome amplification (WGA) of single cells for PGD and, as has recently been proven, multiple displacement amplification (MDA) using Phi29 polymerase is on its way to becoming the standard WGA method in PGD applications (Coskun and Alsmadi 2007, Peng et al. 2007, Spits and Sermon 2009).

However, there are still several problems to be resolved. For example, high ADO rates in the range of 20-30% achieved in subsequent PCR analysis using fresh cells can be by-passed only if a sufficient number of informative polymorphic markers is available (Spits and Sermon 2009, Glentis et al. 2009). This raises the same problems as mentioned for multiplex PCR when linkage analysis is not feasible. Another factor is the time that is needed for MDA reactions (up to 16 hours), especially when using commercially available WGA kits. Additionally, the time necessary for subsequent analysis also needs to be considered, as time constitutes an essential parameter in PGD. One possibility of increasing the sensitivity of MDA could be downscaling of the assay to low-volume reactions, which has proven to be successful for PCR. Yet, commercially available WGA kits are designed for larger volumes in the range of 50 µl and a prerequisite for downscaling is to adjust reagent concentrations and reaction conditions. For example, when MDA is to be performed on the planar glass slide, the compatibility of the reaction mixture with the covering mineral oil has been taken into account. In fact, single cell whole genome amplification resulting in a high DNA yield is a great advantage for PGD, as successful applications have shown (Glentis et al. 2009, Ren et al. 2009).

In comparison with other PGD studies heterozygosity rates for polymorphic microsatellite markers and mutation-specific amplification products were achieved from fixed single lymphocytes in nearly the same range as those from fresh cells (Ray et al.

2001, Lee et al. 2007, Spits et al. 2007). Moreover, this single cell genetic test system was applied to polar body diagnosis for three female patients with mutations (a 1 bp and a 5 bp deletion, respectively; Fig. 26) in the *APC* gene mentioned above (diagnosis was done at the Medical Genetics Center). In five PGD cycles, polar bodies of 60 oocytes were analyzed and 13 of the oocytes were identified as normal. These polar body PGDs resulted in one clinical pregnancy. Although polar bodies enable the analysis of only the maternal genome, they nevertheless have some advantages. Polar body diagnosis is an adequate method applicable for inherited diseases in those couples where only the woman is affected. In addition, ADO rates are considerably less in polar body than in blastomere analysis and it is easier to find informative polymorphic markers, which can be important in challenging cases (Altarescu et al. 2008). Removal of cells from the embryo (as is the case in blastomere and blastocyst PGD) can also be circumvented.

PGD of blastomeres where one or two cells are taken from the eight-cell stage embryo at day three postfertilization is still the method of choice in many laboratories (Spits and Sermon 2009). However, PGD of several trophectoderm cells extracted from the blastocyst stage of the embryo recently is becoming more important (McArthur et al. 2005, Fragouli et al. 2009). Accuracy and reliability of analysis indisputably increases with the number of cells or template DNA, respectively, but even if, e. g., up to 10 cells, which together contain about 70 pg, were analyzed, this still lies within the range of minute amounts of DNA and requires sensitive analysis methods which the developed system provides (Lutz-Bonengel et al. 2007). There are many reasons for or against the use for both blastomere and blastocyst PGD. For example, advantages of trophectoderm cells, in contrast to blastomeres, include reduced ADO rates and amplification failure as well as higher implantation rates and approximately equal pregnancy rates (Pangalos et al. 2008). On the other hand, cryoconservation caused by the strictly limited time available for analysis has the potential to harm the embryo and prevent its implantation (McArthur et al. 2005, Spits and Sermon 2009). This problem could be overcome by applying the genetic test system to blastocyst cells as it was shown that analysis can be done within 12 h also necessary for polar body diagnosis. In fact, the application of polar body, blastomere or blastocyst PGD depends on several factors ranging from legal restrictions, and the genetic background of patients to the type of disease analyzed. However, it is clear that PGD will only ever be performed on few or single cells.

Thus, this investigation successfully validates reliable genetic testing for as little as one single cell by means of mutation detection in the *APC* gene.

Moreover, the combination of single cell isolation, horizontal particle transfer and subsequent analysis can also be optimized for a wide range of other inherited diseases or genetic disorders and is not limited to polar bodies or PGD in general. This technique enables a variety of molecular analyses where isolation of few or single cells is important for genetic characterization. The whole analysis procedure performed in this work has proven to be successfully applicable for different questions in molecular research, from characterization of tumour polyp tissue to single cell analysis in PGD.

7 References

Aaltonen L, Johns L, Järvinen H, Mecklin J-P, Houlston R: Explaining the familial colorectal cancer risk associated with mismatch repair (MMR)-deficient and MMR-stable tumors. Clin Cancer Res 2007; 13 (1): 356-361

Altarescu G, Brooks B, Eldar-Geva T, Margalioth EJ, Singer A, Levy-Lahad E, Renbaum P: Polar body-based preimplantation genetic diagnosis for *N*-Acetylglutamate synthase deficiency. Fetal Diagn Ther 2008; 24: 170-176

Al-Tassan N, Chmiel NH, Maynard J, Fleming N, Livingston AL, Williams GT, Hodges AK, Davies DR, David SS, Sampson JR, Cheadle JP: Inherited variants of *MYH* associated with somatic G:C→T :A mutations in colorectal tumors. Nat Genet 2002; 30: 227-232

Ao A, Wells D, Handyside AH, Winston RML, Delhanty JDA: Preimplantation genetic diagnosis of inherited cancer: familial adenomatous polyposis coli. J Assist Reprod Gen 1998; 15 (3): 140-144

Auroux P-A, Iossifidis D, Reyes DR, Manz A: Micro total analysis systems. 2. Analytical standard operations and applications. Anal Chem 2002; 74 (12): 2637-2652

Ballhausen WG: Genetic testing for familial adenomatous polyposis. Ann NY Acad Sci 2000; 910: 36-49

Bazan V, La Rocca G, Corsale S, Agnese V, Macaluso M, Migliavacca M, Gregorio V, Cascio S, Sisto PS, Di Fede G, Buscemi M, Fiorentino E, Passantino R, Morello V, Tomasino RM, Russo A: Laser pressure catapulting (LPC): Optimization LPC-system and genotyping of colorectal carcinomas. J Cell Physiol 2005; 202: 503-509

Boiteux S, Radicella JP: The human *OGG1* gene: Structure, functions, and its implication in the process of carcinogenesis. Arch Biochem Biophys 2000; 377 (1): 1-8

Boland CR, Thibodeau SN, Hamilton SR, Sidransky D, Eshleman JR, Burt RW, Meltzer SJ, Rodriguez-Bigas MA, Fodde R, Ranzani N, Srivastava S: A National Cancer Institute workshop on microsatellite instability for cancer detection and familial predisposition: Development of international criteria for the determination of microsatellite instability in colorectal cancer. J Cancer Research 1998; 58: 5248-5257

Bonner WA, Hulett HR, Sweet RG, Herzenberg LA: Fluorescence activated cell sorting. Rev Sci Instrum 1972; 43 (3): 404-409

Bova GS, Eltoum IA, Kiernan JA, Siegal GP, Frost AR, Best CJM, Gillespie JW, Su GH, Emmert-Buck MR: Optimal molecular profiling of tissue and tissue components. Molecular Biotechnol 2005; 29: 119-152

Brown WM, Prager EM, Wang A, Wilson AC: Mitochondrial DNA sequences of primates: tempo and mode of evolution. J Mol Evol 1982; 18: 225-239

Burton MP, Schneider BG, Brown R, Escamilla-Ponce N, Gulley ML: Comparison of histologic stains for use in PCR analysis of microdissected, paraffin-embedded tissues. Biotechniques 1998; 24 (1): 86-92

Calabrese P, Tsao J-L, Yatabe Y, Salovaara R, Mecklin J-P, Järvinen HJ, Aaltonen LA, Tavaré S, Shibata D: Colorectal pretumor progression before and after loss of DNA mismatch repair. Am J Pathol 2004; 164 (4): 1447-1453

Carvajal-Carmona LG, Howarth KM, Lockett M, Polanco-Echeverry GM, Volikos E, Gorman M, Barclay E, Martin L, Jones AM, Saunders B, Guenther T, Donaldson A, Paterson J, Frayling I, Novelli MR, Philips R, Thomas HJW, Silver A, Atkin W, Tomlinson IPM: Molecular classification and genetic pathways in hyperplastic polyposis syndrome. J Pathol 2007; 121: 378-385

Casula M, Colombino M, Satta MP, Cossu A, Asierto PA, Bianchi-Scarrà G, Castiglia D, Budroni M, Rozzo C, Manca A, Lissia A, Carboni A, Petretto E, Satriano SMR, Botti G, Mantelli M, Ghirorzo P, Stratton MR, Tanda F, Palmieri G: *BRAF* gene is somatically mutated but does not make a major contribution to malignant melanoma susceptibility: The Italian Melanoma Intergroup Study. J Clin Oncol 2004; 22 (2): 286-292

Cawkwell L, Quirke P: Direct multiplex amplification of DNA from a formalin fixed, paraffin wax embedded tissue section. J Clin Pathol: Mol Pathol 2000; 53: 51-52

Clevers H: Wnt breakers in colon cancer. Cancer Cell 2004; 5-6

Collins DW, Jukes TH: Rates of transition and transversion in coding sequences since the human-rodent divergence. Genomics 1994; 20: 386-396

Coskun S, Alsmadi O: Whole genome amplification from a single cell: a new era for preimplantation genetic diagnosis. Prenat Diagn 2007; 27 (4): 297-302

Croner RS, Guenther K, Foertsch T, Siebenhaar R, Brueckl WM, Stremmel C, Hlubek F, Hohenberger W, Reingruber B: Tissue preparation for gene expression profiling of colorectal carcinoma: Three alternatives to laser microdissection with preamplification. J Lab Clin Med 2004; 143 (6): 344-351

Curran S, McKay JA, McLeod HL, Murray GI: Laser capture microscopy. J Clin Pathol: Mol Pathol 2000; 53: 64-68

Davies H, Bignell GR, Cox C, Stephens P, Edkins S, Clegg S, Teague J, Woffendin H, Garnett MJ, Bottomley W, Davis N, Dicks E, Ewing R, Floyd Y, Gray K, Hall S, Hawes R, Hughes J, Kosmidou V, Menzies A, Mould C, Parker A, Stevens C, Watt S, Hooper S, Wilson R, Jayatilake H, Gusterson BA, Cooper C, Shipley J, Hargrave D, Pritchard-Jones K, Maitland N, Chenevix-Trench G, Riggins GJ, Bigner DD, Palmieri G, Cossu A, Flanagan A, Nicholson A, Ho JWC, Leung SY, Yuen ST, Weber BL, Seigler HF, Darrow TL, Paterson H, Marais R, Marshall CJ, Wooster R, Stratton MR, Futreal PA: Mutations of the *BRAF* gene in human cancer. Nature 2002; 417: 949-954

Deng G, Bell I, Crawley S, Gum J, Terdiman JP, Allen BA, Truta B, Sleisenger MH, Kim YS: *BRAF* mutation is frequently present in sporadic colorectal cancer with methylated *hMLH1*, but not in hereditary nonpolyposis colorectal cancer. Clin Cancer Res 2004; 10: 191-195

Dillon D, Zheng K, Costa J: Rapid, efficient genotyping of clinical tumor samples by laser-capture microdissection/PCR/SSCP. Exp Mol Pathol 2001; 70: 195-200

Di Martino D, Giuffrè G, Staiti N, Simone A, Todaro P, Saravo L: Laser microdissection and DNA typing of cells from single hair follicles. Forensic Sci Int 2004; 146: 155-157

Dittrich PS, Tachikawa K, Manz A: Micro total analysis systems. Latest advancements and trends. Anal Chem 2006; 78 (12): 3887-3907

Domingo E, Niessen RC, Oliveira C, Alhopuro P, Moutinho C, Espìn E, Armengol M, Sijmons RH, Kleibeuker JH, Seruca R, Aaltonen LA, Imai K, Yamamoto H, Schwartz S, Hofstra RMW:

BRAF-V600E is not involved in the colorectal tumorigenesis of HNPCC in patients with functional *MLH1* and *MSH2* genes. Oncogene 2005; 24: 3995-3998

Esteller M, Risques RA, Toyota M, Capella G, Moreno V, Peinado MA, Baylin SB, Herman JG: Promoter hypermethylation of the DNA repair gene O^6-*methylguanine-DNA Methyltransferase* is associated with the presence of G:C to A:T transition mutations in p53 in human colorectal tumorigenesis. Cancer Res 2001; 61: 4689-4692

Fearon ER, Vogelstein B: A genetic model for colorectal tumorigenesis. Cell 1990; 61: 759-767

Fiegler H, Geigl JB, Langer S, Rigler D, Porter K, Unger K, Carter NP, Speicher MR: High resolution array-CGH analysis of single cells. Nucleic Acids Res 2007; 35 (3): e15 (DOI: 10.1093/nar/gkl1030)

Findlay I: Pre-implantation genetic diagnosis. Brit Med Bull 2000; 56 (3): 672-690

Fragouli E, Katz-Jaffe M, Alfarawati S, Stevens J, Colls P, Goodall N, Tormasi S, Gutierrez-Mateo C, Prates R, Schoolcraft WB, Munne S, Wells D: Comprehensive chromosome screening of polar bodies and blastocysts from couples experiencing repeated implantation failure. Fertil Steril 2009; DOI 10.1016/j.fertnstert.2009.04.053

Fransén K, Klintenäs M, Österström A, Dimberg J, Monstein HJ, Söderkvist P: Mutation analysis of the *BRAF*, *ARAF* and *RAF-1* genes in human colorectal adenocarcinomas. Carcinogenesis 2004; 25 (4): 527-533

Friedl W, Propping P : Familiärer Darmkrebs. Medgen 2007; 19: 216-224

Garnett MJ, Marais R: Guilty as charged: *B-RAF* is a human oncogene. Cancer Cell 2004; 6: 313-319

Gebert J, von Knebel Doeberitz C: Hereditäre Tumoren des Gastrointestinaltrakts (FAP/HNPCC). Chir Gastroenterol 1999; 15: 163-172

Giuffrè G, Müller A, Brodegger T, Bocker-Edmonston T, Gebert J, Kloor M, Dietmaier W, Kullmann F, Büttner R, Tuccari G, Rüschoff J, the German HNPCC Consortium, German Cancer Aid (Deutsche Krebshilfe): Microsatellite analysis of hereditary nonpolyposis colorectal

cancer-associated colorectal adenomas by laser-assisted microdissection. J Mol Diagn 2005; 7 (2): 160-170

Glentis S, SenGupta S, Thornhill A, Wang R, Craft I, Harper JC: Molecular comparison of single cell MDA products derived from different cell types. Reprod Biomed Online 2009; 19 (1): 89-98

Grimmond SM, Raghavan D, Russel PJ: Detection of a rare point mutation in *Ki-ras* of a human bladder cancer xenograft by polymerase chain reaction and direct sequencing. Urol Res 1992; 20: 121-126

Groden J, Thliveris A, Samowitz W, Carlson M, Gelbert L, Albertsen H, Joslyn G, Stevens J, Spirio L, Robertson M, Sargeant L, Krapcho K, Wolff E, Burt R, Hughes JP, Warrington J, McPherson J, Wasmuth J, Le Paslier D, Abderrahim H, Cohen D, Leppert M, White R: Identification and characterization of the familial adenomatous polyposis coli gene. Cell 1991; 66: 589-600

Hagen-Mann K, Zacher T, Khanaga O, Baukloh V, Mann W, Schön U: Molekularbiologische Analyse von Einzelzellen. Medgen 2005; 17: 240-245

Hashimoto Y, Itho Y, Fujinaga Y, Khan AQ, Sultana F, Miyake M, Hirose K, Yamamoto H, Ezaki T: Development of nested PCR based on the ViaB sequence to detect *Salmonella typhi*. J Clin Microbiol 1995; 33 (3): 775-777

Hehr A, Gross C, Bals-Pratsch M, Paulmann B, Tomi D, Seifert B, Hehr U, Schwinger E: Polkörperdiagnostik für monogene Erkrankungen als deutsche Alternative zur Präimplantationsdiagnostik. Das Deutsche IVF-Register 1996-2006. Springer 2007; DOI: 10.1007/978-3-540-49928-2

Hehr A, Seifert B, Hehr U, Bals-Pratsch M: Polar body diagnosis for monogenic disorders in Regensburg. J Reproduktionsmed Endokrinol 2009; 6 (1): 27-31

Herzenberg LA, Parks D, Sahaf B, Perez O, Roederer M, Herzenberg LA: The history and future of the fluorescence activated cell sorter and flow cytometry: a view from Stanford. Clin Chem 2002; 48 (10): 1819-1827

Holinski-Feder E, Morak M: Hyperplastische Polypen, sessile serratierte Adenome, konventionelle Adenome: Molekulare Pathways und deren klinische Relevanz. J Gastroenterol Hepatol Erkr 2010; 8: pre-publishing online

Hoque MO, Lee C-CR, Cairns P, Schoenberg M, Sidransky D: Genome-wide genetic characterization of bladder cancer: A comparison of high-density single-nucleotide polymorphism arrays and PCR-based microsatellite analysis. Cancer Res 2003; 63: 2216-2222

Hunt JL: Molecular pathology in anatomic pathology practice. Arch Pathol Lab Med 2008; 132: 248-260

Issa J-P: CpG island methylator phenotype in cancer. Nat Rev Cancer 2004; 4: 988-993

Jass JR: Classification of colorectal cancer based on correlation of clinical, morphological and molecular features. Histopathology 2007; 50: 113-130

Jones PA, Baylin SB: The fundamental role of epigenetic events in cancer. Nat Rev Genet 2002; 3: 415-428

Kinzler KW, Vogelstein B: Lessons from hereditary colorectal cancer. Cell 1996; 87: 159-170

Kirchner T, Reu S: Entwicklung molekularpathologischer Entitäten beim Dickdarmkarzinom. Pathologe 2008; 29 (Suppl 2): 264-269

Kirschner J, Plaschke-Schluetter A: Advanced forensics with precise target excision: the CellCut Plus laser microdissetion instrument. Nat Methods 2007; 4

Klein CA, Schmidt-Kittler O, Schardt JA, Pantel K, Speicher MR, Riethmüller G: Comparative genomic hybridization, loss of heterozygosity, and DNA sequence analysis of single cells. P Natl Acad Sci USA 1999; 96: 4494-4499

Klein CA: Single cell amplification methods for the study of cancer and cellular ageing. Mech Ageing Dev 2005; 126: 147-151

Koinuma K, Shitoh K, Miyakura Y, Furukawa T, Yamashita Y, Ota J, Ohki R, Choi YL, Wada T, Konishi F, Nagai H, Mano H: Mutations of *BRAF* are associated with extensive *hMLH1* promoter methylation in sporadic colorectal carcinomas. Int J Cancer 2004; 108: 237-242

Kranenburg O: The *KRAS* oncogene: past, present, and future. Biochim Biophys Acta 2005; 1756: 81-82

Kuliev A, Rechitsky S, Verlinsky Y: Preimplantation Diagnosis. Encyclopedia of Life Sciences (ELS) 2007; DOI: 10.1002/9780470015902.a0005570.pub2

Kumar R, Angelini S, Czene K, Sauroja I, Hahka-Kemppinen M, Pyrhonen S, Hemminki K: *BRAF* mutations in metastatic melanoma: a possible association with clinical outcome. Clin Cancer Res 2003; 9: 3362-3368

Lechner S, Müller-Ladner U, Renke B, Schölmerisch J, Rüschoff J, Kullmann F: Gene expression pattern of laser microdissected colonic crypts of adenomas with low grade dysplasia. Gut 2003; 52: 1148-1153

Lee JW, Yoo NJ, Soung Ark WS, Kim SY, Lee JH, Park JY, Cho YG, Kim CJ, Ko YH, Kim SH, Nam SW, Lee JY, Lee SH: *BRAF* mutations in non-Hodgkin's lymphoma. Br J Cancer 2003; 89: 1958-1960

Lee H-S, Jun JH, Choi HW, Lim CK, Yoo H-W, Koong MK, Kang IS: Preimplantation genetic diagnosis for ornithine transcarbamylase deficiency by simultaneous analysis of duplex-nested PCR and Fluorescence *in situ* hybridization: a case report. J Korean Med Sci 2007; 22: 572-576

Lehmann U, Kreipe H: Real-time PCR analysis of DNA and RNA extracted from formalin-fixed and paraffin-embedded biopsies. Methods 2001; 25: 409-418

Lindor NM, Rabe K, Petersen GM, Haile R, Casey G, Baron J, Gallinger S, Bapat B, Aronson M, Hopper J, Jass J, LeMarchand L, Grove J, Potter J, Newcomb P, Terdiman JP, Conrad P, Moslein G, Goldberg R, Ziogas A, Anton-Culver H, de Andrade M, Siegmund K, Thibodeau SN, Boardman LA, Seminara D: Lower cancer incidence in Amsterdam-I criteria families without mismatch repair deficiency. J Amer Med Assoc 2005; 293 (16): 1979-1985

Lu X, Huang W-H, Wang Z-L, Cheng J-K: Recent developments in single-cell analysis. Anal Chim Acta 2004; 510: 127-138

Lutz-Bonengel S, Saenger T, Heinrich M, Schoen U, Schmidt U: Low volume amplification and sequencing of mitochondrial DNA on a chemically structured chip. Int J Legal Med 2007; 121: 68-73

Lykke-Andersen J, Shu M-D, Steitz JA: Communication of the position of exon-exon junctions to the mRNA surveillance machinery by the protein RNPS1. Science 2001; 293 (5536): 1836-1839

Lynch HT: Hereditary nonpolyposis colorectal cancer (HNPCC). Cytogenet Cell Genet 1999; 86: 130-135

Mäkinen MJ: Colorectal serrated adenocarcinoma. Histopathology 2007; 50: 131-150

Maquat LE: Nonsense-mediated mRNA decay in mammals. J Cell Sci 2005; 118: 1773-1776

Matsubara Y, Kerman K, Kobayashi M, Yamamura S, Morita Y, Tamiay E: Microchamber array based DNA quantification and specific sequence detection from a single copy via PCR in nanoliter volumes. Biosens Bioelectron 2005; 20: 1482-1490

Mayer V, Schoen U, Holinski-Feder E, Koehler U, Thalhammer S: Single cell analysis of mutations in the *APC* gene. Fetal Diagn Ther 2009; 26: 148-156

McArthur SJ, Leigh D, Marshall JT, de Boer KA, Jansen RPS: Pregnancies and live births after trophectoderm biopsy and preimplantation genetic testing of human blastocysts. Fertil Steril 2005; 84 (6): 1628-1636

McDonald GR, Hudson AL, Dunn SM, You H, Baker GB, Whittal RM, Martin JW, Jha A, Edmondson DE and Holt A: Bioactive contaminants leach from disposable laboratory plasticware. Science 2008; 322 (5903): 917

Minoo P, Baker K, Goswami R, Chong G, Foulkes WD, Ruszkiewicz AR, Barker M, Buchanan D, Young J, Jass JR: Extensive DNA methylation in normal colorectal mucosa in hyperplastic polyposis. Gut 2006; 55: 1467-1474

Mitelman F, Johansson B, Mertens F: The impact of translocations and gene fusions on cancer causation. Nat Rev Cancer 2007; 7: 233-245

Moutou C, Viville S: Improvement of preimplantation genetic diagnosis (PGD) for the Cystic Fibrosis mutation ΔF508 by fluorescent polymerase chain reaction. Prenat Diagn 1999; 19: 1248-1250

Murray GI: An overview of laser microdissection technologies. Acta histochem 2007; 109: 171-176

Nakamoto T: Evolution and the universality of the mechanism of initiation of protein synthesis. Gene 2009; 432 (1-2): 1–6

Nakamura Y: The adenomatous polyposis coli gene and human cancers. J Cancer Res Clin 1995; 121: 529-534

Nunes MC, Roy NS, Keyoung HM, Goodman RR, McKhann II G, Jiang L, Kang J, Nedergaard M, Goldman SA: Identification and isolation of multipotential neural progenitor cells from the subcortical white matter of the adult human brain. Nat Med 2003; 9 (4): 439-447

O'Brien MJ, Yang S, Mack C, Xu H, Huang CS, Mulcahy E, Amorosino M, Farraye FA: Comparison of microsatellite instability, CpG island methylation phenotype, *BRAF* and *KRAS* status in serrated polyps and traditional adenomas indicates separate pathways to distinct colorectal carcinoma end points. Am J Surg Pathol 2006; 30: 1491-1501

Ogino S, Kawasaki T, Kirkner GJ, Loda M, Fuchs CS: CpG island methylator phenotype-low (CIMP-low) in colorectal cancer: Possible associations with male sex and *KRAS* mutations. J Mol Diagn 2006; 8 (5): 582-588

Oliveira C, Velho S, Moutinho C, Ferreira A, Preto A, Domingo E, Capelinha AF, Duval A, Hamelin R, Machado JC, Schwartz Jr. S, Carneiro F, Seruca R: *KRAS* and *BRAF* oncogenic mutations in MSS colorectal carcinoma progression. Oncogene 2007; 26: 158-163

Olsson L, Lindblom A: Familiy history of colorectal cancer in a Swedish county. Fam Cancer 2003; 2: 87-93

Pangalos CG, Hagnefelt B, Kokkali G, Pantos K, Konialis CP: Birth of a healthy histocompatible sibling following preimplantation genetic diagnosis for Chronic Granulomatous Disease at the blastocyst stage coupled to HLA typing. Fetal Diagn Ther 2008; 24: 334-339

Peng W, Takabayashi H, Ikawa K: Whole genome amplification from single cells in preimplantation genetic diagnosis and prenatal diagnosis. Eur J Obstet Gyn R B 2007; 131: 13-20

Peto J, Houlston RS: Genetics and the common cancers. Eur J Cancer 2001; 37 (8): 88-96

Piyamongkol W, Bermúdez MG, Harper JC, Wells D: Detailed investigation of factors influencing amplification efficiency and allele drop-out in single cell PCR: implications for preimplantation genetic diagnosis. Mol Hum Reprod 2003; 9 (7): 411-420

Proff C, Rothschild MA, Schneider PM: Low volume PCR (LV-PCR) for STR typing of forensic casework samples. Int Congr Ser 2006; 1288: 645-647

Rajagopalan H, Bardelli A, Lengauer C, Kinzler KW, Vogelstein B, Velculescu VE: *RAF/RAS* oncogenes and mismatch-repair status. Nature 2002; 418: 934

Ray PF, Winston RML, Handyside AH: Reduced allele dropout in single-cell analysis for preimplantation genetic diagnosis of cystic fibrosis. J Assist Reprod Gen 1996; 13 (2): 104-106

Ray PF, Vekemans M, Munnich A: Single cell multiplex PCR amplification of five dystrophin gene exons combined with gender determination. Mol Hum Reprod 2001; 7 (5): 489-494

Ren Z, Zeng H, Xu Y, Zhuang G, Deng J, Zhang C, Zhou C: Preimplantation genetic diagnosis for Duchenne muscular dystrophy by multiple displacement amplification. Fertil Steril 2009; 91 (2): 359-364

Renwick P, Ogilvie CM: Preimplantation genetic diagnosis for monogenic diseases: overview and emerging issues. Expert Rev Mol Diagn 2007; 7 (1): 33-43

Reyes DR, Iossifidis D, Auroux P-A, Manz A: Micro total analysis systems. 1. Introduction, theory, and technology. Anal Chem 2002; 74 (12): 2623-2636

Robert Koch-Institut: Krebs in Deutschland 2003-2004. Häufigkeiten und Trends. 6. überarbeitete Auflage. Robert Koch-Institut (Hrsg.) und die Gesellschaft der epidemiologischen Krebsregister in Deutschland e. V. (Hrsg.). Berlin 2008

Roehrl MH, Becker K-F, Becker I, Höfler H: Efficiency of single-cell polymerase chain reaction from stained histologic slides and integrity of DNA in archival tissue. DiagnMol Pathol 1997; 6 (5): 292-297

Salovaara R, Loukola A, Kristo P, Kääriäinen H, Ahtola H, Eskelinen M, Härkönen N, Julkunen R, Kangas E, Ojala S, Tulikoura J, Valkamo E, Järvinen H, Mecklin J-P, Aaltonen LA, de la Chapelle A: Population-based molecular detection of hereditary nonpolyposis colorectal cancer. J Clin Oncol 2000; 18: 2193-2200

Samowitz WS, Sweeney C, Herrick J, Albertsen H, Levin TR, Murtaugh MA, Wolff RK, Slattery ML: Poor survival associated with the *BRAF* V600E mutation in microsatellite-stable colon cancers. Cancer Res 2005; 65 (14): 6063-6070

Sampson JR, Jones S, Dolwani S, Cheadle JP: *MutYH* (*MYH*) and colorectal cancer. Biochem Soc T 2005; 33 (4): 679-683

Sarkozy A, Carta C, Moretti S, Zampino G, Digilio MC, Pantaleoni F, Scioletti AP, Esposito G, Cordeddu V, Lepri F, Petrangeli V, Dentici ML, Mancini GMS, Selicorni A, Rossi C, Mazzanti L, Marino B, Ferrero GB, Silengo MC, Memo L, Stanzial F, Faravelli F, Stuppia L, Puxeddu E, Gelb BD, Dallapiccola B, Tartaglia M: Germline *BRAF* muttions in Noonan, LEOPARD, and Cardiofaciocutaneous Syndromes: Molecular diversity and associated phenotypic spectrum. Hum Mutat 2009; 30 (4): 695-702

Schmidt U, Lutz-Bonengel S, Weisser H-J, Sänger T, Pollak S, Schön U, Zacher T, Mann W: Low-volume amplification on chemically structured chips using the PowerPlex16 DNA amplification kit. Int J Legal Med 2005; 120 (1): 42-48

Schubbert S, Zenker M, Rowe SL, Boell S, Klein C. Bollag G, van der Burgt I, Musante L, Kalscheuer V, Wehner L-E, Nguyen H, West B, Zhang KYJ, Sistermans E, Rauch A, Niemeyer CM, Shannon K, Kratz CP: Germline *KRAS* mutations cause Noonan syndrome. Nat Genet 2006; 38: 331-336

Schütze K, Lahr G: Identification of expressed genes by laser-mediated manipulation of single cells. Nat Biotechnol 1998; 16: 737-742

Sermon K: Current concepts in preimplantation genetic diagnosis (PGD): a molecular biologist's view. Hum Reprod Update 2002; 8 (1): 11-20

Sermon K, van Steirteghem A, Liebaers I: Preimplantation genetic diagnosis. Lancet 2004; 363: 1633-1641

Seruca R, Velho S, Oliveira C, Leite M, Matos P, Jordan P: Unmasking the role of *KRAS* and *BRAF* pathways in MSI colorectal tumors. Expert Rev Gastroenterol Hepatol 2009; 3 (1): 5-9

Seth R, Crook S, Ibrahem S, Fadhil W, Jackson D, Ilyas M: Concomitant mutations and splice variants in *KRAS* and *BRAF* demonstrate complex perturbation of the Ras/Raf signaling pathway in advanced colorectal cancer. Gut 2009; 58: 1234-1241

Shine J, Dalgarno L: The 3'-terminal sequence of *Escherichia coli* 16S ribosomal RNA: Complementarity to nonsense triplets and ribosome binding sites. Proc Nat Acad Sci 1974; 71 (4): 1342-1346

Simone NL, Bonner RF, Gillespie JW, Emmert-Buck MR, Liotta LA: Laser-capture microdissection: opening the microscopic frontier to molecular analysis. Trends Genet 1998; 14 (7): 272-276

Speicher MR, Carter NP: The new cytogenetics: Blurring the boundaries with molecular biology. Nat Rev Genet 2005; 6: 782-792

Spirio LN, Samowitz W, Robertson J, Robertson M, Burt RW, Leppert M, White R: Alleles of *APC* modulate the frequency and classes of mutations that lead to colon polyps. Nat Genet 1998; 20: 385-388

Spits C, De Rycke M, Van Ranst N, Verpoest W, Lissens W, Van Steirteghem A, Liebaers I, Sermon K: Preimplantation genetic diagnosis for cancer predisposition syndromes. Prenat Diagn 2007; 27: 447-456

Spits C, Sermon K: PGD for monogenic disorders: aspects of molecular biology. Prenat Diagn 2009; 29: 50-56

St. John DJB, McDermott FT, Hopper JL, Debney EA, Johnson WR, Hughes ESR: Cancer risk in relatives of patients with common colorectal cancer. Ann Intern Med 1993; 118: 785-790

Tam IYS, Chung LP, Suen WS, Wang E, Wong MCM, Ho KK, Lam WK, Chiu SW, Girard L, Minna JD, Gazdar AF, Wong MP: Distinct epidermal growth factor receptor and *KRAS* mutation patterns in non-small lung cancer patients with different tobacco exposure and clinicopathologic features. Clin Cancer Res 2006; 12: 1647-1653

Thalhammer S, Lahr G, Clement-Sengewald A, Heckl WM, Burgemeister R, Schütze K: Laser microtools in cell biology and molecular medicine. Laser Phys 2003; 13 (5): 681-692

Thalhammer S, Langer S, Speicher M, Heckl WM, Geigl JB: Generation of chromosome painting probes from single chromosomes by laser microdissection and linker-adaptor PCR. Chromosome Res 2004; 12: 337-343

Tomi D, Griesinger G, Schultze-Mosgau A, Eckhold J, Schoepper B, Al-Hasani S, Diedrich K, Schwinger E: Polar body diagnosis for Hemophilia A using multiplex PCR for linked polymorphic markers. J Histochem Cytochem 2005; 53 (3): 277-280

Toyota M, Ahuja N, Ohe-Toyota M, Herman JG, Baylin SB, Issa JPJ: CpG island methylator phenotype in colorectal cancer. Proc Natl Acad Sci 1999; 96: 8681-8686

Turnbull C, Hodgson S: Genetic predisposition to cancer. Clin Med 2005; 5 (5): 491-498

Umetani N, Sasaki S, Watanabe T, Ishigami H, Ueda E, Nagawa H: Diagnostic primer sets for microsatellite instability optimized for a minimal amount of damaged DNA from colorectal tissue samples. Ann Surg Oncol 2000; 7 (4): 276-280

Van der Klift H, Wijnen J, Wagner A, Verkuilen P, Tops C, Otway R, Kohonen-Corish M, Vasen H, Oliani C, Barana D, Moller P, DeLozier-Blanchet C, Hutter P. Foulkes W, Lynch H, Burn J, Möslein G, Fodde R: Molecular characterization of the spectrum of genomic deletions in the mismatch repair genes *MSH2*, *MLH1*, *MSH6*, and *PMS2* responsible for hereditary nonpolyposis colorectal cancer (HNPCC). Gene Chromosome Canc 2005; 44: 123-138

Vanneste E, Melotte C, Delbrock S, D'Hooghe T, Brems H, Fryns JP, Legius E, Vermeesch JR: Preimplantation genetic diagnosis using fluorescent in situ hybridization for cancer predisposition syndromes caused by micro-deletions. Human Reprod 2009; 24: 1522-1528

Vogelstein B, Fearon ER, Hamilton SR, Kern SE, Preisinger AC, Leppert M, Nakamura Y, White R, Smits AM, Bos JL: Genetic alterations during colorectal-tumor development. New Engl J Med 1988; 319: 525-532

Wang J, Chang Y-F, Hamilton JI, Wilkinson MF: Nonsense-associated altered splicing: A frame-dependent response distinct from nonsense-mediated decay. Mol Cell 2002; 10: 951-957

Wang Y, Friedl W, Lamberti C, Jungck M, Mathiak M, Pagenstecher C, Propping P, Mangold E: Hereditary nonpolyposis colorectal cancer: frequent occurrence of large genomic deletions in *MSH2* and *MLH1* genes. Int J Cancer 2003; 103: 636-641

Weimer J, Koehler MR, Wiedemann U, Attermeyer P, Jacobsen A, Karow D, Kiechle M, Jonat W, Arnold N: Highly comprehensive karyotype analysis by a combination of spectral karyotyping (SKY), microdissection and reverse painting (SKY-MD). Chromosome Res 2001; 9: 395-402

Weinberg RA: Fewer and fewer oncogenes. Cell 1982; 30: 3-4

Weisenberger DJ, Siegmund KD, Campan M, Young J, Long TI, Faasse MA, Kang GH, Widschwendter M, Weener D, Buchanan D, Koh H, Simms L, Barker M, Leggett B, Levine J, Kim M, French AJ, Thibodeau SN, Jass J, Haile R, Laird PW: CpG island methylator phenotype underlies sporadic microsatellite instability and is tightly associated with *BRAF* mutation in colorectal cancer. Nat Genet 2006; 38 (7): 787-793

Woide D, Schlentner V, Neumaier T, Wachtmeister T, Paretzke HG, von Guttenberg Z, Wixforth A, Thalhammer S: Programmable cytogenetic submicrolitre lab-on-a-chip for molecular diagnostic applications. IEEE Transactions on Biomedical Circuits and Systems, International Conference on Biomedical Electronics and Devices 2007

Woide D, Mayer V, Wachtmeister T, Hoehn N, Zink A, Koehler U, Thalhammer S: Single particle adsorbing transfer system. Biomed Microdevices 2009; 11 (3): 609-614

Wood RD, Mitchell M, Sgouros J, Lindahl T: Human DNA repair genes. Science 2001; 291: 1284-1289

Yang S, Farraye FA, Mack C, Posnik O, O'Brien MJ: *BRAF* and *KRAS* mutations in hyperplastic polyps and serrated adenomas of the colorectum. Am J Surg Pathol 2004; 28 (11): 1452-1459

Yeung SHI, Greenspoon SA, McGuckian A, Crouse CA, Emrich CA, Ban J, Mathies RA: Rapid and high-throughput forensic short tandem repeat typing using a 96-lane microfabricated capillary array electrophoresis microdevice. J Forensic Sci 2006; 51 (4): 740-747

Young J, Jass JR: The case for a genetic predisposition to serrated neoplasia in the colorectum: Hypothesis and review of the literature. Cancer Epidemiol Biomarkers Prev 2006; 15 (10): 1778-1784

Zhang C, Xing D: Miniaturized PCR chips for nucleic acid amplification and analysis: latest advances and future trends. Nucleic Acids Res 2007; 35 (13): 4223-4237

Appendix

Publications

Woide D, Schlentner V, Neumaier T, Wachtmeister T, Paretzke HG, von Guttenberg Z, Wixforth A, Thalhammer S: Programmable cytogenetic submicrolitre lab-on-a-chip for molecular diagnostic applications. IEEE Transactions on Biomedical Circuits and Systems, International Conference on Biomedical Electronics and Devices 2007

Woide D, Mayer V, Wachtmeister T, Hoehn N, Zink A, Koehler U, Thalhammer S: Single particle adsorbing transfer system. Biomedical Microdevices 2009; 11 (3): 609-614

Mayer V, Schoen U, Holinski-Feder E, Koehler U, Thalhammer S: Single cell analysis of mutations in the *APC* gene. Fetal Diagnosis and Therapy 2009; 26: 148-156

PROGRAMMABLE CYTOGENETIC SUBMICROLITRE LAB-ON-A-CHIP FOR MOLECULAR DIAGNOSTIC APPLICATIONS

Daniela Woide, Veronika Schlentner, Teresa Neumaier, Thorsten Wachtmeister
Herwig G. Paretzke, Zeno von Guttenberg[1], Achim Wixforth[2]and Stefan Thalhammer[*]

GSF, National Research Center for Environment and Health, Institute of Radiation Protection
Ingolstädter Landstrasse 1, 85764 Neuherberg, Germany
[1]Advalytix AG, Sauerbruchstrasse 50, 81377 Munich, Germany
[2]University Augsburg, Chair for Experimental Physics I, Universitätsstrasse 1, 86135 Augsburg, Germany
[*] stefan.thalhammer@gsf.de[£]

Keywords: Nanobiotechnology, lab-on-a-chip, cytogenetics, microfluidic PCR, surface acoustic waves, laser-based microdissection.

Abstract: This project focuses on the development of an acoustic driven, freely programmable multifunctional biochemical lab-on-a-chip. By combining different platform elements, like microdissection-, nanofluidic- and detection-modules, the lab-on-a-chip can be adapted to question- and patient-specific cytogenetic and forensic applications. In contrast to many common lab-on-a-chip approaches presently available, the fluidic handling is done on a planar surface of the lab-on-a-chip. Minute amounts of biochemical fluids are confined in 'virtual' reaction chambers and 'virtual' test tubes in the form of free droplets. The droplets, fluidic tracks and reaction sites are defined at the chip surface by a monolayer chemical modification of the chip surface. Surface acoustic waves are employed to agitate and actuate these little 'virtual' test tubes along predetermined trajectories. Well-defined investigations, controlled in the submicrolitre regime, can be conducted quickly and gently on the lab-on-a-chip.

1 INTRODUCTION

Over the past decade, advances in molecular biology have helped to enhance understanding of the complex interplay between genetic, transcriptional and translational alterations in, e.g., human cancers. These molecular changes are the basis for an evolving field of high-throughput cancer discovery techniques using microscopic amounts of patient-based material to detect genetic changes such as mutations, insertions, deletions or imbalances.

To be able to reproducibly and reliably handle, process and analyse such small samples, many laboratories all over the world are intensively investigating the applicability of biochips for this purpose. Biochips are small sample carriers, where biological material is attached for analysis. In dependence of the kinds of molecules attached to the surface analytical biochips are divided into DNA-

chips, protein-chips, cell-chips and lab-on-a-chip systems. Most progress in this field occurs especially in the area of DNA-chips (Schneegass et al., 2001; Lagally et al., 2001; Ng and Ilag, 2003). Existing gene chips developed by the Affymetrix Company are a new approach in microarray technology. Oligonucleotide arrays (e.g. genome-wide human SNP array as well as human gene array) are based on hybridisation to small, high-density arrays containing tens of thousands of synthetic oligonucleotides. The arrays are designed based on sequence information alone and are synthesized *in situ* using a combination of photolithography and oligonucleotide chemistry. Chromatin immuno-precipitation (ChiP) coupled with whole-genome DNA-microarrays allows determination of the entire spectrum of *in vivo* DNA binding sites for any given protein (Buck and Lieb, 2004).

In parallel, another kind of test systems was developed, i.e. bead-technologies (Edelmann et al., 2004) and microfluidic systems (Harrison et al.,

---

[£]The authors wish to be known that, in their opinion the first two authors should be regarded as joint First Author.

PROGRAMMABLE CYTOGENETIC SUBMICROLITRE LAB-ON-A-CHIP FOR MOLECULAR DIAGNOSTIC
APPLICATIONS

1993; Thorsen et al., 2002; Kwakye and Baeumner, 2003). There is growing interest in performing chemical reactions in microfluidic devices as they offer a variety of significant advantages over macroscopic reactors, such as high surface-area-to-volume ratios and improved control over mass and heat transfer.

Several companies and universities are working on programs employing new electronic DNA analysis technologies. These automated techniques are often developed in non-forensic fields, such as medical research, genetics or biochemistry. In genetic forensics, nucleic acid is usually extracted from saliva, blood, semen, bone, hair and dried skin; these are the sources for most crime scene DNA isolations. Chemical kits for DNA isolation, amplification and detection are available today. The future of forensic testing will follow the path of greater automation e.g. of the DNA fingerprinting process. If a particular kind of polymorphism can be detected through automation, reducing the analysis time and expense, it may be of interest to the forensic community. Developments, however, for forensic applications are rare. Only Nanogen Inc. has developed this technology with applications to STR analysis termed APEX® - automated programmable electronic matrix, by using an electric chip as heart of the analysis (Ibrahim et al., 1998; Rau, 1997).

While DNA-chips become commercially important, scientific and technical development in the last years generated different approaches of multiparameter tests particular for medical applications, so-called 'lab-on-a-chip' systems (LOCs). Miniaturisation of analysis systems will yield in an enormous cost-saving in regard to materials like test tubes or microtitre plates as well as biochemical reagents. Furthermore, a smaller sample volume implies in the end a higher sensitivity and homogeneity of detection. Additionally, in comparison to serial single analyses, parallelisation of analyses enables an enormous time saving due to automation. These micro- and nanolaboratories on the scale of a computer chip are equipped with all components necessary for cytogenetic analysis, they are portable, easy to use, flexible, inexpensive, biocompatible and, like computer chips, full programmable.

Here, we present an acoustic driven lab-on-a-chip for cytogenetic and forensic applications (Thalhammer et al., 2007). In contrast to many other lab-on-a-chip approaches, the fluidic handling is done on the planar surface of this chip, the fluids being confined in 'virtual' reaction chambers and 'virtual' test tubes in form of free droplets. The droplets, fluidic tracks and reaction sites are defined at the chip surface by a monolayer chemical modification of the chip surface. In comparison to conventional closed microfluidic systems with external pumping, afflicted with the difficulty to further miniaturize, surface acoustic waves are employed to agitate and actuate these little 'virtual' test tubes along predetermined trajectories. These surface acoustic waves propagate on a substrate surface, to move and mix smallest fluidic volumina. Liquid amounts in the range from 1 micro- down to 100 picolitre are precisely moved on monolayers of thin, chemical processed fluidic 'tracks' without any tubing system. The surface acoustic waves are generated by high frequency electrical impulses on microstructured interdigital transducers embedded into the lab-on-a-chip.

Minute amount of sample material is extracted by laser-based microdissection out of e.g. histological sections (Thalhammer et al., 2003; Thalhammer et al., 2004). A few picogram of genetic material are isolated and transferred via a low-pressure transfer system onto the lab-on-a-chip. Subsequently the genetic material inside single droplets, which behave like 'virtual' beakers, is transported to the reaction and analysis centres on the chip surface via surface acoustic waves, probably best known from their use as high frequency filters in mobile phones. At these 'biological reactors' the genetic material is processed, e.g. amplified via polymerase chain reaction methods, and genetically characterized (Guttenberg et al., 2005).

Well-defined analyses, controlled in the submicrolitre regime, can be quickly and gently conducted on the lab-on-a-chip. Apart from its nearly unlimited applicability for many different biological assays, its programmability and extremely low manufacturing costs are another definite advantage of this 'cytochip'. In fact, those LOCs can be made so cheap that their use as disposables in many areas of diagnostics can be envisioned.

2   MATERIAL & METHODS

In most microfluidic systems liquids are confined and moved in tubes or capillaries. Usually, the application of such systems is restricted to continuous flow processes. However, when carefully looking at a microscale fluid, one realizes that the effects of e.g. surface tension by far exceed those of gravity. The shape of a droplet on a surface is given

by the properties of the substrate. It either remains a droplet or it wets the surface, depending on whether the substrate is hydrophobic or hydrophilic. The technology to create such fluidic tracks (fig. 1) is very much similar to define conducting paths on an electronic semiconductor device.
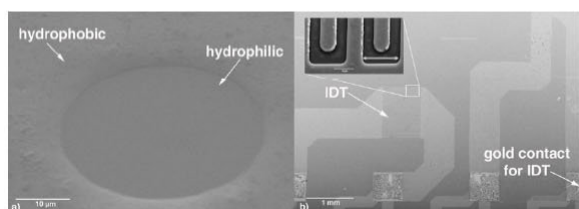

Figure 1: Chemical functionalization of the chip surface creating a hydro-philic/hydrophobic structure. Electron microscopy of a) the hydrophilic reaction centre on the hydrophobic LOC surface, scale bar 10 μm, and b) the arrangement of interdigital transducers (IDT) and electric conduction to control the SAW, scale bar 1 mm. Enlargement in b), electron microscopy of the interdigital transducer in detail with comb periodicity of the double-headed arrow, scale bar 10 μm.

Small amounts of liquids do not really need to be confined in tubes and trenches. They form their own test tubes, held together by surface tension effects. These micro volumina, due to the fact that in small droplets the effect of surface tension dominates gravity, do not need any reservoir as surface tension keeps the droplets in shape. Visualizing dewdrops hanging on a spider's web, one can observe that average droplet size obviously depends on the thickness of the strand: smaller droplets are attached to finer fibres and bigger ones to thicker threads. Apparently droplet shape conforms to the geometry as well as the wettability of the subsurface.

    A 'lab-on-a-chip', however, requires more than just test tubes. More important, their cargo has to be moved around, mixed, stirred or processed in general.

2.1 Lab-on-a-Chip Design

The layout of the lab-on-a-chip is shown layer by layer in a schematic drawing (fig. 2). The basic material of the lab-on-a-chip is a lithium niobate ($LiNbO_3$) single crystal wafer polished on both sides. The first metal layer is platinum (Pt) or nickel (Ni) for the heater and sensor structure, followed by a gold layer for the SAW transducer and the contact wires. The complete chip is protected with sputter oxide, which is removed above the contact pads. All structures are patterned by photolithography.

    A chemical functionalization of the surface or parts thereof can be employed to laterally define a

modulation of the wetting properties, thus creating fluidic pathways or tracks forming virtual potential wells for a fluid on the flat surface of a chip (fig. 3). To form a high contact angle of the oil on the chips, the surface has to be lipophilic. However, the hybridization array has to be wetted easily and needs active coupling groups for the oligo DNA spots. Therefore a chemically heterogeneous surface modification is needed achieved by photo-lithography. The tracking system for biochemical reactants and oil droplet movement and heaters on the chip is patterned with photoresist. An organic layer of a hydrophobic silane is bound to the whole surface. After removing the photoresist, epoxysilane is grafted from an organic solution.
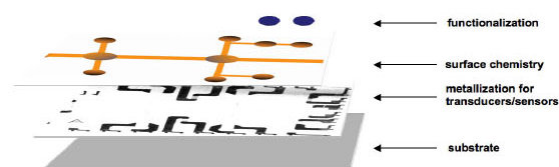

Figure 2: Design of LOC functionality. The ground substrate ($LiNbO_3$) is covered by a layer of Pt, Ni and Au for transducers and sensor metallization. Subsequent silanisation of the surface accounts for a hydrophilic/hydrophobic surface chemistry, facilitating a planar tracking system, which could be further functionalised.

2.2 Actuation

Actuation of single droplets or closed loops of liquid on a fluidic track is achieved by so-called surface acoustic waves, which have been widely used in the completely different field of radio frequency signal processing over the last twenty years or so. Each cell phone, for instance, contains two or more devices operating on SAW.

    Actuation of small droplets on the surface of a SAW chip is caused by the effect of acoustic streaming. This phenomenon appears when intensive sound fields are travelling through a liquid. Two major actuation forms can be described: internal flow inside the droplet versus transport of the droplet.

2.2.1 Interdigital Transducer

Electronic devices employing the SAW normally utilize one or more interdigital transducers (IDTs) to convert acoustic waves to electrical signal and vice versa utilizing the piezo-electric effect of certain materials (i.e. $LiNbO_3$) (fig. 1). These devices are

PROGRAMMABLE CYTOGENETIC SUBMICROLITRE LAB-ON-A-CHIP FOR MOLECULAR DIAGNOSTIC
APPLICATIONS

fabricated utilizing common processes used in the manufacture of silicon integrated circuits. Piezo-electricity is the ability of crystals to generate a voltage in response to applied mechanical stress. Depending on their design, the interdigital transducers produce a special type of acoustic surface wave, which can efficiently transfer energy into liquids. Typical SAW frequencies for the fluidic application presented here range from 100 to 200 MHz, the wavelengths are then around 20 micrometers. Transducers are copied from a transducer mask (Advalytix); a distance of 26.5 μm between two combs results in a resonance frequency on the LiNbO$_3$ of 150.6 MHz (fig. 1).
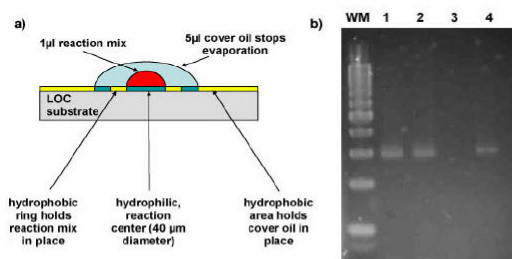

Figure 3: a) Side-view of the lab-on-a-chip amplification unit displaying single droplet PCR. The PCR reaction mix (1 μl) on the hydrophilic reaction centre (40 μm in diameter) is covered with mineral oil to avoid evaporation. The hydrophobic area around the reaction centre holds reaction mix and cover oil in place. b) Gel electrophoresis of 1 μl β-Actin PCR. WM: weight marker, PeqGold 100 bp DNA ladder; lane 1+2: positive control; lane 3: negative probe; lane 4: LOC-PCR, 500 pg target DNA.

2.2.2 Surface Acoustic Wave

Surface waves, so-called Rayleigh-waves, are applied on the piezo-electric system without any mechanical contact to realize actuation of the reactants on the LOC with interdigital transducers.

A surface acoustic wave is an acoustic wave travelling along the surface of a material having some elasticity, with amplitude that typically decays exponentially with the depth of the substrate. It is the nanometre analogue of an earthquake. This kind of wave is commonly used in piezo-electric devices called SAW devices in electronic circuits. Its amplitude and wavelength, however, can be controlled by an electrical signal applied to an appropriate transducer.

At low amplitudes, e.g. below one nanometre, a striking SAW pulse creates internal streaming within the fluid. Its energy is strongly absorbed and radiated into the fluid under the Rayleigh angle. At larger amplitudes, the internal streaming becomes a movement of the whole droplet into the desired

direction on the chip with a desired speed (Wixforth et al., 2004). Velocities close to one m/sec can be achieved in this way. In this sense, the transducer generating the surface acoustic waves can be regarded as pump without moving parts that may be remotely operated to control the position of one or more single droplets on the planar fluidic network on a LOC system.

3 PROTOTYPE

Here, we present a multifunctional lab-on-a-chip combining different platform elements like microdissection-, nanofluidic- and detection-modules (fig. 4) with the aim of providing a new platform for fast, cheap and easy investigation of genetic material in patient or forensic samples.

Without any mechanical structuring the lab-on-a-chip exhibits 'virtual' tracks, whereon samples and reagents are acoustically driven, actuated by electrical nanopumps (fig. 5). For the LOC, specific reaction-predefined 'spots' can be generated for total genome amplification via PCR, labelling of the amplified material and detection.

The recent developed lab-on-a-chip system combines serial processing with parallel downstream applications by using a minimum amount of genetic material as source for further investigation. Amplification, labelling and detection of the isolated genetic material are subsequently carried out on the chip surface driven by surface acoustic waves.

Each lab-on-a-chip (fig. 5) has two areas operating as biochemical reaction points, controlled by the temperature sensor. The sensors of the chip are calibrated by a thermoplate and resistance measurements controlled by a *LabView* program. The chip has 10 separately addressable SAW transducers, two on each side for aligning the reactant droplet on the heaters and for mixing during the biochemical reactions. Opposing transducers have different spatial periods to avoid crosstalk.

Extraction of sample material is performed via laser-based microdissection providing the possibility to isolate samples in the range from several cells down to a single chromosomal band with minimum risk of contamination. These small amounts of genetic material, which lay in the range of several picogram, are then transferred via a low-pressure transfer system onto the lab-on-a-chip. This newly developed transfer system (publication in preparation) extracts microdissected material using
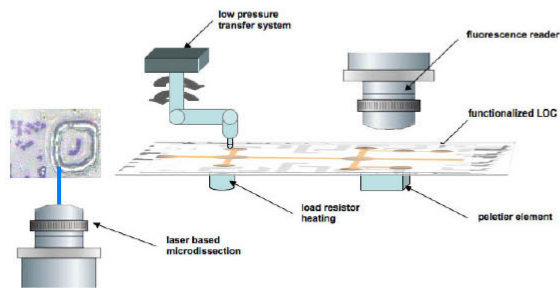
Figure 4: The modular lab-on-a-chip system consists of several units for isolating, processing and analysing minute amounts of sample material: laser-based microdissection is followed by processing of the extracted material and detection of hybridized probes or amplified material by a fluorescence reader. All operations on the LOC are controlled by SAW actuated microfluidics.

low-pressure and transfers it to the reaction centre on the LOC. The patented transfer device allows the precise positioning of the isolated material on top of the LOC.

Subsequently, the sample material inside single droplets is transported very efficiently and contact-less to the reaction and analysis centres on the chip surface via surface acoustic waves. Processing of isolated genetic material like specific or unspecific amplification is conducted on the nanofluidic device via polymerase chain reaction methods followed by labelling with fluorochromes.

Qualitative as well as quantitative analyses such as real-time PCR or microarray will be carried out using a novel 'fluorescence reader', especially designed for the LOC system and forming the principal component of the detection unit. Thus different applications for point-of-care diagnostics are practicable on one single lab-on-a-chip.

4 POSSIBLE APPLICATIONS

This freely programmable lab-on-a-chip system will open new potentials in research and development in different fields of applications ranging from cytogenetics to pathology and forensics.

Apart from its nearly unlimited applicability for many different biological assays, possible applications of this system in cytogenetics are e.g. detection of chromosomal imbalances and detection of genomic imbalances in solid tumour tissue. After isolation of the genetic material by laser-based microdissection the sample is transferred to the lab-on-a-chip using a low- pressure transfer system. Furthermore, in a first biochemical reaction the

extracted material is enzymatically digested and prepared for subsequent amplification e.g. *Alu* PCR for SNP analyses. Whole genome amplification of e.g. individually isolated single cells and chromosomes followed by labelling the material with fluorochromes can be used for e.g. fluorescence *in situ* hybridization (FISH) experiments. After mixing with different-labelled reference-DNA the mixture can be transferred to the specific CGH array via wetting modulated surface chemistry, hybridized and finally detected. To make sure that fluorochromes are incorporated uniformly into the sample DNA as well as the reference DNA, the labelling process can be monitored using online PCR detection. In the same way the amount of DNA product after amplification can be determined exactly. This provides the possibility to mix equal amounts of sample and reference DNA for the hybridization mixture. The detection array, microarray on the lab-on-a-chip, will be question- and patient-specific spotted by dot blot technology. Again acoustic actuation will be adopted to solve e.g. lyophilized reagents in a specific buffer.

With regard to the emerging field of forensics, this LOC system can also be applied to genomic sample material as blood cells, buccal swaps or other human cell material performing DNA fingerprint, paternity tests or SNP analysis. As forensic analysis should be cost and time saving, the development of a new miniature analytical lab-on-a-chip system could serve the market in a novel and promising way. Real-time PCR and STR analysis could not only be applied to the novel LOC system separately but also be combined on one single lab-on-a-chip in a modular way.
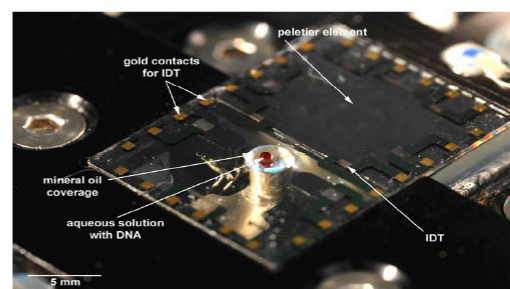

Figure 5: SAW driven lab-on-a-chip system with 10 interdigital transducers, two heaters and biochemical reactant containers. Transport of minute amounts of sample material in 'virtual' beakers is actuated by surface acoustic waves generated via interdigital transducers. The liquid phase comprising the genetic material (red) is covered by a thin layer of mineral oil avoiding evaporation. A load resistor heating and a peltier element provide for precise temperature profiles required for molecular biological methods.

PROGRAMMABLE CYTOGENETIC SUBMICROLITRE LAB-ON-A-CHIP FOR MOLECULAR DIAGNOSTIC
APPLICATIONS

A further application in the field of systems radiation biology is to investigate the influence of low-dose irradiation on cell-cell interactions and possible bystander effects. The medical use of ionizing radiation contributes the largest fraction to the population's anthropogenic radiation exposure. Thus, biopsies of suspicious diagnostic findings, which were irradiated with standard low-dose, will be extracted for histological examination and isolated cell clusters will be analysed on the LOC. By spotting a specific protein array on one part of the LOC and moving cells and media via SAW onto this particular array, it should be possible to detect cancer cascades and involved proteins. This method can be further used to determine the relation and interaction between cancer associated proteins i.e. p53, TGF-β and caspase.

5   OUTLOOK

This system, the acoustically driven, freely programmable multifunctional biochemical lab-on-a-chip system, will be applied on different diagnostic approaches at the single cell or single chromosome level e.g. cytogenetics, tumour genetics and genetic forensics.

Competitive LOCs, combining these techniques, are worldwide not on the market. An essential advantage of the LOC system is the modular set-up, which allows reacting to different diagnostic questions in a preventive medical check-up. This implements the rapid adaptation to patient-specific point-of-care diagnostics as well as the operator-specific development of new molecular markers for imaging techniques. Fields of applications for the newly developed LOC system range from the analysis of cell compartments and single cells in tumour diagnosis to chromosomal imbalances in the human genome.

ACKNOWLEDGEMENTS

REFERENCES

Buck M.J. and Lieb J.D., 2004. ChiP-chip: considerations for the design, analysis, and application of genome-wide chromatin immunoprecipitation experiments. *Genomics* 83: 349-360

Edelmann, L., Hashmi, G., Song, Y., Han, Y., Kornreich, R., Desnick, R.J., 2004. Cystic fibrosis screening: validation of a novel method using Bead Chip technology. *Genet Med.* 6(5): 431-438

Guttenberg, Z., Müller, H., Habermüller, H., Geisbauer, A., Pipper, J., Felbel, J., Kielpinski, M., Scriba, J., Wixforth, A., 2005. Planar chip device for PCR and hybridization with surface acoustic wave pump. *Lab on a chip* 5: 308-317

Harrison, D.J., Fluri, K., Seiler, K., Fan, Z., Effenhauser, C.S., Manz, A., 1993. Micromaching a miniaturized capillary electrophoresis-based chemical analysis system on a chip. *Science* 261: 895-897

Ibrahim, M.S., et al., 1998. Real-time microchip PCR for detecting single-base differences in viral and human DNA. *Anal Chem.* 70: 2013

Kwakye, S., Baeumner, A., 2003. A microfluidic biosensor based on nucleic acid sequence recognition. *Anal. Bioanal. Chem.* 376(7): 1062-1068

Lagally, E.T., Emrich, C.A., Mathies, R.A., 2001. Fully integrated PCR-capillary electrophoresis microsystem for DNA analysis. *Lab on a chip* 1: 102-107

Ng, J.H., Ilag, L.L., 2003. Biochips beyond DNA: technologies and applications. *Biotechnol. Annu. Rev.* 9: 1-149

Rau, R., 1997. The National Institute of Justice Forensic DNA Laboratory Improvement Program. *Profiles DNA* 1: 5

Schneegass, I., Brautigam, R., Kohler, J.M., 2001. Miniaturized flow-through PCR with different template types in a silicon chip thermocycler. *Lab Chip* 1(1): 42-49

Thalhammer, S., Lahr, G., Clement-Sengewald, A., Heckl, W.M., Burgemeister, R., Schütze, K., 2003. Laser microtools in cell biology and molecular medicine. *Laser Physics* 13(5): 681-692

Thalhammer, S., Langer, S., Speicher, M.R., Heckl, W.M., Geigl, J.B., 2004. Generation of chromosome painting probes from single chromosomes by laser microdissection and linker-adaptor PCR. *Chromosome Research* 12: 337-343

Thalhammer, S., von Guttenberg, Z., Koehler, U., Zink, A., Heckl, W.M., Franke, T., Paretzke, H.G., Wixforth, A., 2007. Programmierbares, zytogenetisches Submikroliter-Chiplabor für molekular-diagnostische Anwendungen. *GenomXPress* ISBN: 1617-562X, 1.07: 29-31

Thorsen, T., Maerkl, S.J., Quake, S.R., 2002. Microfluidic large-scale integration. Science 298: 580-584

Wixforth, A., Strobl., C., Gauer, C., Toegl, A., Scriba, J., Guttenberg, Z., 2004. Acoustic manipulation of small droplets. *Anal. Bioanal. Chem.* 379: 982-991

Single particle adsorbing transfer system

**Daniela Woide · Veronika Mayer ·
Thorsten Wachtmeister · Norbert Hoehn · Albert Zink ·
Udo Koehler · Stefan Thalhammer**

Abstract Here we present a novel approach for horizontal transfer of single particles after laser microdissection. The developed technique is a single particle adsorbing system for highly selective and gentle horizontal transfer of microdissected fixed and living material. As mediated via low-pressure technology, the transfer process can be precisely controlled, thus facilitating horizontal particle transfer of any isolated material, e.g. tissue material, single cells or chromosomes, in addition to precise positioning for sample release. This collection method allows one to predefine target positions and enables material transfer without contamination to any planar microchip device. This contamination free transfer is indispensable for novel lab-on-a-chip systems performing nanoscale polymerase chain reaction analyses. Using *virtual* reaction chamber micro-

Daniela Woide and Veronika Mayer contributed equally to this paper.

D. Woide · V. Mayer · T. Wachtmeister · S. Thalhammer (✉)
Helmholtz Zentrum Munich,
German Research Center for Environmental Health (GmbH),
Institute of Radiation Protection,
Ingolstädter Landstrasse 1,
85764 Neuherberg, Germany
e-mail: stefan.thalhammer@helmholtz-muenchen.de

N. Hoehn
Xyz high precision,
Heinestrasse 20,
64295 Darmstadt, Germany

A. Zink
EURAC, Institute for the iceman,
Viale Druso 1,
39100 Bolzano, Italy

U. Koehler
Medizinisch Genetisches Zentrum,
Bayerstrasse 3-5,
80335 Munich, Germany

devices, small amounts of microdissected material—as little as one single cell—can be directly transmitted and immediately used for single cell analysis.

Keywords Laser microdissection · Single particle handling · Low pressure · LV-PCR microchip

1 Introduction

Modern molecular research and diagnosis relies increasingly on the capability to isolate pure samples of single particles and their precise positioning for further biochemical analysis. A major goal in human genetic diagnosis is the genomic characterization of one single cell, e.g. a blastomere or a polar body in preimplantation genetic diagnosis (PGD). Such applications require reliable methods for single cell analyses, the most promising of which are microdissection techniques.

Microdissection techniques enable the precise manipulation and isolation of genetic material in the range of several micrometers, from fragments of histological tissue sections down to single cells or single chromosomes. Using glass needle microdissection, where the tip of an extended glass needle is in contact with the sample, dissected material is typically in the range of 1 μm, depending on the needle diameter. Chromosomal aberrations, for instance, were characterized in a highly specific manner by microdissection and reverse FISH painting of single chromosome fragments (Weimer et al. 2001). However, the limited visible area at high light microscopic magnifications makes it difficult to trace the target, and procedures are tedious and time-consuming.

In contrast, non-contact techniques based on laser microdissection enable highly selective extraction of small-

est fractions of genetic material with minimum risk of contamination (Thalhammer et al. 2003). Using laser capture microdissection (LCM) samples are extracted thermally via local fusion of a synthetic membrane to the sample surface by an IR laser. This technique is applicable for the extraction of single particles down to 3–5 μm particle size (Simone et al. 1998). In contrast to LCM, using the laser pressure catapulting approach the sample material is fixed on an ultra thin PEN-carrier membrane (2 μm). Via the light-pressure of an UV-A laser microdissected material can selectively be isolated "bottom-up" into a collection device (Thalhammer et al. 2003). A similar technology providing transfer of microdissected material via short laser impulse into microtubes deals with sample preparation performed via a sandwich system where samples are placed on a PET-membrane (1.4 μm) and turned upside down onto a standard glass slide (Kirschner and Plaschke-Schluetter 2007). Non-contact transport of microdissected material can further occur via gravity effects; while turning tissue samples mounted on special foil slides upside down, UV laser isolated material falls by gravity directly into a PCR cap centered below (Di Martino et al. 2004). All the above-mentioned laser microdissection methods transfer isolated material into collection tubes or wells.

Here we present a novel system for transferring laser microdissected material in form of single particles via low-pressure technology. This *s*ingle *p*article *a*dsorbing *t*ransfer *s*ystem (SPATS) provides a totally new approach for controlled horizontal material transfer after laser microdissection directly to any planar microdevice with μm-precision.

2 Material and methods

2.1 Technical description

Via an adaptor the SPATS can be fixed to any inverted microscope. Here, all non-contact microdissection and transfer procedures were performed using an inverted optical microscope (Axiovert, Zeiss, Oberkochen, Germany) with a 337 nm nitrogen laser coupled into the light path, a CCD camera (Q Imaging, Surrey, Canada) and the novel SPATS device combining mechanical, optical, pneumatic and electronic components for low-pressure transfer of single microdissected particles.

All functions and parameters of hardware components like XY-scanning stage, camera, transfer system and pressure supply could be custom adapted with flexible control software ('Nanosauger' Version 2.4, XYZ High Precision, Darmstadt, Germany), ensuring control and flexible usage of the equipment. Thus parameters like position, height and running speed of the device as well as distance control, duration and pressure of the adsorption

and release processes could be varied for different applications. In addition, the transfer process can be programmed and run automatically in future.

Visualization of the transfer process, or rather visual verification of sample uptake and release, was mediated via a miniature detection unit of an inverted optical microscope and a CCD camera with a flexible application programmer interface (A.P.I.).

Due to its modular character the novel SPATS could be application specific optimized and adjusted to an existing inverted optical microscope used for laser microdissection. Isolation of sample material fixed on a 2 μm thick supporting membrane was performed via laser microdissection as previously described (Thalhammer et al. 2004). Take-up positions on sample slides were moved into the field of view via a precision open-loop XY-scanning technology, providing motion accuracy beyond 1 μm. The whole SPATS instrument was fixed on the microscope tripod in combination with a conventional micrometer step motor providing the required technology for the transfer process. Four degrees of freedom, comprising one rotatory and three translational motions (xyz), enabled the exact positioning of a carrier trunk associated sample adsorbing head above the sample take-up area with micrometer accuracy (Fig. 1(a), (b)). Thus, maximum precision and rapid collection of even the smallest specimens were possible. The degrees of freedom of the microscope XY-scanning stage as well as those of the transfer device were controlled by the developed software. Additionally, a LTA-02 laser sensor auto-focus unit (Selectronet AG, Krefeld, Germany) was integrated for automatic distance control, by constantly measuring the distance of sample adsorbing head to sample surface. For optimal sample uptake, the sample adsorbing head is stopped at approximately 100 μm above the sample surface. Via the micrometer step motor the laser sensor is mechanically maneuverable in the same way as the head allowing calibration.

The sample adsorbing head consisted of a copper collection grid attached to a transparent glass tube with 1.7–2.0 mm external diameter, 500 μm internal diameter and 60 mm in length (Fig. 1(b)). For pressure supply, this transparent glass tube was connected to a pneumatic picopump via low- and high-pressure adaptors. Via the collection grid, featuring an adsorption field of 500 μm and pores with less than 5 μm in diameter, particles in the range of at least 5 μm could be adsorbed and released again (Fig. 1(c)). The collection grid was biologically inert, antistatic and UV-C resistant. For different applications the sample head and so the collection grid could easily be exchanged according to sample requirements via 'easy-to-fit' click system. Thus, even for individual extraction processes a new adsorbing head could be used to limit the risk of contamination. Designed as a disposable, it is also
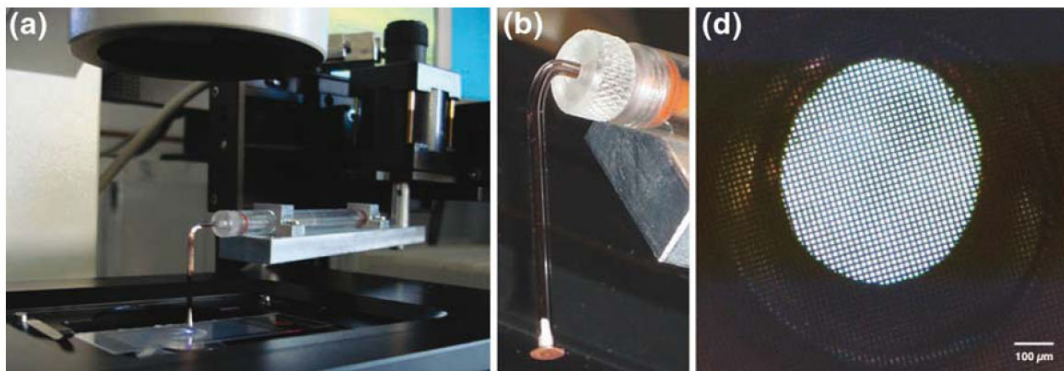
Springer

Fig. 1 Single particle adsorbing transfer system (SPATS) for high precise low-pressure transfer of genetic material onto a glass surface for further biochemical processing: (**a**) SPATS system, integrated into a conventional inverted optical microscope: micrometer step motor providing exact positioning, the carrier trunk with easy-to-fit click system, the sample adsorbing head and the collection grid centered to a sample slide; (**b**) exchangeable adsorbing head via an easy-to-fit click system, comprising the low-pressure capillary and the sample collection grid; (**c**) collection grid: grid diameter 500 μm, pore diameter 5 μm

possible to clean the adsorbing head in use by dipping into 70% EtOH and subsequently drying under UV-C irradiation after each isolation session. Additionally, grid as well as pore size could precisely be adjusted to accommodate different sample sizes and sample states.

A computerized sensitive PLI-100 pressure control unit (Harvard Apparatus, Holliston, US) allowed fine-tuning of both low-pressure (0–0.75 kPa) and high-pressure (413 kPa) for sample adsorption and release, respectively.

2.2 PCR analyses of isolated and transferred material

As proof of contamination free transfer PCR reactions were performed after single particle isolation of a) bone material from Egyptian mummies for sex determination using primer-specific Amelogenin PCR and b) single fibroblast isolation for unspecific *Alu*-PCR amplification. Experiments were performed in several independent approaches whereas adsorbing head devices were replaced after each experiment.

a) *Primer-specific Amelogenin PCR from Egyptian mummy bone sections*

After decalcification 3–5 μm sections from a tissue block of the occipital bone were placed on 2 μm laser supporting polyethylene-naphtalate membrane (PEN) mounted on microscopic slides (MicroDissect GmbH, Herborn, Germany). To avoid external contamination, nested paraffin embedded blocks were used. Deparaffinization was achieved by rehydration steps in fact 30 min Xylol, 5 min 100% EtOH, 5 min 90% EtOH and 5 min 70% EtOH; then tissue slides were dried at 37°C. Small particles of about 350 μm in diameter were isolated via laser microdissection out of bone sections and transferred via the SPATS directly into a 0.2 ml reaction tube containing 10 μl of lysis solution (First-DNA All-tissue

DNA blue kit, Gen-ial GmbH, Troisdorf, Germany). DNA extraction was performed using the First-DNA All-tissue DNA blue kit (Gen-ial GmbH, Troisdorf, Germany) and isolated DNA was resolved in 10 μl of ddH_2O (the detailed methodical description can be found in Woide et al. 2008, publication in preparation). 1 μl of 10 μl extraction solution was used for PCR analysis and dried at 30°C on reaction sites of a virtual reaction chamber (VRC) PCR device (AmpliGrid, Advalytix AG, Munich, Germany). 1 μl Amelogenin PCR reaction mix contained 1× Qiagen master mix (Fast Cycling PCR Kit, Qiagen GmbH, Hilden, Germany), 1× Q-Solution (Fast Cycling PCR Kit, Qiagen GmbH, Hilden, Germany) and 1 μM of each primer Amel1 (5′-CCC-TGG-GCT-CTG-TAA-AGA-ATA-GTG-3′; Metabion GmbH, Martinsried, Germany) and Amel2 (5′-ATC-AGA-GCT-TAA-ACT-GGG-AAG-CTG-3′; Metabion GmbH, Martinsried, Germany). Each 1 μl PCR mixture was immediately covered with 5 μl sealing solution (Advalytix AG, Munich, Germany) to avoid evaporation. PCR was performed on an AmpliSpeed thermocycler (Advalytix AG, Munich, Germany) using the following conditions: 30 s at 94°C, 30 s at 60°C, 30 s at 72°C for 40 cycles after an initial denaturation step of 5 min at 95°C.

PCR products were analyzed on polyacrylamide gels (CleanGel HyRes, ETC GmbH, Kirchentellinsfurt, Germany) after silver staining (DNA silver staining kit, GE Healthcare, Uppsala, Sweden). All experiments were done in duplicates.

b) *Single fibroblast isolation for unspecific Alu-PCR amplification*

Fibroblast cells were cultured in RPMI +10%FCS +10,000 U Streptomycin (Biochrom AG, Berlin, Germany) on a 2 μm PEN-microscopic slide (MicroDissect GmbH, Herborn, Germany) at 37°C, 5% CO_2, for 1–2 days. After drying on the membrane at 37°C, single fibroblast cells

were isolated via laser microdissection, transferred via SPATS to reaction points on a VRC ChromoChip PK 60 PCR slide (Advalytix AG, Munich, Germany), released into a 200 nl water droplet and subsequently dried at room temperature. 1 μl of *Alu*-PCR reaction mix containing 0.025 U HotStarTaq polymerase (Qiagen GmbH, Hilden, Germany), 1× HotStarTaq master mix (Qiagen GmbH, Hilden, Germany) and *Alu*-primers (Advalytix AG, Munich, Germany) was pipetted on each single fibroblast cell at reaction sites on the chip. Each 1 μl PCR mixture was immediately covered with 5 μl sealing solution (Advalytix AG, Munich, Germany) to avoid evaporation. 1 μl VRC PCR was performed on the ChromoChip PK 60 using a conventional thermocycler (Eppendorf, Hamburg, Germany) using the following conditions: 30 s at 94°C, 30 s at 62°C, 30 s at 72°C, for 40 cycles after an initial denaturation step of 15 min at 95°C. PCR products were analyzed on 6% polyacrylamide gels.

3 Results and discussion

3.1 Mode of operation

The transfer device SPATS is designed to transfer any kind of fixed particles in the range of at least 5 μm up to 500 μm in diameter selectively via low-pressure. The adsorption limit of 5 μm particle size, however, applies to the size of microdissected PEN-membrane carrier fragments. The size of the biological sample isolated can be smaller (e.g. single metaphase chromosome isolation see Fig. 2(g), (h)). Particle shape should be planar and particle weight depends on the applied pressure and the suction volume according to the grid diameter. Due to the chemical composition of the supporting membrane, the PEN membrane is stable up to 155°C and doesn't interfere the subsequent PCR analyses and is also resistant to solvents. During the transfer process the sample is neither changed morphologically, chemically nor biologically. As an important feature the transfer process can visually be controlled at any time during the isolation process.

Biological material for microdissection is fixed on ultra thin PEN-carrier-membrane and positioned onto the scanning stage slide holder of an inverted optical microscope. After laser micro-isolation of a specific fragment, the low-pressure transfer device SPATS is swiveled in the field of view and maneuvered to the sample surface. This is accomplished either manually or by laser sensor via automatic distance-control operation. Subsequently, by applying low-pressure (0–0.75 kPa), the microdissected material is adsorbed to a collection grid. Then, the low-pressure transfer system is maneuvered out of the field of
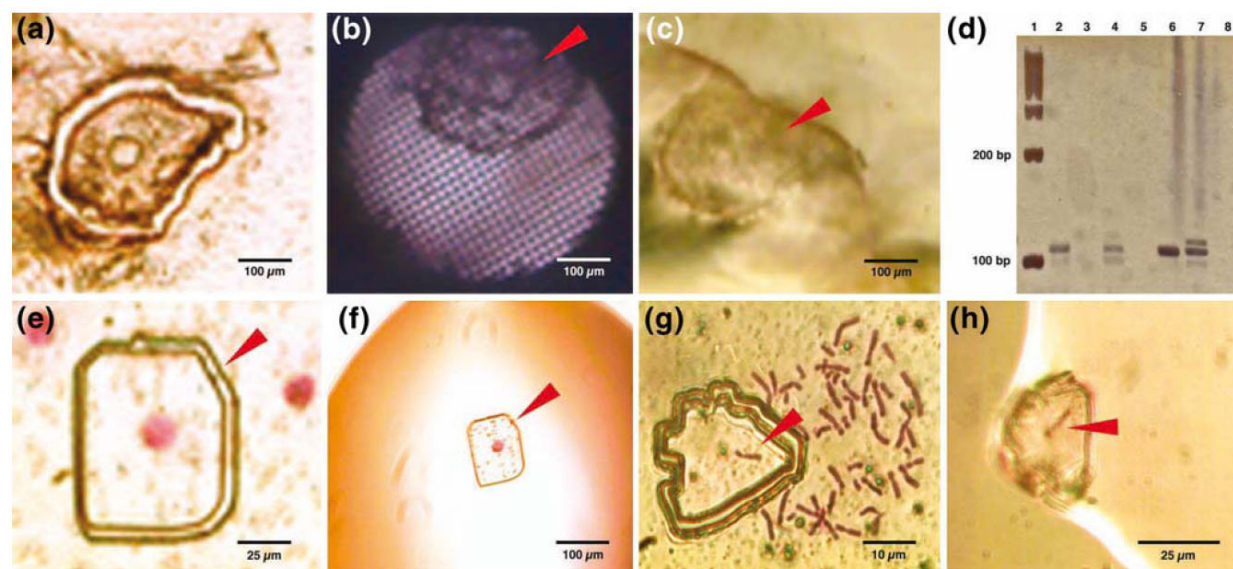

Fig. 2 Workflow of the transfer process via low-pressure single particle adsorbing transfer system demonstrated by microdissection of sample material in the range from 350 μm down to 5 μm and subsequent PCR analysis: (**a**) hard material like paraffin-embedded bone tissue sections (~300 μm) and soft material like (**e**) single cells (~20 μm, see *red arrow*) or (**g**) single chromosomes (~1–10 μm, see *red arrow*). Low-pressure transfer of single particles can visually be controlled: sample take-up via adsorption of isolated bone material to the collection grid of the adsorbing head ((**b**), see *red arrow*) and precisely controlled release of adsorbed sample material into a small droplet of fluid, e.g. 0.2 μl buffer solution, via high-pressure impulse ((**c**), (**f**), (**h**); see *red arrows*). PCR analysis of bone tissue material on the Amelogenin gene for sex determination (**d**): lane *1*: 100 bp molecular weight marker (PeqLab Biotechnologie GmbH, Erlangen, Germany); lane *2* and *4*: 106 bp female mummy DNA amplification product (see *red arrows*); lane *6* and *7*: reference products of 106 bp female and 106/112 bp male DNA; lanes *3*, *5* and *8*: negative controls of PEN-membrane, PCR master mix and lysis buffer mix

view and moved horizontally to the surface of an analysis device (e.g. a VRC microdevice). For further processing of the extracted sample, a small volume of fluid is applied onto the sample take-up device. Those fluid volumina for sample uptake can be chosen very small, e.g. 0.2–1.0 µl of buffer solution. During this whole process, low-pressure is maintained to avoid loosing the sample. When positioned at a close distance, approximately 100 µm, to the surface of the buffer droplet, release of sample material is achieved by switching from low-pressure operation to a short high-pressure impulse (413 kPa, 2 ms) (Fig. 2(c), (f), (h)). In this way, sample material can be transferred either into the cap of a conventional reaction tube or, more importantly, onto an integrated microdevice, being available for further biochemical processing. By this means sample material is adsorbed, transferred and released in a highly precise, safe, reliable and gentle way at a predefined, designated position, in fact from the collection grid into smallest amounts of fluid, without dispersing the fluid. Adsorbing heads and collection grids respectively can easily be exchanged for every single isolation procedure and for different kinds of samples. Concerns about the feasibility, that the suction technique may also remove tissue pieces besides the target sample, which are not firmly enough attached to the supporting membrane, can be invalidated due to the following facts: the suction power lateral to the grid area is minimal, and the low-pressure used for isolation is too low to extract whole unisolated particles or fragments from the supporting membrane or the supporting membrane itself. Only completely isolated material can be adsorbed.

3.2 Applications: proof of principle

This novel transfer device offers a wide range of applications. Proof of principle was realized in numerous experiments with two kinds of materials, hard ones like bone tissue particles (Fig. 2(a–c)), and soft ones like single cells or chromosomes (Fig. 2(e–h)).

Experiments were performed on bone tissue particles originating from Egyptian mummies (Fig. 2(a–c)). Bone particles in the range of about 300 µm in diameter (corresponds to 10–52 preserved cells (Vashishth et al. 2000)) were microdissected selectively (Fig. 2(a)). After approaching the sample adsorbing head to the bone particle surface, microdissected material was adsorbed to the collection grid via low-pressure for sample take-up (Fig. 2(b)) and released into a 0.2 ml collection tube (Fig. 2(c)) being available for further conventional DNA extraction and analysis methods like primer-specific PCR amplification. For molecular sex determination a segment of the Amelogenin gene was amplified (Fig. 2(d)), which is located on the human sex chromosomes. The amplification product of the amelogenin gene results in a 112 bp fragment from the Y-chromosome and a 106 bp fragment of the X-chromosome (Shadrach et al. 2004). Therefore males show two PCR products, while females give a single amplification product. Experiments were performed several times and results were extremely reproducible each time (Woide et al. 2008), publication in preparation).

Moreover, soft samples like single fibroblast cells were isolated via laser microdissection (Fig. 3(a)), adsorbed via SPATS (Fig. 3(b)) and then precisely transferred to reaction points on a planar VRC ChromoChip PK 60 slide (Fig. 3(c)). Despite spot distances of about 2 mm, reaction sites on the chip could be filled in a highly precise manner, thus samples could be released exactly within marked reaction sites. For reproducibility, during the experiment 50–100 single microdissected fibroblast cells were each released precisely into 0.2 µl of sterile water on the ChromoChip PK 60 surface and subsequently dried at room temperature, being available for whole genome amplification of single cells e.g. in Alu-PCR analysis, resulting in a typical DNA fragment 'smear' (Fig. 3(d)) showing successfully amplified Alu-sequences (a kind of SINE (short interspersed nuclear elements)-repeats in genomic DNA. Alu-PCR thus is a kind of whole genome
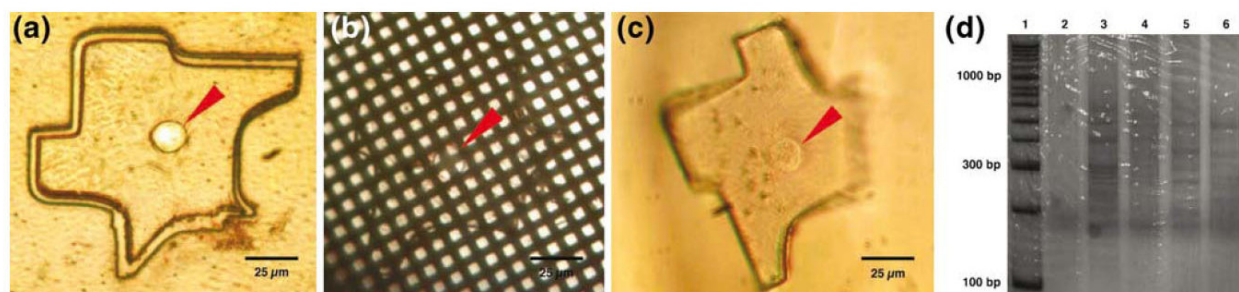

Fig. 3 Isolation and transfer of a single living fibroblast cell via SPATS (see *red arrows* in (**a**) to (**c**)) followed by Alu-PCR analysis. (**d**) Polyacrylamide gel of *Alu*-PCR products: lane *1*: length standard Hyper Ladder II (Bioline, London, UK); lane *2*: negative control; lanes *3–6*: *Alu*-PCR whole genome amplification products of single fibroblast cells (see *red arrows*)

amplification method to increase the amount of starting material for several different downstream analyses like PCR or sequencing for detection of specific mutations (Van Orsouw et al. 1997). Besides the cell preparations, first tests of the low-pressure transfer method have been performed on historic human tissue sections just as a clear evidence, that even sample material that is that difficult to handle can reliably be extracted and transferred for analysis.

In summary we present a novel device for extracting and transferring laser microdissected sample material further to analysis devices via low-pressure technology. Compared to established transfer technologies after laser microdissection, the advantage of this novel approach lies in the gentle way to release isolated biological material not only into conventional microtubes but also directly and very precisely onto horizontal surfaces of planar microdevices for further molecular analysis. Consequently, intermediate steps of comparable methodologies need not be applied reducing essentially the possibility of contamination and risk of loosing material.

The local release of isolated sample material can be performed exactly at any predefined target position, an important feature which all the other microdissection transfer systems lack. In addition possible alterations of tissue, cells or genetic material are minimized in comparison to available laser microdissection techniques due to the low-pressure procedure.

The SPATS device is part of a novel multifunctional submicroliter lab-on-a-chip system (LOC) for molecular diagnostic applications (Thalhammer et al. 2007; Woide et al. 2008). This LOC combines two very important pre-analytical aspects in handling minute amounts of biological samples like non-contact laser microdissection and well-directed transfer of isolated material onto specific reaction sites without contamination. However, an important fact was, that in principle this low-pressure transfer system works autonomous of further pre- or post-analysis steps thus facilitating not only its modular integration in existing systems but also the ability to update novel adaptations and upgrades.

3.3 Outlook

There exist although several other techniques for the transfer of isolated material into analytic vessels. To our knowledge, no comparable system for transferring biological sample material has neither commercially been available nor presented. The convenience of possible horizontal transfer of sample material via SPATS even to planar microdevice surfaces provides convincing evidence that this novel technique is improved capable to well established and widely used techniques. A huge potential arises from the application of the totally new methodology of low-pressure transfer in respect to scientific applications and also for possible future applications besides DNA analyses. The system has high potential in RNA and protein analyses microchip systems. The SPATS system is patent-registered (EU patent 08150662.8).

References

D. Di Martino, G. Giuffrè, N. Staiti, A. Simone, P. Todaro, L. Saravo, Forensic Sci. Int **146**, 155–157 (2004). doi:10.1016/j.forsciint.2004.09.047

J. Kirschner, A. Plaschke-Schluetter, Nat. Methods **4** (2007)

B. Shadrach, M. Commane, C. Hren, I. Warshawsky, J. Mol. Diagn **6**(4), 401–405 (2004)

N.L. Simone, R.F. Bonner, J.W. Gillespie, M.R. Emmert-Buck, L.A. Liotta, TIG **14**(7), 272–276 (1998)

S. Thalhammer, G. Lahr, A. Clement-Sengewald, W.M. Heckl, R. Burgemeister, K. Schütze, Laser Phys **13**(5), 681–692 (2003)

S. Thalhammer, S. Langer, M.R. Speicher, W.M. Heckl, J.B. Geigl, Chromosome Res **12**, 337–343 (2004). doi:10.1023/B:CHRO.0000034132.77192.5f

S. Thalhammer, Z. von Guttenberg, U. Koehler, A. Zink, W.M. Heckl, T. Franke et al., GenomXPress **1/07**, 29–31 (2007)

N.J. Van Orsouw, D. Li, J. Vijg, Mol. Cell. Probes **11**(2), 95–101 (1997). doi::10.1006/mcpr.1996.0089

D. Vashishth, O. Verborgt, G. Divine, M.B. Schaffler, D.P. Fyhrie, Bone **26**(4), 375–380 (2000). doi:10.1016/S8756-3282(00)00236-2

J. Weimer, M.R. Koehler, U. Wiedemann, P. Attermeyer, A. Jacobsen, D. Karow et al., Chromosome Res **9**, 395–402 (2001). doi:10.1023/A:1016735618513

D. Woide, V. Mayer, T. Neumaier, T. Wachtmeister, H.G. Paretzke, Z. von Guttenberg, et al, Proceedings of the first international conference on biomedical electronics and devices Vol 2, ISBN: 978-989-8111-17-3: 265–271 (2008)

Original Paper

Fetal Diagnosis and Therapy

Single Cell Analysis of Mutations in the *APC* Gene

Veronika Mayer[a]   Ulrike Schoen[b]   Elke Holinski-Feder[b]   Udo Koehler[b]
Stefan Thalhammer[a]

[a]Helmholtz Zentrum Munich, German Research Center for Environmental Health, Institute of Radiation Protection, Neuherberg, and [b]MGZ Medical Genetics Center, Munich, Germany

Abstract
Introduction: Mutation analysis of inherited monogenic diseases is an important aspect of preimplantation genetic diagnosis. Familial adenomatous polyposis of the colon is an autosomal dominant inherited disorder caused by mutations in the tumor suppressor gene adenomatous polyposis coli *(APC)*. A characteristic of this severe disease is the development of thousands of polyps in the colon which untreated evolve into malignant colon carcinomas. Here we present a novel approach for the establishment of mutation detection in the *APC* gene in single cells applicable for preimplantation genetic diagnosis. ***Methods:*** Single fixed lymphocytes were isolated via laser microdissection and transferred to reaction centers of planar chemically structured glass slides via a recently developed horizontal low-pressure single particle adsorbing transfer system (SPATS). A multiplex nested polymerase chain reaction protocol in a 1-μl reaction volume, followed by sequencing and fragment length analysis was applied in order to detect mutations in the *APC* gene. ***Results:*** Reliable isolation and transfer of single lymphocytes was demonstrated. High amplification efficiency and low allelic drop out (ADO) rates for polymorphic microsatellite markers and mutation specific amplification products of various mutations in the *APC* gene were obtained from fixed single cells. ***Conclusions:*** This novel nanotechnological downscaling approach enables a reliable validation of genetic testing using diploid single lymphocytes, and will open a wide range of single cell diagnostics.

Copyright © 2009 S. Karger AG, Basel

Introduction

The ability to analyze individual single cells plays an increasingly important role in molecular genetic diagnostics. In preimplantation genetic diagnosis (PGD), mutation analysis has to be performed on only a few or even single cells: blastomeres, blastocyst cells and polar bodies. Recently, mutation analysis of inherited monogenic disorders has successfully been established [1–4].

Here we present a fast and reliable technique for mutation analysis of single cells. The isolation of specific single cell samples and their precise positioning for further analysis constitutes a basic aspect. Up to now, different methods for the isolation of single cells have been in rou-

Dr. Stefan Thalhammer, Helmholtz Zentrum Munich
German Research Center for Environmental Health, Institute of Radiation Protection
Ingolstädter Landstrasse 1, DE–85764 Neuherberg (Germany)
Tel. +49 89 3187 2893, Fax +49 89 3187 3323
E-Mail stefan.thalhammer@helmholtz-muenchen.de

tine laboratory use, e.g. extraction via fluorescence-activated cell sorting (FACS) [5, 6], glass needle microdissection [7] and a broad variation of laser-based microdissection techniques, like laser capture [8], laser pressure catapulting [9], laser impulse [10], or isolation via gravity effects [11]. Microdissection techniques enable the precise manipulation and isolation of genetic material within a range of several micrometers, from fragments of histological tissue sections down to single cells or single chromosomes. The low quantity of DNA on single cells leads to a number of complications in mutation analysis which are rarely found in normal routine diagnostics. Mutation analysis must therefore be carefully validated and optimized as regards amplification efficiency and the evaluation of allelic drop out (ADO) rates before application to PGD, e.g. haploid polar body analysis. In this study, isolation of fixed single lymphocytes is achieved using laser microdissection in combination with the recently developed low-pressure single particle adsorbing transfer system (SPATS). This approach allows the transfer of the isolated material to a planar chemically structured glass slide with micrometer precision [12]. The deposition of a single cell to a reaction center, either conventional reaction tubes or chemically structured devices, is facilitated by microscopic control of the entire process. On a planar polymerase chain reaction (PCR) device, a 1-μl droplet of PCR mixture forms its own 'virtual' reaction chamber, held together by surface tension due to the hydrophilic/hydrophobic chemically structured surface [13]. Markedly reduced thermal mass of the entire PCR system effects rapid heating and cooling rates and therefore enables PCR reactions in less time with increased efficiency (for review, see [14]).

As proof of concept we show the specific detection of mutations in the tumor suppressor gene adenomatous polyposis coli (*APC;* OMIM 611731). Mutations of the *APC* gene (chromosome 5q22.2, 15 exons) are associated with familial adenomatous polyposis of the colon (FAP; OMIM 175100). FAP is an autosomal-dominant disorder with a >95% risk of colorectal cancer without prophylactic colectomy. This inherited disorder is characterized by multiple polyps occurring in the colon during the second decade of life [15].

Material and Methods

Preparation and Isolation of Single Cells

Human lymphocytes were isolated from peripheral blood samples of three FAP patients heterozygous for mutations in exon 15 of the *APC* gene (patient A: c.2612delG; patients B and C:

c.3183–3187delACAAA) and were prepared following standard techniques [16]. Fixed single lymphocytes were applied to a 2-μm polyethylene-naphthalate membrane mounted on a glass slide (Carl Zeiss MicroImaging GmbH, Munich, Germany) and isolated via laser-based microdissection [16]. The isolated cells were transferred horizontally via the low-pressure transfer system SPATS to reaction centers of a planar hydrophilic/hydrophobic structured glass slide (AmpliGrid, Advalytix-Olympus GmbH, Munich, Germany) [12]. Cells were released into 300-nl sterile water droplets and dried at room temperature. All preparative steps were performed under optical control.

Single Cell PCR Analysis

All single cell PCR reactions were carried out as multiplex PCRs with primers specific for the *APC* gene region of interest together with primers for the polymorphic microsatellite markers D5S346 and D5S82 (table 1). When only a minute amount of DNA is available, the simultaneous amplification of polymorphic marker sequences combined with the amplification of the mutated gene region is important in order to avoid misdiagnosis due to preferential amplification, allelic drop out or contamination. The low-volume PCR reactions were carried out in 1 μl total reaction volume covered with 5 μl mineral oil to prevent evaporation and external contamination (fig. 1). The PCR products from the slides were transferred into 0.2 ml reaction tubes and diluted 1:10 with sterile water. Aliquots of 3 μl of each diluted sample were used as templates in secondary PCRs with mutation-specific and marker specific primers respectively. Primer sequences, mutation positions and the detection methods used are listed in table 1. First PCR was performed using an AmpliSpeed slide cycler (Advalytix-Olympus GmbH), secondary PCR using a Primus Advanced96 Peqlab Cycler (Peqlab Biotechnologie GmbH, Erlangen, Germany). A detailed overview of all PCR protocols is presented in table 2. PCR was carried out using the QIAGEN Multiplex PCR Kit (Qiagen GmbH, Hilden, Germany) according to the manufacturer's instructions. Secondary mutation-specific nested PCR products were separated on 2% agarose gels (E-gel 96) to control the presence and quality of amplification products. Subsequently, PCR reactions were further analyzed via fragment length analysis and sequencing analysis.

Sequencing Analysis

Double-strand sequencing of mutation-specific nested PCR products was performed with the BigDyeB Terminator v1.1 Cycle Sequencing Kit (Applied Biosystems, Foster City, Calif., USA) and the AB Hitachi 3730 DNA Analyzer (Applied Biosystems) according to the manufacturer's instructions. Data were analyzed using Mutation Surveyor V3.10 Software. Sequencing was performed to detect the specific deletions and to confirm the results of fragment length analysis.

Fragment Length Analysis

An aliquot of 1 μl secondary PCR with FAM-labeled primers was mixed with 12.7 μl of Hi-Di™ formamide (Applied Biosystems) and 0.3 μl of GeneScan™-500LIZ™ size standard (Applied Biosystems) and prepared for analysis on an AB/Hitachi 3130xL Genetic Analyzer (Applied Biosystems). Data were analyzed using GeneScan™ software (Applied Biosystems).

Table 1. Details on primer sequences and mutation detection methods

Primer	Sequence (5′–3′)	Mutation/marker location	Detection method
PA1-F PA1-R	GAA TAC TAC AGT GTT ACC CAG CTC TCA GTG GTA GAC CCA GAA CTT	c.2612delG	
PA2-F PA2-R	AGA ACG CGG AAT TGG TCT AGG CA TGA CTT TGG CAA TCT GGG CTG CA	c.2612delG	gel electrophoresis sequencing analysis
PA-S1-F PA-S2-R	CAT CCA GCA ACA GAA AAT CCA G GCA AAC CTC GCT TTG AAG AAG TTC	c.2612delG	SNaPshot analysis
PB1-F PB1-R	CAG TTG AAC TCT GGA AGG CAA GGA GAA ACA CAT TCC TGC TGT C	c.3183–3187delACAAA	
PB2-F PB2-R PB2-F[1]	AAG ATG GGC AAG ACC CAA ACA C TGC TGT CCA AAA TGT GGT TGG AAG ATG GGC AAG ACC CAA ACA C	c.3183–3187delACAAA	gel electrophoresis sequencing analysis fragment length analysis
D5S346-F[1] D5S346-R	ACT CAC TCT AGT GAT AAA TCG GG AGC AGA TAA GAC AGT ATT ACT AGT T	5q22–q23	fragment length analysis
D5S82-F[1] D5S82-R	ATC AGA GTA TCA GAA TTT CT CCC AAT TGT ATA GAT TTA GAA GTC	5q21.3	fragment length analysis

Nested PCR reactions were carried out with primer pairs PA1-F/R and PA2-F/R for the analyses of the 1-bp deletion of patient A and with primers PB1-F/R and PB2-F/R for the 5-bp deletion of patients B and C.

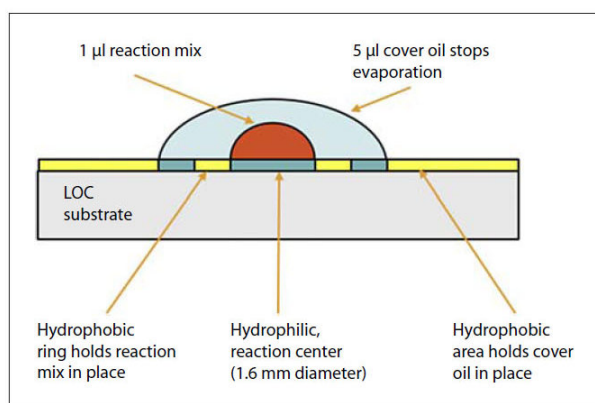[1] Labeled with 6-FAM.

Color version available online

Fig. 1. Scheme of the planar hydrophilic/hydrophobic structured glass slide with 1 µl PCR reaction mixture covered with 5 µl mineral oil.

Single Nucleotide Primer Extension (SNaPshot) Analysis

Aliquots of 3 µl of purified first PCR were used as templates for SNaPshot reactions. They were performed using the ABI PRISM® SNaPshot® Multiplex Kit (Applied Biosystems) according to the manufacturer's instructions. 0.5 µl of the SNaPshot product was mixed with 10 µl of Hi-Di™ formamide (Applied Biosystems) and 0.5 µl of GeneScan™-120LIZ™ size standard (Applied Biosystems) and prepared for analysis on an AB/Hitachi 3130xL Genetic Analyzer (Applied Biosystems). Data were analyzed using GeneScan™ software (Applied Biosystems) [17].

Results

Single Cell Isolation and Transfer

Isolation of unstained fixed single lymphocytes was performed reliably using laser microdissection and the horizontal low-pressure transfer system SPATS. Cells were transferred and positioned precisely in 300 nl of sterile water droplets to the reaction centers (1.6 mm diameter, fig. 1) on the modified glass surface. All single cell isolation, transfer and deposition processes were controlled optically via light microscopy (fig. 2).

Single Cell Analysis

Multiplex PCR was carried out for a total of 108 fixed single lymphocytes and 23 negative controls. The mutation-specific amplification products were part of the initial nested PCR reactions. The amplification products of microsatellite marker PCR served as control for the detection of allelic drop out or contamination events. To

Fig. 2. Isolation of a single human lymphocyte (for picture, cells were stained with Giemsa, see arrows) prepared from whole peripheral blood. **a** Laser microdissected single cell fixed on a 2-μm polyethylene-naphthalate membrane mounted on an object slide. **b** Isolated single cell released into a 300 nl droplet of sterile water on the surface of a planar PCR device after horizontal transfer via the single particle adsorbing transfer system. The specific form of the particle was chosen in order to identify the single cell.
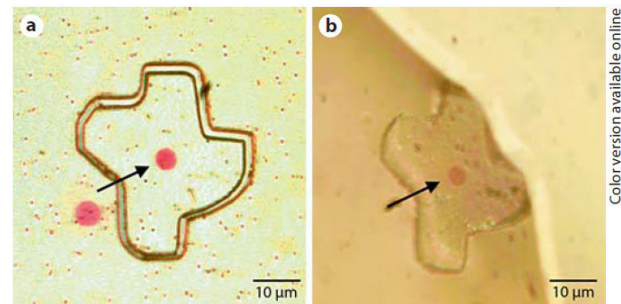
Color version available online

Table 2. Overview of all PCR protocols

Patient/loci	First PCR	PCR conditions	Loci	Secondary PCR	PCR conditions
Patient A/ c.2612delG	2 μmol/l PA1-F/R	97°C, 20 min 94°C, 30 s 64°C[1], 90 s } 15× 72°C, 30 s 94°C, 30 s 50°C, 30 s } 15× 72°C, 30 s 72°C, 7 min	c.2612delG	1 μmol/l PA2-F/R SNaPshot, 0.2 μmol/l S1/S2-F/R	95°C, 15 min 94°C, 30 s 62°C, 60 s } 30× 72°C, 30 s 72°C, 7 min 96°C, 10 s 50°C, 5 s } 25× 60°C, 30 s
Patient B/ c.3183–3187 delACAAA and D5S346	2 μmol/l PB1-F/R 2 μmol/l D5S346	97°C, 20 min 94°C, 30 s 64°C[1], 90 s } 15× 72°C, 30 s 94°C, 30 s 50°C, 30 s } 15× 72°C, 30 s 72°C, 7 min	c.3183–3187delACAAA D5S346	1 μmol/l PB2-F/R, 62°C 1 μmol/l PB2-F/R-FAM, 64°C 1 μmol/l D5S346-F/R-FAM	95°C, 15 min 94°C, 30 s 62/64°C, 60 s } 30× 72°C, 30 s 72°C, 7 min 95°C, 15 min 94°C, 30 s 57°C[1], 60 s } 7× 72°C, 30 s 94°C, 30 s 50°C, 30 s } 25× 72°C, 30 s 72°C, 7 min
Patient C/ c.3183–3187 delACAAA, D5S346 and D5S82	2 μmol/l PB1-F/R 2 μmol/l D5S346-F/R-FAM 2 μmol/l D5S82-F/R-FAM	97°C, 20 min 94°C, 30 s 64°C[1] 90 s } 15× 72°C, 30 s 94°C, 30 s 50°C, 30 s } 10× 72°C, 30 s 72°C, 7 min	c.3183–3187delACAAA D5S346 D5S82	2 μmol/l PB2-F/R-FAM 2 μmol/l D5S346-F/R-FAM 2 μmol/l D5S82-F/R-FAM	95°C, 15 min 94°C, 30 s 59°C, 60 s } 25× 72°C, 30 s 72°C, 7 min 95°C, 15 min 94°C, 30 s 57°C[1], 60 s } 7× 72°C, 30 s 94°C, 30 s 50°C, 30 s } 20× 72°C, 30 s 72°C, 7 min

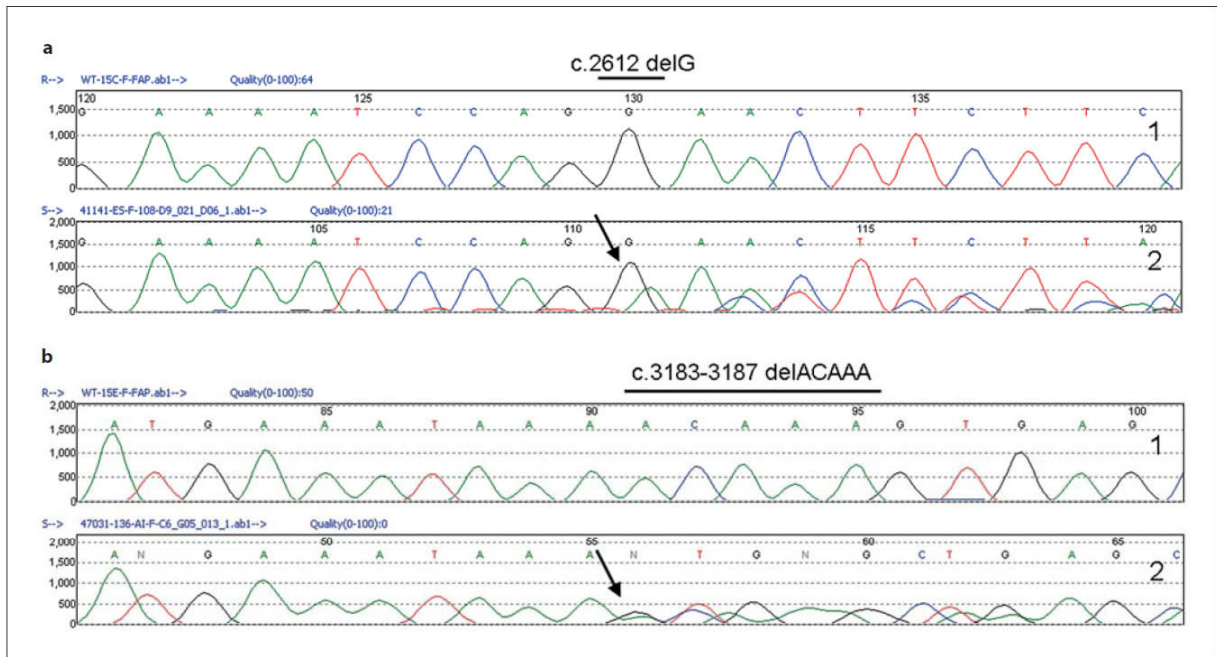[1] Temperature increment of –1°C per cycle.

Fig. 3. Specific mutations in the *APC* gene of FAP patients A, B and C. **a** Sequencing shows the heterozygous 1 bp deletion (c.2612delG) (arrow) of patient A. Lane 1: wild-type sequence of exon 15; lane 2: forward patient specific sequence. **b** Shows the wild-type sequence in lane 3 and the heterozygous sequence (forward) with the 5-bp deletion (c.3183–3187delACAAA) (arrow) of patients B and C in lane 4.

Fig. 4. Results of the fragment length analysis of the multiplex PCR for patient C (c.3183–3187delACAAA). Full profile consisting of 6 alleles (opaque peaks), generated with the three primer pairs D5S346: alleles 111 bp/119 bp; PB2-FAM: 137 bp (mutated)/142 bp (wild type) and D5S82: 173 bp/179 bp. Size standard: transparent peaks.
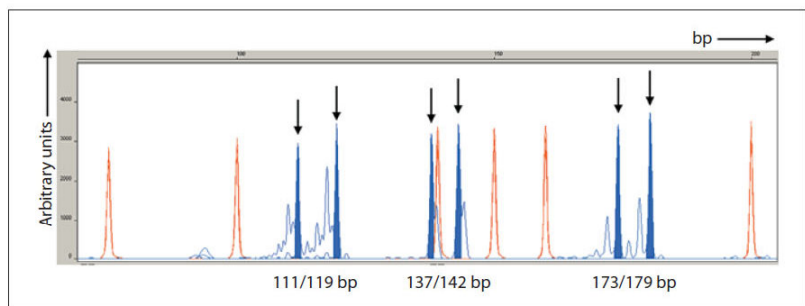
detect patient-specific deletions, the PCR products were sequenced (fig. 3). In addition to sequencing, fragment length analysis (patients A and B) and SNaPshot analysis (patient A) was carried out. Amplification efficiency of single cell PCR ranged from 77.3 to 93.8%, shown with gel electrophoresis and fragment length analysis. Heterozygosity rates between 72.2 and 100.0% were achieved. For the 5 bp deletion c.3183–3187delACAAA (patients B and C) heterozygosity efficiency was determined for full profiles of the multiplex PCRs in fragment length analysis. The full profile for patient B (82.3%) consists of the alleles 118/120 bp (D5S346) and 137/142 bp (PB2-FAM), for patient C (57.4%) of the alleles 111 bp/119 bp (D5S346), 137 bp/142 bp (PB2-FAM) and 173 bp/179 bp (D5S82) (fig. 4). For the 1-bp deletion c.2612delG (patient A) the results of the sequencing analysis were confirmed using

Table 3. Results of single cell analysis

Patient/loci	Amplification, %	Heterozygosity, %	Analysis method
Patient A/c.2612delG	77.3 (17/22)	81.3 (13/16)[1]	gel electrophoresis, sequencing analysis
Patient B/c.3183–3187delACAAA	90.5 (19/21)	72.2 (13/18)[1]	gel electrophoresis, sequencing analysis
	85.7 (18/21)	83.3 (15/18)	fragment length analysis
Patient B/D5S346	85.7 (18/21)	100.0 (18/18)	fragment length analysis
Patient C/c.3183–3187delACAAA	93.8 (61/65)	83.6 (51/61)	fragment length analysis
Patient C/D5S346	89.2 (58/65)	93.1 (54/58)	fragment length analysis
Patient C/D5S82	92.3 (60/65)	76.7 (46/60)	fragment length analysis

[1] One of the amplified samples could not be analyzed in sequencing or fragment length analysis.

the SNaPshot approach which allows reliable genotyping of the mutation (data not shown). All results of the single cell analysis are summarized in table 3. Contamination of one negative control occurred only in one of the three parallel patient-specific secondary PCR reactions showing the mutated 137 bp allele. As there was no amplification product detected in all other secondary PCR reactions for markers D5S346 and D5S82, contamination in the multiplex low-volume PCR could be excluded. Contamination probably occurred during nested PCR preparation as the amplified loci is consistent with the mutated allele. Contaminations in 4 of 179 (2.2%) secondary PCR reactions (table 3, patient C: 61 + 58 + 60 amplified samples) refer to unspecific extraneous alleles in the single cell samples clearly distinguishable from patient-specific alleles which seem to be a kind of stuttering peak but do not influence the single cell analysis results.

Discussion

Single cell analysis plays an important role in numerous fields of genetic testing, especially in preimplantation genetic diagnosis (PGD) [18, 19].

Recent years have seen a considerable increase in mutation analysis of monogenic diseases in the context of PGD due to advances in single cell analysis techniques. Up to now, mutation analysis of inherited monogenic disorders has been a well-established procedure [20]. As there is a need for validation prior to PGD, a test system is required to optimize the work flow, thus increasing the detection efficiency of mutations and to reduce allelic drop out 2 (ADO). The precise and reproducible acces-

sibility to single cells is a basic prerequisite to establishing such a test system.

In our study the successful combination of single cell laser microdissection, single particle transfer and low-volume multiplex PCR is presented. Subsequently, it was shown that fragment length analysis, SNaPshot and sequencing analysis could be performed on single cell PCR products. Our approach displays not only the establishment of a genetic test system prior to PGD but beyond single cell PCR, and analysis is also applicable to conventional isolated polar bodies, blastomeres or blastocyst cells which are transferred to a planar glass slide.

In comparison to other preliminary testing for PGD, some significant differences can be observed. The horizontal transfer of a series of isolated single lymphocytes to a planar PCR device constitutes a basic aspect of our approach. Optical control of the entire single cell handling including horizontal transfer ensures the reliability of the system in contrast to other isolation methods [12].

A striking advantage is the use of easily accessible fixed single lymphocytes. Storage of fixed lymphocytes for several months in sufficient quality for PCR analysis allows repeated optimization experiments without the need for fresh blood samples. Considering the template DNA quality, primer pairs were chosen which amplify only short sequences no more than 200 bp in length. Furthermore, short fragments increase amplification efficiency and decrease allelic drop out in single cell PCR reactions [21].

In contrast to the majority of investigations for PGD, we use heat denaturation of fixed lymphocytes prior to the first PCR cycle instead of chemical or enzymatic lysis of the cells [1]. Higher denaturing temperatures of at least

96°C reduce ADO rates dramatically without affecting amplification efficiency [22]. Therefore, we chose an initial denaturing step for single cell PCR of 97°C. This process enables time savings of up to 1 h, depending on the lysis method, since the time needed for enzyme incubation or washing can be omitted. The overall time for the single cell analysis procedure, excluding laser microdissection, is about 8–12 h, depending on which method is used, e.g. fragment length, sequencing or SNaPshot analysis. Time is an important factor in PGD and in polar body (PB) diagnosis, analysis time is limited to about 20 h in Germany [23].

Another advantage of heat denaturation is the reduced risk of contamination. Several lysis preparation steps and therefore unessential contact with potentially contaminated reagents or laboratory equipment can be avoided as the isolated cell on the reaction center of the planar PCR slide is covered only with reaction mix and mineral oil before starting PCR. Precise isolation and transfer of only one single cell under optical control and dry conditions additionally ensures that the risk of co-isolation of contaminating particles such as cell debris or DNA which may be present in aqueous cell solutions is minimized. On the basis of PCR on a glass slide the possibility of releasing contaminant substances from plastic PCR tubes into the reaction mix, especially when the tube is heated, can thus be circumvented [24]. The use of a nested PCR assay allows a reduced number of cycles during the first PCR and thus minimizes the risk of amplifying unspecific products. During the second PCR reaction, amplification products of the first PCR serve as a template for the inner primers, and so the yield of specific amplification products increases. Contamination from other sources is reduced to a minimum due to extreme care and appropriate facilities in the laboratory.

In our study, multiplex PCR in a total reaction volume of 1 μl was performed. Compared to PCR analysis in larger reaction volumes, this leads to an increased amplification sensitivity and efficiency of PCR which is necessary for minute amounts of DNA [25, 26]. Application of fluorescent PCR, which is standard in PGD nowadays, as well as the optimization of PCR conditions and nested PCR protocols are further strategies for additionally increasing amplification efficiency and detection sensitivity [1, 27]. The combination of at least two polymorphic markers and a mutation-specific fragment ensures an accurate analysis of the heterozygosity status of a single lymphocyte cell. Such multiplex reactions not only allow the reliable detection of ADO but are an important element for indirect diagnosis with linked polymorphic markers. Although multiplex PCR exclusively carried out with polymorphic markers has the advantage of being applied to many patients with different mutations, we could show that a multiplex assay combining different markers and mutation-specific primers can also be applied to several patients with the same mutation.

Furthermore, our approach enables the possibility of direct analysis of specific mutations, as nested PCR of single cells yields enough DNA for sequencing analysis (if necessary). This could be the case if linkage analysis for polymorphic markers is not feasible for couples who wish to perform PGD (for review, see [1]). Whole genome single cell amplification which enables the combination of several different analysis methods such as mutation, polymorphic marker or STR analysis, comparative genomic hybridization (CGH) or fluorescence in situ hybridization (FISH) would display a great facilitation in PGD. Some efforts have been taken to establish whole genome amplification (WGA) of single cells for PGD and, as has recently been proven, multiple displacement amplification (MDA) using Phi29 polymerase is on its way to becoming the standard WGA method in PGD applications [1, 28].

However, there are still several problems to be resolved. For example, high ADO rates in the range of 20–30% achieved in subsequent PCR analysis using fresh cells can be by-passed only if a sufficient number of informative polymorphic markers is available [1, 29]. This raises the same problems as mentioned for multiplex PCR when linkage analysis is not feasible. Another factor is the time that is needed for MDA reactions (up to 16 h), especially when using commercially available WGA kits. Additionally, the time necessary for subsequent analysis also needs to be considered, as time constitutes an essential parameter in PGD. One possibility of increasing the sensitivity of MDA could be downscaling of the assay to low-volume reactions, which has proven to be successful for PCR. Yet, commercially available WGA kits are designed for larger volumes in the range of 50 μl and a prerequisite for downscaling is to adjust reagent concentrations and reaction conditions. For example, when MDA is to be performed on our planar glass slide, the compatibility of the reaction mixture with the covering mineral oil has been taken into account. In fact, single cell whole genome amplification resulting in a high DNA yield is a great advantage for PGD, as successful applications have shown [29, 30].

In comparison with other PGD studies we achieved heterozygosity rates for polymorphic microsatellite markers and mutation-specific amplification products from

fixed single lymphocytes in nearly the same range as those from fresh cells [31–33]. Moreover, we applied our single cell genetic test system to polar body diagnosis for 3 female patients with mutations in the APC gene mentioned above (a 1-bp and a 5-bp deletion, respectively). In five PGD cycles, polar bodies of 60 oocytes were analyzed and 13 of the oocytes were identified as normal. These polar body PGDs resulted in one clinical pregnancy.

The main reason why we chose polar body diagnosis for demonstrating our approach is the legal situation in Germany where manipulation of embryos is forbidden by law and polar bodies are the only option for PGD [23]. Although PBs enable the analysis of only the maternal genome, they nevertheless have some advantages. Polar body diagnosis is an adequate method applicable for inherited diseases in those couples where only the woman is affected. In addition, ADO rates are considerably less in PB than in blastomere analysis and it is easier to find informative polymorphic markers, which can be important in challenging cases [34]. Removal of cells from the embryo (as is the case in blastomere and blastocyst PGD) can also be circumvented.

PGD of blastomeres where one or two cells are taken from the eight-cell stage embryo at day three postfertilization is still the method of choice in many laboratories [1]. However, PGD of several trophectoderm cells extracted from the blastocyst stage of the embryo is becoming more important [35, 36]. Accuracy and reliability of analysis indisputably increases with the number of cells or template DNA, respectively, but even if, e.g., up to 10 cells, which together contain about 70 pg, were analyzed, this still lies in the range of minute amounts of DNA and requires sensitive analysis methods which our system provides [37]. There are many reasons for or against the use for both blastomere and blastocyst PGD. For example, advantages of trophectoderm cells, in contrast to blastomeres, include reduced ADO rates and amplification fail-

ure as well as higher implantation rates and approximately equal pregnancy rates [38]. On the other hand, cryoconservation caused by the strictly limited time available for analysis has the potential to harm the embryo and prevent its implantation [1, 35]. This problem could be overcome by applying our approach to blastocyst cells as we have shown that analysis can be done within the 12 h also necessary for polar body diagnosis. In fact, the application of PB, blastomere or blastocyst PGD depends on several factors ranging from legal restrictions, and the genetic background of patients to the type of disease analyzed. However, it is clear that PGD will only ever be performed on a few or single cells.

Thus, our investigation successfully validates reliable genetic testing for as little as one single cell by means of mutation detection in the *APC* gene. Moreover, the combination of single cell isolation, horizontal particle transfer and subsequent analysis can also be optimized for a wide range of other inherited diseases or genetic disorders and is not limited to polar bodies or PGD in general. This technique enables a variety of molecular analyses where isolation of a few or single cells is important for genetic characterization, e.g. heterogeneous cell populations or mosaics. Even the isolation and analysis of specific regions from tissue sections (e.g. tumor sections) is facilitated with our system. Due to the selective isolation and single particle transfer processes, cross-contamination with tissue cells of neighboring regions can be circumvented.

Funding

References

▶1 Spits C, Sermon K: PGD for monogenic disorders: aspects of molecular biology. Prenat Diagn 2009;29:50–56.

▶2 Hehr A, Seifert B, Hehr U, Bals-Pratsch M: Polar body diagnosis for monogenic disorders in Regensburg. J Reproduktionsmed Endokrinol 2009;6:27–31.

▶3 Vanneste E, Melotte C, Debrock S, D'Hooghe T, Brems H, Fryns JP, Legius E, Vermeesch JR: Preimplantation genetic diagnosis using fluorescent in situ hybridization for cancer predisposition syndromes caused by microdeletions. Human Reprod 2009;24:1522–1528.

▶4 Sermon K: Current concepts in preimplantation genetic diagnosis (PGD): a molecular biologist's view. Hum Reprod Update 2002; 8:11–20.

▶5 Nunes MC, Roy NS, Keyoung HM, Goodman RR, McKhann II G, Jiang L, Kang J, Nedergaard M, Goldman SA: Identification and isolation of multipotential neural progenitor cells from the subcortical white matter of the adult human brain. Nat Med 2003; 9:439–447.

6 Herzenberg LA, Parks D, Sahaf B, Perez O, Roederer M, Herzenberg LA: The history and future of the fluorescence activated cell sorter and flow cytometry: a view from Stanford. Clin Chem 2002;48:1819–1827.

7 Weimer J, Koehler MR, Wiedemann U, Attermeyer P, Jacobsen A, Karow D, Kiechle M, Jonat W, Arnold N: Highly comprehensive karyotype analysis by a combination of spectral karyotyping (SKY), microdissection and reverse painting (SKY-MD). Chromosome Res 2001;9:395–402.

8 Simone NL, Bonner RF, Gillespie JW, Emmert-Buck MR, Liotta LA: Laser-capture microdissection: opening the microscopic frontier to molecular analysis. Trends Genet 1998;14:272–276.

9 Thalhammer S, Lahr G, Clement-Sengewald A, Heckl WM, Burgemeister R, Schütze K: Laser microtools in cell biology and molecular medicine. Laser Phys 2003;13:681–692.

10 Kirschner J, Plaschke-Schluetter A: Advancing forensics with precise target excision: the CellCut Plus laser microdissection instrument. Nature Methods 2007;4.

11 Di Martino D, Giuffrè G, Staiti N, Simone A, Todaro P, Saravo L: Laser microdissection and DNA typing of cells from single hair follicles. Forensic Sci Int 2004;146:155–157.

12 Woide D, Mayer V, Wachtmeister T, Hoehn N, Zink A, Koehler U, Thalhammer S: Single Particle Adsorbing Transfer System, Biomed Microdevices. DOI 10.1007/s10544–008–9270–8.

13 Woide D, Schlentner V, Neumaier T, Wachtmeister T, Paretzke HG, von Guttenberg Z, Wixforth A, Thalhammer S: Programmable cytogenetic submicrolitre lab-on-a-chip for molecular diagnostic applications. IEEE Transactions on Biomedical Circuits and Systems, International Conference on Biomedical Electronics and Devices, 2007.

14 Zhang C, Xing D: Miniaturized PCR chips for nucleic acid amplification and analysis: latest advances and future trends. Nucleic Acids Res 2007;35:4223–4237.

15 Nakamura Y: The adenomatous polyposis coli gene and human cancers. J Cancer Res Clin 1995;121:529–534.

16 Thalhammer S, Langer S, Speicher M, Heckl WM, Geigl JB: Generation of chromosome painting probes from single chromosomes by laser microdissection and linker-adaptor PCR. Chromosome Res 2004;12:337–343.

17 Murphy KM, Geiger T, Hafez MJ, Eshleman JR, Griffin CA, Berg KD: A single nucleotide primer extension assay to detect the *APC* I1307K gene variant. J Mol Diagn 2003;5:222–226.

18 Klein CA, Schmidt-Kittler O, Schardt JA, Pantel K, Speicher MR, Riethmüller G: Comparative genomic hybridization, loss of heterozygosity, and DNA sequence analysis of single cells. Proc Natl Acad Sci USA 1999;96:4494–4499.

19 Ao A, Wells D, Handyside AH, Winston RML, Delhanty JDA: Preimplantation genetic diagnosis of inherited cancer: familial adenomatous polyposis coli. J Assist Reprod Gen 1998;15:140–144.

20 Renwick P, Ogilvie CM: Preimplantation genetic diagnosis for monogenic diseases: overview and emerging issues. Expert Rev Mol Diagn 2007;7:33–43.

21 Piyamongkol W, Bermúdez MG, Harper JC, Wells D: Detailed investigation of factors influencing amplification efficiency and allele drop-out in single cell PCR: implications for preimplantation genetic diagnosis. Mol Hum Reprod 2003;9:411–420.

22 Ray PF, Winston RML, Handyside AH: Reduced allele dropout in single-cell analysis for preimplantation genetic diagnosis of cystic fibrosis. J Assist Reprod Gen 1996;13:104–106.

23 Tomi D, Griesinger G, Schultze-Mosgau A, Eckhold J, Schoepper B, Al-Hasani S, Diedrich K, Schwinger E: Polar body diagnosis for hemophilia A using multiplex PCR for linked polymorphic markers. J Histochem Cytochem 2005;53:277–280

24 McDonald GR, Hudson AL, Dunn SM, You H, Baker GB, Whittal RM, Martin JW, Jha A, Edmondson DE, Holt A: Bioactive contaminants leach from disposable laboratory plasticware. Science 2008;322:917.

25 Schmidt U, Lutz-Bonengel S, Weisser HJ, Sänger T, Pollak S, Schön U, Zacher T, Mann W: Low-volume amplification on chemically structured chips using the PowerPlex16 DNA amplification kit. Int J Legal Med 2006;120:42–48.

26 Proff C, Rothschild MA, Schneider PM: Low volume PCR (LV-PCR) for STR typing of forensic casework samples. Int Congr Ser 2005;1288:645–647.

27 Moutou C, Viville S: Improvement of preimplantation genetic diagnosis (PGD) for the Cystic Fibrosis mutation ΔF508 by fluorescent polymerase chain reaction. Prenat Diagn 1999;19:1248–1250.

28 Coskun S, Alsmadi O: Whole genome amplification from a single cell: a new era for preimplantation genetic diagnosis. Prenat Diagn 2007;27:297–302.

29 Glentis S, SenGupta S, Thornhill A, Wang R, Craft I, Harper JC: Molecular comparison of single cell MDA products derived from different cell types. Reprod Biomed Online 2009;19:89–98.

30 Ren Z, Zeng H, Xu Y, Zhuang G, Deng J, Zhang C, Zhou C: Preimplantation genetic diagnosis for Duchenne muscular dystrophy by multiple displacement amplification. Fertil Steril 2009;91:359–364.

31 Ray PF, Vekemans M, Munnich A: Single cell multiplex PCR amplification of five dystrophin gene exons combined with gender determination. Mol Hum Reprod 2001;7:489–494.

32 Lee H-S, Jun JH, Choi HW, Lim CK, Yoo H-W, Koong MK, Kang IS: Preimplantation genetic diagnosis for ornithine transcarbamylase deficiency by simultaneous analysis of duplex-nested PCR and fluorescence in situ hybridization: a case report. J Korean Med Sci 2007;22:572–576.

33 Spits C, De Rycke M, Van Ranst N, Verpoest W, Lissens W, Van Steirteghem A, Liebaers I, Sermon K: Preimplantation genetic diagnosis for cancer predisposition syndromes. Prenat Diagn 2007;27:447–456.

34 Altarescu G, Brooks B, Eldar-Geva T, Margalioth EJ, Singer A, Levy-Lahad E, Renbaum P: Polar body-based preimplantation genetic diagnosis for *N*-acetylglutamate synthase deficiency. Fetal Diagn Ther 2008;24:170–176.

35 McArthur SJ, Leigh D, Marshall JT, de Boer KA, Jansen RPS: Pregnancies and live births after trophectoderm biopsy and preimplantation genetic testing of human blastocysts. Fertil Steril 2005;84:1628–1636.

36 Fragouli E, Katz-Jaffe M, Alfarawati S, Stevens J, Colls P, Goodall N, Tormasi S, Gutierrez-Mateo C, Prates R, Schoolcraft WB, Munne S, Wells D: Comprehensive chromosome screening of polar bodies and blastocysts from couples experiencing repeated implantation failure. Fertil Steril 2009;DOI 10.1016/j.fertnstert.2009.04.053

37 Lutz-Bonengel S, Saenger T, Heinrich M, Schoen U, Schmidt U: Low volume amplification and sequencing of mitochondrial DNA on a chemically structured chip. Int J Legal Med 2007;121:68–73.

38 Pangalos CG, Hagnefelt B, Kokkali G, Pantos K, Konialis CP: Birth of a healthy histocompatible sibling following preimplantation genetic diagnosis for chronic granulomatous disease at the blastocyst stage coupled to HLA typing. Fetal Diagn Ther 2008;24:334–339.

Mayer/Schoen/Holinski-Feder/Koehler/Thalhammer

One- and Three-letter-code of amino acids and RNA codon table

The table shows the 64 codons of the mRNA and the amino acids for each. The direction of the mRNA is 5' to 3'. Uracile (U) instead of thymine (T) is the corresponding base in mRNA.

		2nd base			
		U	**C**	**A**	**G**
1st base	**U**	UUU (Phe/F) Phenylalanine UUC (Phe/F) Phenylalanine UUA (Leu/L) Leucine UUG (Leu/L) Leucine	UCU (Ser/S) Serine UCC (Ser/S) Serine UCA (Ser/S) Serine UCG (Ser/S) Serine	UAU (Tyr/Y) Tyrosine UAC (Tyr/Y) Tyrosine UAA Ochre (*Stop*) UAG Amber (*Stop*)	UGU (Cys/C) Cysteine UGC (Cys/C) Cysteine UGA Opal (*Stop*) UGG (Trp/W)Tryptophan
	C	CUU (Leu/L) Leucine CUC (Leu/L) Leucine CUA (Leu/L) Leucine CUG (Leu/L) Leucine	CCU (Pro/P) Proline CCC (Pro/P) Proline CCA (Pro/P) Proline CCG (Pro/P) Proline	CAU (His/H) Histidine CAC (His/H) Histidine CAA (Gln/Q) Glutamine CAG (Gln/Q) Glutamine	CGU (Arg/R) Arginine CGC (Arg/R) Arginine CGA (Arg/R) Arginine CGG (Arg/R) Arginine
	A	AUU (Ile/I) Isoleucine AUC (Ile/I) Isoleucine AUA (Ile/I) Isoleucine AUG˙ (Met/M) Methionine	ACU (Thr/T)Threonine ACC (Thr/T)Threonine ACA (Thr/T)Threonine ACG (Thr/T)Threonine	AAU (Asn/N) Asparagine AAC (Asn/N) Asparagine AAA (Lys/K) Lysine AAG (Lys/K) Lysine	AGU (Ser/S) Serine AGC (Ser/S) Serine AGA (Arg/R) Arginine AGG (Arg/R) Arginine
	G	GUU (Val/V) Valine GUC (Val/V) Valine GUA (Val/V) Valine GUG (Val/V) Valine	GCU (Ala/A) Alanine GCC (Ala/A) Alanine GCA (Ala/A) Alanine GCG (Ala/A) Alanine	GAU (Asp/D) Aspartic acid GAC (Asp/D) Aspartic acid GAA (Glu/E) Glutamic acid GAG (Glu/E) Glutamic acid	GGU (Gly/G) Glycine GGC (Gly/G) Glycine GGA (Gly/G) Glycine GGG (Gly/G) Glycine

˙ The codon AUG both codes for methionine and serves as an initiation site: the first AUG in an mRNA's coding region is where translation into protein begins (Shine and Dalgarno 1974, Nakamoto 2009).

nonpolar	polar	basic	acidic	(stop codon)

Inverse RNA codon table with One- and Three-letter-code of the amino acids.

Inverse codon table			
Ala/A	GCU, GCC, GCA, GCG	**Leu/L**	UUA, UUG, CUU, CUC, CUA, CUG
Arg/R	CGU, CGC, CGA, CGG, AGA, AGG	**Lys/K**	AAA, AAG
Asn/N	AAU, AAC	**Met/M**	AUG
Asp/D	GAU, GAC	**Phe/F**	UUU, UUC
Cys/C	UGU, UGC	**Pro/P**	CCU, CCC, CCA, CCG
Gln/Q	CAA, CAG	**Ser/S**	UCU, UCC, UCA, UCG, AGU, AGC
Glu/E	GAA, GAG	**Thr/T**	ACU, ACC, ACA, ACG
Gly/G	GGU, GGC, GGA, GGG	**Trp/W**	UGG
His/H	CAU, CAC	**Tyr/Y**	UAU, UAC
Ile/I	AUU, AUC, AUA	**Val/V**	GUU, GUC, GUA, GUG
START	AUG	**STOP**	UAA, UGA, UAG

(codon tables from Wikipedia: http://en.wikipedia.org/wiki/Genetic_code)

Curriculum Vitae

Personalien:

Vor- und Zuname:	Veronika Mayer
Geburtstag:	29.12.1980
Geburtsort:	Rosenheim
Wohnort:	83115 Neubeuern (Deutschland), Elandstr. 4
Staatsangehörigkeit:	deutsch
Familienstand:	verheiratet

Schulbildung:

1987 - 1991	Grundschule in Neubeuern
1991 - 2000	Karolinengymnasium Rosenheim Abschluss: Abitur

Studium:

2000 - 2006   Biologiestudium an der Ludwig-Maximilians-Universität München
Hauptfach: Humangenetik
Nebenfächer: Genetik, Immunologie, Zoologie

Thema der Diplomarbeit:
„Untersuchungen zur Isolierung von Chromosomen aus verschieden fixierten Wurzelmeristemzellen der Gerste (*Hordeum vulgare* L.)"

Studienabschluss: Diplom

Berufstätigkeit/Promotion:

2007 - 2009   Wissenschaftliche Mitarbeiterin an der Ludwig-Maximilians-Universität München, Ausübung der Tätigkeit mit Gastvertrag am Helmholtz Zentrum München

2009   Wissenschaftliche Mitarbeiterin an der Universität Augsburg, Ausübung der Tätigkeit mit Gastvertrag am Helmholtz Zentrum München

2010   Abschluss der Promotion

Berufsweiterbildung:

Frühjahr 2007   Workshop „Whole Genome Amplification"

Veröffentlichungen:

2007
Woide D, Schlentner V, Neumaier T, Wachtmeister T, Paretzke HG, von Guttenberg Z, Wixforth A, Thalhammer S: Programmable cytogenetic submicrolitre lab-on-a-chip for molecular diagnostic applications. IEEE Transactions on Biomedical Circuits and Systems, International Conference on Biomedical Electronics and Devices 2007

2009
Woide D, Mayer V, Wachtmeister T, Hoehn N, Zink A, Koehler U, Thalhammer S: Single particle adsorbing transfer system. Biomedical Microdevices 2009; 11 (3): 609-614

Mayer V, Schoen U, Holinski-Feder E, Koehler U, Thalhammer S: Single cell analysis of mutations in the *APC* gene. Fetal Diagnosis and Therapy 2009; 26: 148-156

Tätigkeitsschwerpunkte:

Lasermikrodissektion
PCR und low-volume PCR (AmpliGrid-Technologie)
Einzelzellanalyse
Sequenzierung
Fragmentanalyse